2024

The Role of Notch1 Signaling in Regulating Neurogenesis in the Olfactory Bulb Following Traumatic Brain Injury

Sarah A. Baig
Virginia Commonwealth University

The Role of Notch1 Signaling in Regulating Neurogenesis in the Olfactory Bulb Following Traumatic Brain Injury

A thesis submitted in partial fulfillment of the requirements for the degree of Master of Science in Anatomy and Neurobiology at Virginia Commonwealth University

By:

Sarah Baig

Bachelor of Arts in Biology and Psychology – University of Virginia, 2019

Major Advisor: Dr. Dong Sun, MD, Ph.D.

Professor

Department of Anatomy and Neurobiology

Virginia Commonwealth University

Richmond, Virginia

May 2024

Acknowledgements

It has been a great honor and privilege to participate in this invaluable research at Virginia Commonwealth University School of Medicine. Foremost, I would like to express my sincere gratitude to my advisor, Dr. Dong Sun, for her continuous support, patience, motivation, and immense knowledge throughout my research. Thank you for giving me the opportunity to conduct research, while inspiring my independence and personal growth throughout the years.

I thank my committee members, Dr. Kristy Dixon and Dr. Andrew Ottens, for providing valuable perspectives and profound knowledge in the direction of my research. I thank my program director, Dr. Kimberle Jacobs, for her guidance and support in completing my degree. To the Microscopy Facility, especially Frances White, thank you for your continuous assistance, training, and collaboration throughout my project and troubleshooting LSM 880.

To my mother, Zanobia Afghan Baig, and my late father, Mirza Afghan Baig, thank you for your continuous support and unconditional love. I would not be where I am today without the both of you and I hope I can continue to make you both proud In Sha Allah. To my four sisters and two brothers, I would not be who I am today without all of you, and I am truly grateful for your incredible support and guidance throughout my journey. I am incredibly appreciative to have such amazing individuals nurturing and supporting me in my life.

Lastly, thank you to my lab mates who have encouraged and supported me throughout the years. I wish all of you the best of luck in your future endeavors.

Table of Contents

List of Figures....4
List of Tables....7
List of Abbreviations....8
Chapter 1: Introduction....13
1.1 Traumatic Brain Injury....13
1.1.1 Epidemiology....13
1.1.2 Mechanism and Biomechanics....15
1.1.4 Pathophysiology of TBI....18
1.1.5 Experimental TBI Models....22
1.2 Olfactory Bulb....23
1.2.1 Olfactory Dysfunction....23
1.2.3 Anatomy of the Olfactory Bulb....28
Layers of the Olfactory Bulb....29
Cells of the Olfactory Bulb....30
1.2.4 Adult Neurogenesis and Plasticity in the Olfactory Bulb....34
1.2.5 TBI Induced Neurogenesis in the Olfactory Bulb....37
1.3 Notch1 Signaling....38
1.4 Dissertation objectives/Hypothesis....42
Chapter 2: Materials and Methods....42
2.1 Experimental Subjects....42
2.2 Transgenic Mice Strain....43
2.3 Surgical Procedure....44
2.4. Tissue Processing....48
2.4.1 Transcardial Perfusion....48
2.4.2 Tissue Embedding in Agarose....48
2.4.3 Tissue Preparation and Collection....49
2.5 Immunohistochemistry....50
2.6 Confocal microscopy....51
2.7 Quantification and Stereology....52
2.8 Statistical Analysis....52
Chapter 3: Results....54
3.2 Changes of GFP+ Cell Populations with Increased Time from Injury....65
3.3 Loss of Notch1 Results in an Increase of Neuronal Differentiation and Proliferation Dependent on GCL....69
Conclusion and Future Direction....94
Vita....95
References....96

List of Figures

Figure 1.1 Post-TBI 5 Year Outcome **15**

Figure 1.1.4.1 Primary Injury Pathophysiology **20**

Figure 1.1.4.2 Secondary Injury Post-TBI Pathophysiology **23**

Figure 1.2.2 Post-Traumatic Olfactory Dysfunction Mechanisms **28**

Figure 1.2.4 Neurogenesis Pathway in the Olfactory Bulb **35**

Figure 1.2.3.1 Layers of the Olfactory Bulb **38**

Figure 1.2.3.2 Cells of the Olfactory Bulb **39**

Figure 1.3 Notch Signaling Pathway **41**

Figure 2.2 Transgenic Mice Strains **43**

Figure 2.3.1 LFPI Model **45**

Figure 2.3.2 FPI Percussion Device **46**

Figure 2.4.2 Dorsal View of the Olfactory Bulb **48**

Figure 2.4.3 Tissue Collection **49**

Figure 3.1 Olfactory Bulb Staining **53**

Figure 3.2 BrdU+ Staining Pattern at 4WPI **56**

Figure 3.3 Quantification of BrdU+ Cells in the GCL, EPL, and GL of the Olfactory Bulb 4 WPI **57**

Figure 3.4 BrdU+/Neun+ Staining Pattern at 4WPI **58**

Figure 3.5 Quantification of BrdU+/NeuN+ Cells in the GCL, EPL, and GL of the Olfactory Bulb 4 WPI **59**

Figure 3.6 BrdU+ Staining Pattern at 8 WPI **60**

Figure 3.7 Quantification of BrdU+ in the GCL, EPL, and GL of the Olfactory

Bulb 8 WPI **61**

Figure 3.8 BrdU+/Neun+ Staining Pattern at 8 WPI **62**

Figure 3.9 Quantification of BrdU+/NeuN in the GCL, EPL, and GL of the Olfactory Bulb 8 WPI **63**

Figure 3.10 GFP Staining Pattern at 4 WPI **65**

Figure 3.11 Quantification of GFP+ Cells in the GCL, EPL, and GL of the Olfactory Bulb 4 WPI **66**

Figure 3.12 GFP Staining Pattern at 8 WPI **67**

Figure 3.13 Quantification of GFP+ in the GCL, EPL, and GL of the Olfactory Bulb 8 WPI **68**

Figure 3.14 GFP/BrdU Double-Labeling Staining Pattern at 4 WPI **70**

Figure 3.15 Quantification of GFP+ /BrdU+ Cells in the GCL, EPL, and GL of the Olfactory Bulb at 4 WPI **71**

Figure 3.16 GFP/BrdU/NeuN Triple-Labeling Staining Pattern at 4 WPI **72**

Figure 3.17 Quantification of GFP+ /BrdU+/NeuN Cells in the GCL, EPL, and GL of the Olfactory Bulb at 4 WPI **73**

Figure 3.18 GFP/BrdU Double-Labeling Staining Pattern at 8 WPI. **74**

Figure 3.19 Quantification of GFP+/BrdU+ in the GCL, EPL, and GL of the Olfactory Bulb at 8 WPI. **75**

Figure 3.20 GFP/BrdU Triple-Labeling Staining Pattern at 8 WPI **76**

Figure 3.21 Quantification of GFP+/BrdU+/NeuN in the GCL, EPL, and GL of the Olfactory Bulb at 8 WPI **77**

Figure 3.22 Comparison of the number of GFP+ cells between 4 and 8 weeks WPI

83

Figure 3.23 Comparison of the number of BrdU+ cells between 4 and 8 weeks WPI

83

Figure 3.24 Comparison of the number of GFP+/BrdU+ cells between 4 and 8 weeks WPI

84

Figure 3.25 Comparison of the number of BrdU+/NeuN+ cells between 4 and 8 weeks WPI

84

Figure 3.26 Comparison of the number of GFP+/BrdU+/NeuN+ cells between 4 and 8 weeks WPI

85

List of Tables

Table 2.1 Total Animals Used in 4 WPI and 8 WPI IHC **43**

Table 3.1 P values of Two-Way ANOVA Post-hoc Test at 4 WPI. **78**

Table 3.2 P values of Two-Way ANOVA Post-hoc Test at 8 WPI. **79**

Table 3.3: P values of Two-Way ANOVA Post-hoc Test Comparing 4 WPI vs. 8 WPI **80**

List of Abbreviations

ABC	Avidin-Biotin Complex
AD	Alzheimer's disease
ANOVA	Analysis of variance
aNSCs	Adult Neural Stem Cells
BBB	Blood Brain Barrier
BrdU	5-Bromo-2-deoxyuridine
CCI	Controlled Cortical Impact Injury
CHI	Closed Head Injury
CDC	Center for Disease Control and Prevention
cKO	conditional Knock Out
CNS	Central Nervous System
DAB	3,3'-Diaminobenzadine-tetra-hydrochloride
DAI	Diffuse Axonal Injury
DG	Dentate Gyrus
DPI	Days post-injury
EPL	External Plexiform Layer
EYFP	Enhanced Yellow Fluorescent Protein
FPI	Fluid Percussion Injury
GL	Glomerular Layer
GC	Granule cell

GCL	Granule Cell Layer
GCS	Glasgow Coma Score
GFP	Green fluorescent protein
IHC	Immunohistochemistry
IF	Immunofluorescence
i.p.	Intraperitoneal injection
IPL	Internal Plexiform Layer
LOC	Loss of Consciousness
LFPI	Lateral fluid percussion injury
LSM	Laser Scanning Microscope
MCL	Mitral Cell Layer
MVA	Motor Vehicle Accident
NeuN	Neuronal nuclear protein
NICD	Notch intracellular domain
NSHAP	National Social Life, Health and Aging Proj
NC-Y	Control
NC-NKO-Y	Notch1 cKO
NSC	Neural Stem Cell
NPCs	Neural progenitor cells
OB	Olfactory Bulb
OD	Olfactory dysfunction
ORNs	Olfactory Receptor Neurons

ONL	Olfactory Nerve Layer
PGCs	Periglomerular Cells
PBS	Phosphate buffer saline
PD	Parkinson’s Disease
PFA	Paraformaldehyde
RMS	Rostral Migratory Stream
SVZ	Subventricular Zone
TAM	Tamoxifen
TBI	Traumatic brain injury
WHO	World Health Organization
WPI	Weeks post-injury

Abstract

In the United States, more than 20.5 million adults over the age of 40 suffer from olfactory dysfunction, with TBI attributing to 5-17% of all olfactory dysfunction cases. Although often initially undetected and less conspicuous than other cognitive and behavioral impairments, olfactory dysfunction may have a significant negative impact on patients' quality of life and ability to accomplish activities of daily living, therefore the pathophysiology of these disorders should be understood. The production of neural stem cells enhances the repair and regeneration of the injured brain following a TBI. One of the primary endogenous neural stem cell generation sites in the adult mammalian brain is the subventricular zone (SVZ) of the lateral ventricles. Neuroblasts born in the SVZ migrate via the rostral migratory stream to the olfactory bulb (OB), giving rise to fully functional integrated cells. One of the major issues with new cells is their ability to survive to maturation and integrate into the neuronal network.

Following a TBI, the generation of new neurons and the regulatory mechanism driving their maturation and integration into the neuronal circuitry of the olfactory bulb is poorly understood. Notch1, a highly conserved transmembrane pathway plays a critical role in neural stem cell proliferation, differentiation, dendritic complexity, and apoptosis. In this current study, experiments were conducted to better understand neurogenesis in the OB following TBI and the regulatory role of Notch1 signaling. We hypothesized that TBI alters the developmental processes of adult generated neurons in the olfactory bulb and Notch1 signaling plays and important role in regulating this process. To test this hypothesis, we used transgenic mice with conditional knockout of Notch1 in nestin+ cells, along with matched control mice aged approximately 2-3 months. These mice underwent either a lateral fluid percussion injury (LFPI) or sham surgery. Following the injury, they received intraperitoneal injections of BrdU (50

mg/kg) immediately after for 7 days to label newly generated injury-induced cells. At 4 or 8 weeks post-injury, the animals were sacrificed, and sections of the olfactory bulb were processed to detect the total number of cells positive for GFP and BrdU alone, or double and triple-labeled with the mature neuronal marker NeuN. The sections were then quantified using stereology.

We found that the absence of Notch1 in nestin+ cells significantly affected neural stem cell survival in the OB particularly at 8 weeks post-injury (WPI), where the injury group showed significantly higher numbers of BrdU+ and BrdU+/NeuN+ cells. These results suggest a time-dependent proliferation of neural stem cells, with notable differences observed at 8WPI compared to 4WPI. Additionally, consistent findings at 8WPI highlight the granule cell layer (GCL) as a crucial site for understanding injury's impact on OB neurogenesis and cell survival. For future studies, examining time points beyond 8 weeks could provide insights into the long-term survival of injury-dependent neurons and the effects of Notch1 inactivation on neural stem cell differentiation and proliferation in the OB. Additionally, incorporating a more severe injury model and functional assessments of olfaction would enhance our understanding of these processes.

Chapter 1: Introduction

Despite the staggering statistics, traumatic brain injury (TBI) is referred to as the "silent" epidemic with limited awareness of its implications worldwide. It afflicts millions of Americans and their families each year with no effective treatment to improve neural structural repair and functional recovery of patients following TBI. However, with advancements in research, medications, and rehabilitation strategies, cognitive recovery and a reduction in neurological and olfactory deficits can be better elucidated. Specifically, investigating endogenous neural stem cells and the regulatory role of Notch1 can provide valuable insight in enhancing cognitive and functional recovery following TBI.

1.1 Traumatic Brain Injury

1.1.1 Epidemiology

The Center for Disease Control and Prevention (CDC) defines TBI as a disruption in the normal functioning of the brain that may be caused by a bump, blow, jolt to the head, or penetrating head injury (CDC, 2023). Each year, over 1.5 million Americans sustain a TBI, and as a consequence of these injuries over 230,000 people are hospitalized, 50,000 die representing one-third of all injury-related deaths, and approximately 80,000-90,000 people experience the onset of long-term disability (CDC, 2023). Alarmingly, these statistics do not include the many TBI cases that go untreated, nor the ones treated in primary or urgent care facilities. In the United States alone, TBI is the leading cause of death and disability in children and adults under the age of 45 years old, and as of today, 5.3 million men, women, and children are living with a permanent TBI-related disability (CDC, 2023).

Depending on the severity of the injury, those afflicted by TBI face various health problems that can last a couple days or the rest of their lives. The CDC reports 5-year outcomes

of persons with TBI estimates based on the TBIMS National Database **(Figure 1.1)**. The data includes people 16 years of age and older who received inpatient rehabilitation services for a primary diagnosis of TBI (CDC, 2023). The report states that 5 years post TBI, 22% died, 30% became worse, 22% stayed the same, and only 26% improved. Even after surviving a TBI and receiving rehabilitation services, the long-term negative impacts of TBI are significant, with the person's life expectancy predicted to be on average 9 years shorter (CDC, 2023). Among those still alive after 5 years, 57% are moderately or severely disabled, 55% do not hold a job (but were employed at the time of their injury), 50% return to a hospital at least once, 33% rely on others for help with everyday activities, 29% are not satisfied with life, 29% use illicit drugs or misuse alcohol, and 12% reside in nursing homes or other institutions (CDC, 2023).

Figure 1.1 Post-TBI 5 Year Outcome Illustrates the 5-year outcomes of persons with a primary diagnosis of TBI. Data are US population estimated based on the TBIMS National Data base. CDC 2023.

Apart from the profound short-term and long-term physical, emotional, and neurological impairments from permanent disability for injured persons and their loved ones, there is an immense societal and economic expenditure on clinical management of TBIs that has imposed a

heavy burden on the US healthcare and economic system. In 2010, the United States spent approximately $76.5 billion dollars on direct and indirect TBI related medical costs and it has been estimated that TBI annually costs the global economy approximately $400 billion US dollars (Finkelstein et al., 2006; Kureshi et al., 2017).

1.1.2 Mechanism and Biomechanics

The mechanism of injury for TBIs can be divided into 3 categories: closed head injury (CHI), penetrating, and explosive blast (Ng & Lee, 2019). Closed head TBI, which has the highest incidence and accounts for nearly half of TBI related hospitalizations, refers to blunt impact trauma caused by falls, motor vehicle accidents, and sport concussions. The strong blunt trauma directly disrupts normal functioning of the brain at the site of impact and damage to the brain vasculature, leading to compression of the brain tissues, and reduction of cerebral blood flow. This mechanism of injury eventually results in focal and diffuse injury to other regions of the brain **(Section 1.1.3)**. Types of CHIs include concussion, contusion, diffuse axonal injury, and intracranial hematoma (epidural hematoma, subdural hematoma, subarachnoid hemorrhage, and intraparenchymal hemorrhage) (Ginsburg & Huff, 2023).

Penetrating TBI results when a foreign body penetrates through the skull and the dura and traverses into the brain parenchyma compared to CHI. It is the most severe type of TBI and is a significant cause of mortality in young adults. Types of penetrating TBI include knife or sharp objects, bullets, cavitation, and shockwave injury. Lacerations cause focal injury, cerebral edema, and ischemia. The severity of this type of TBI depends on the energy, speedy of entry, and location (Alao & Waseem, 2022). With the invasive and sharp nature of this TBI, the chance of infection is relatively high, as well as complications such as pneumonitis, cerebrospinal leakage, and respiratory failure.

A relatively new category of TBI, explosive blast TBI is when the brain is compromised by rapid pressure shock waves generated by the explosion as seen during war. Kinetic energy from the blast causes deformation of the brain creating a widespread diffuse injury in both the gray and white matter of the brain, resulting in neuronal and axonal death, as well as a compromised blood brain barrier (BBB) (Cernak & Noble-Hausslein, 2010). The macroscopic acceleration of the brain can result in compression and shearing of the brain tissue. Furthermore, the brain's movement can result in lacerations, subdural hematomas, and micro-hemorrhaging due to increased vascular blood pressure when the BBB is breached (Bryden et al., 2019).

1.1.3 Classification of TBI

TBI classification is extremely heterogeneous and varies based on type, severity, location, mechanism of injury, and physiological response to injury. The severity of TBI is based on the Glasgow Coma Score (GCS) and ranges from 3 (completely unresponsive) to 15 (responsive). TBI can be classified as mild, moderate, and severe based on objective symptoms and neurobehavioral deficits.

According to the World Health Organization (WHO) and the CDC, a mild TBI is defined by a GCS score of 13-15, typically resulting from blunt or mechanical force that rapidly shifts the brain's position. This can lead to transient confusion, disorientation, or loss of consciousness (LOC) lasting no longer than 30 minutes (CDC, 2023). Individuals with a mild TBI or concussion may also encounter cognitive challenges related to learning, memory, concentration, and problem-solving. Symptoms of a mild TBI typically resolve within a few weeks.

A moderate and severe TBI is caused by a bump, blow, or jolt to the head or by a penetrating injury (such as from a gunshot) to the head (CDC, 2023). A moderate TBI has a GCS

score of 9-12 and includes mental status change or LOC of 30 min to 6 hours. A severe TBI has a GCS of <9 and includes mental status change or LOC > 6 hours. A person with a moderate or severe TBI may experience more drastic adverse symptoms such as loss of vision in one or both eyes, a worsening headache, convulsions and seizures, numbness or tingling of arms or legs, and repeated nausea and vomiting (CDC, 2023). Symptoms from a mild to severe TBI may last a couple months to a lifetime.

TBI produces both acute and chronic complications that significantly impair the quality life of afflicted individuals, their loved ones, and society. Apart from the psychological, economical, and physical toll of TBIs, it can result in the long-term mortality, reduced life expectancy, and permanent disabilities. TBI increases the risk for neurodegenerative disorders such as Alzheimer's disease (AD), Parkinson's disease (PD) and chronic traumatic encephalopathy as well as secondary pathological conditions such as sleep disorders, epilepsy, psychiatric conditions (Bramlett et al., 2015). Notably, a study published by Costanzo et al and Zasler found anosmia to occur in 0–16% of patients with mild head injury, 15%–19% of those with moderate head injury, and 25%–30% of those with severe head injury. The relationship between the severity of head injury, assessed by GCS score, and the extent of olfactory dysfunction is significant and will be explored further in **Section 1.2**, constituting the primary focus of this dissertation. Despite the increased prevalence and research regarding TBI, there are limited therapeutic interventions that have shown to improve the long-term complications and neurodegenerations of TBIs as well as olfactory dysfunction (Bramlett et al., 2015).

1.1.4 Pathophysiology of TBI

The pathophysiology of TBI can be divided into two categories: primary injury and secondary injury **(Figure 1.1.4.1).** Primary injury results from the mechanical injury at the time of the trauma. It causes displacement of the brain due to direct impact, acceleration, or penetration at the time of the MVA, fall, or gunshot wound (Stern et al., 2010). Primary injury can cause two types of injury, focal and diffuse or diffuse axonal injury (DAI). The coexistence of both types of primary injuries is common, however, DAI accounts for 70% of TBI cases (Ng & Lee, 2019). Focal injuries are confined to a specific area of the brain and result from a blow to the head resulting in compression of the tissue underneath the site of impact. They result in hematomas (subarachnoid, subdural, and epidural), intracerebral hemorrhages, and cerebral contusions. CHI and penetrating injuries, including skull fractures, contusions, and lacerations, can result in focal primary injuries. Depending on the severity of the injury, it can lead to cognitive deficits, behavioral changes, and hemiparesis (Ng & Lee, 2019). DAI is more commonly seen in injuries involving rapid acceleration, deceleration, and rotational forces as seen in high speed MVA which cause shearing and stretching injury. The strong tensile forces damage cerebral tissue and blood vasculature. The hallmark of DAI is damage to the axons and the degree of axonal injury and neuronal degeneration determines the severity of TBI (Ng & Lee, 2019). DAI also entails widely distributed damage to tissue vasculature, edema, and hypoxic-ischemic injury (Andriessen et al., 2010). Additionally, DAI can lead to deficits in arousal, attention, cognition, and processing speed (Stern et al., 2010). Because primary injury involves mechanical physical damage and acute necrotic cell death, the pathophysiology of primary injury is unlikely to be reversible.

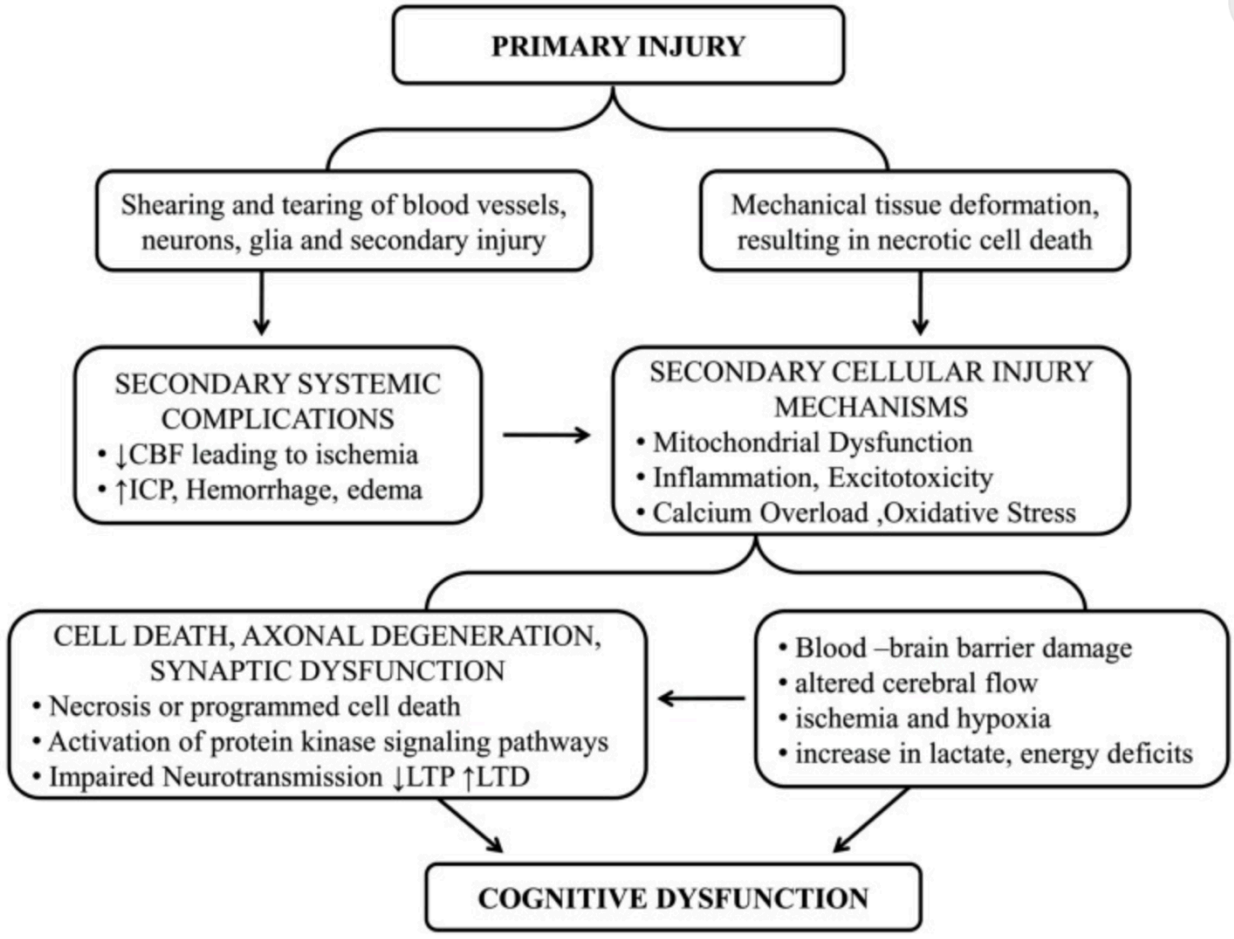

Figure 1.1.4.1 Primary Injury Pathophysiology The diagram illustrates how initial primary injury results in the mechanical deformation of brain tissue and progressing to secondary injury. Image adapted from Kaur & Sharma (2018).

Secondary brain injuries refer to physiological changes that evolve over a period of time (hours to days) in response to the primary injury and can last for years. It involves a cascade of cellular and molecular processes, such as axonal degeneration, excitotoxity, neuroinflammation, apoptotic cell death, ischemic and hypoxic damage, raised intracranial pressure, hydrocephalous, infection, and the release of reactive oxygen species that further result in deformation and

damage to surrounding brain tissue (Graham, 2002). Unlike primary injuries, secondary injuries can be reversible with therapeutic strategies. It is the secondary injury that significantly contributes to the pathophysiology, prognosis, and fatality of TBI and is the focus of TBI research and therapeutic strategies (Ray et al., 2002).

During the initial 24 hours following TBI, immediate mechanical damage leads to Wallerian degeneration of axonal cytoskeleton characterized by degradation of myelin sheath and the impairment of axonal transport (Tang-Schomer et al., 2010). The disruption of the BBB allows infiltration of circulating neutrophils, monocytes, and lymphocytes into the injured brain parenchyma to promote neuroinflammation and edema. The leukocytes release complement factors and pro-inflammatory cytokines such as IL-1β, IL-6 and TNF-α (Lotocki et al., 2009). The upregulation of IL-1β and IL-6 allow further recruitment of leukocytes at the site of injury, while the TNF-α interacts closely with Fas ligand to activate caspases that are essential for programmed cell death ((Morganti-Kossmann et al., 2002). Prolonged and delayed neuroinflammation recruits more macrophages and microglia to promote astrogliosis, as evident in post-TBI survivors that have an accumulation of macrophages and activated microglia (Gentleman et al., 2004; Johnson et al., 2013).

Immediately following a TBI, the breakdown of the BBB and neuroinflammation cause extracellular glutamate and aspartate levels to increase significantly leading to excitotoxicity and the activation of NMDA receptors. Subsequently, there is a rise of Ca^{2+} levels and an influx of positive charges within the cell. Ca^{2+} activates a cascade of secondary messengers that activates programmed cell death and the release of ROS (Baracaldo-Santamaría et al., 2022). The excessive release of excitatory amino acids such as glutamate and aspartate in the extracellular space exacerbates neuronal cell death following TBI.

Another hallmark of pathophysiological neuronal cell death post-TBI is mitochondrial dysfunction. The rise in Ca^{2+} levels in the mitochondria disrupts the electron transport chain, inhibits ATP synthesis, and impairs oxidative phosphorylation preventing essential metabolic reactions for cell survival (Lifshitz et al., 2004; Singh et al., 2006). Mitochondrial dysfunction further allows for the release of ROS and apoptosis of neurons. Endogenous ROS and free radicals are continuously generated following a TBI, and are enhanced via neuroinflammation, release of cytokines, leukocytes, inflammation, mitochondrial dysregulation, and excitotoxicity (Xiong et al., 1997; Shohami and Kohen, 2011). Apoptotic cell death of neurons are hallmarks of secondary injury and is evident in the hippocampus for up to 1-year post-TBI.

Despite advancements in the pathophysiology research of TBI, further investigation in the underlying mechanisms of TBI and its treatment are needed. As stated, while the initial primary injury involves irreversible necrotic cell death, secondary injuries progress over a longer period of time, providing a window for therapeutic interventions. Therefore, much of the research on TBI focuses on exploring strategies to address secondary injury and slow the progression of neuronal cell death, including the use of neurotrophic factors, stem cell therapies, and drug delivery methods (Ng & Lee, 2019).

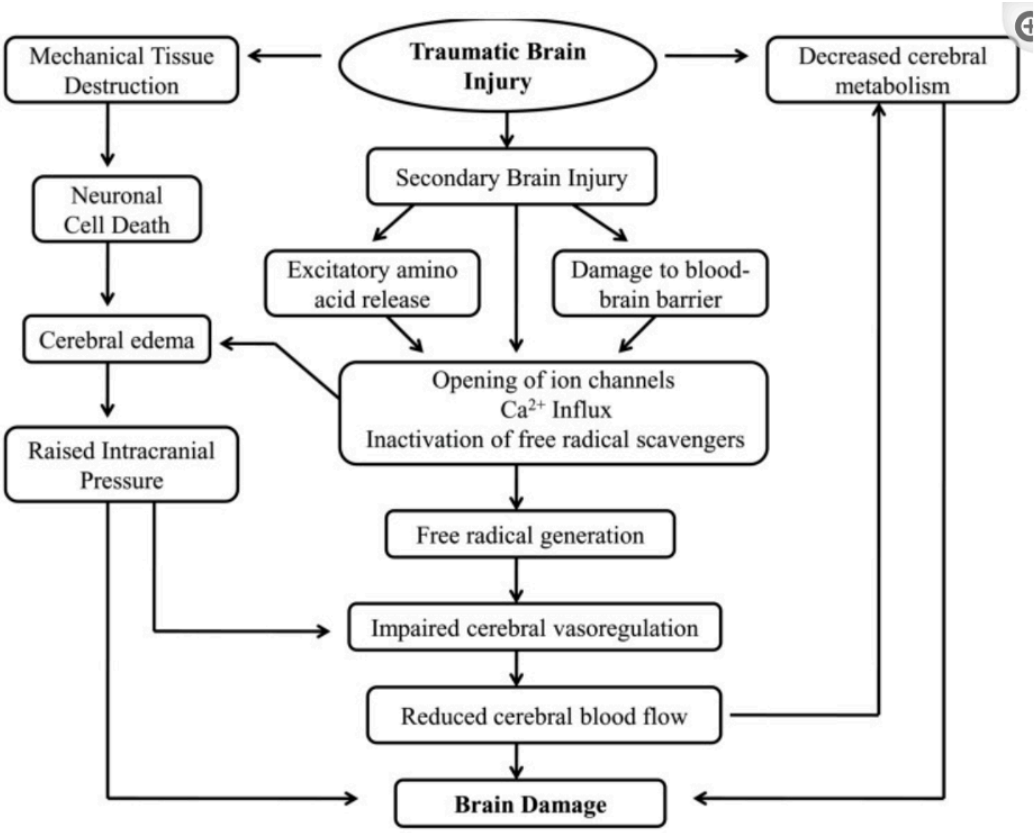

Figure 1.1.4.2 Secondary Injury Post-TBI Pathophysiology The diagram illustrates the pathophysiology of secondary injury post-TBI. Damage to the BBB leads to excitatory glutamate release, Ca influx, generation of ROS, increased ICP, neuronal cell death, and cerebral brain damage. Image adapted from Kaure & Sharma, 2018.

1.1.5 Experimental TBI Models

Mice are commonly used in TBI research because they share structural and genetic similarities with humans, and also offer advantages such as being cost-effective, small in size, and enabling standardized outcome measurements (Xiong et al., 2013). The three widely adapted experimental models that reproduce aspects of TBI observed in humans are: fluid percussion, cortical impact, and weight drop/impact acceleration. There are two types of Fluid Percussion Injury (FPI) models: midline FPI which reproduces diffuse injury, and lateral fluid percussion injury (LFPI) which reproduces mixed focal (ipsilateral hemisphere) and diffuse injury

(contralateral hemisphere). Among the TBI models, the LFPI model is the most well established and commonly used model due to its clinical relevance, reproducibility of mild, moderate, or severe injuries, and standardized parameters (Alder et al., 2011). The LFPI is preferred over the midline FPI because the midline FPI is limited to solely moderate and severe TBI, as well as substantial mortality rate due to severe injuries and neurological deficits (Kabadi et al., 2010). The LFPI is explained in further detail in **Section 2.3**.

1.2 Olfactory Bulb

The two major loci of neurogenesis in the adult mammalian brain are the subventricular zone (SVZ) of the lateral ventricles and the dentate gyrus (DG) of the hippocampus. The SVZ and the DG continuously produce endogenous neural stem cells (NSCs) that mature and become functional neurons integrated in neuronal networks involving odor discrimination and cognition (Landgren & Curtis, 2010). Although there is no effective treatment to improve the neural regulatory mechanisms and functional recovery of patients who suffer from TBIs, harnessing the endogenous population of neural stem and progenitor cells (NS/NPCs) from the SVZ and DG has potential to improve endogenous regeneration of the injured brain (Sun & Rolfe, 2015). Studies from our laboratory have indicated that TBI significantly increases cell proliferation in both the SVZ and DG (Dong & Rolfe, 2015). However, compared to DG, the influence of TBI on SVZ-olfactory neurogenesis is less studied (Sun & Rolfe, 2015).

1.2.1 Olfactory Dysfunction

Although often initially undetected and less conspicuous than other cognitive and behavioral impairments, olfactory dysfunction is a fairly common sequela of a TBI and can have significant detrimental impacts on an individual's quality of life. Therefore, physicians evaluating head injured patients with olfactory dysfunction should understand the

pathophysiology, diagnostic workup, and treatment of these disorders. Upper Respiratory Infection (URI) and head trauma are the two most common causes of OD, with head trauma accounting for about 5-17% of cases of olfactory impairment (Howell et al., 2018). OD can result from any type of head injury, however, not every head injury will result in OD. Olfactory impairment from head injury is estimated to occur in 23.6% of motor vehicle accidents (MVA) and 26.6% of domestic falls (Costanzo et al., 1986).

The presence and degree of olfactory impairment varies depending on the severity of head trauma, type of injury obtained, duration of posttraumatic amnesia, and age. As stated in **Section 1.2.1**, the likelihood of olfactory impairment significantly increases with older age. Gudizo et al. investigated the relationship between the prevalence of olfactory dysfuntion in traumatic brain injury patients by duration of unconsciousness categorized as grades I to III (Gudizo et al., 2014). They found that 18% of grade I TBI patients exhibited olfactory deficits, whereas 57% of patients with grade II or III TBI experienced olfactory impairments (Gudizo et al., 2014). The correlation between TBI severity, as indicated by the Glasgow Coma Scale (GCS), and the degree of olfactory impairment is well established. Based on GCS assessments, 13% of patients with mild TBI demonstrated complete anosmia, while 27% experienced challenges in odor identification. Moreover, "11% of patients with moderate head injury (GCS 9–12) and 25% of patients with severe head injury (GCS 3–8) exhibited complete anosmia" (Heywood et al., 1990; Costanzo et al., 2013).

1.2.2 Pathophysiology of Olfactory Dysfunction

The pathophysiology of olfactory dysfunction can be classified as conductive (physical blockage of airflow to olfactory mucosa) or neurosensory (disruption of the olfactory neural

signaling pathway), with the latter resulting in little to no recovery of olfaction. Neurosensory olfactory dysfunction (sensorineural) results from "URI, traumatic head injury, neurodegenerative disorders, congenital (Kallman's syndrome), and toxins" and are often irreversible with a poor prognosis (Cho, 2014). Conductive olfactory deficits including nasal bone fractures, septal deviation, or mucosal hematoma, as well as diseases of the nasal and paranasal sinuses (nasal stenosis, allergic rhinitis, chronic rhinosinusitis with polyposis, and tumors), show good prognosis and can be treated with surgery (Cho, 2014). Due to the delay in treatment and neglect of olfactory deficits compared to other deficits, the prognosis of post olfactory dysfunction is poor, with approximately only one-third improving overall (Howell et al., 2018).

A functional olfactory system requires a non-obstructed nasal airway and intact neuronal pathway, therefore, a disruption to any portion of those pathways may lead to olfactory dysfunction (Howell et al., 2018). The three most common causes of OD are TBI (15-30%), sinonasal disease (30%), upper respiratory tract infection (URTI) (25%), and neurogenerative diseases (4.2%), all classifying as neurosensory OD (Keller & Malaspina, 2013; Chung et al., 2021).

Recent studies show that MVA account for 51.5% of head injuries with 23.6% of this documenting loss of olfactory function. Since TBI is a sensorineural loss and there are currently no effective treatments, it remains a clinical challenge and point of research. Following a traumatic head injury that results in injury to the direct region of the olfactory bulb, post-traumatic olfactory dysfunction occurs secondary to three specific mechanisms **(Figure 1.2.2):** 1) sinonasal tract disruption or obstruction, 2) direct shearing or stretching of olfactory nerve fibers at the cribriform plate, and 3) focal contusion or hemorrhage within the olfactory

bulb and cortex (Howell et al., 2018). The stretching or shearing of the of the olfactory fibers projecting from the nose across the cribriform plate to connect to the olfactory bulbs, subsequently results in neuronal death and olfactory dysfunction (Howell et al., 2018). Sinonasal tract disruption may be a result of soft tissue or bony trauma to the nasal cavity, leading to direct damage to the olfactory epithelium or the formation of mucosal edema- blocking odorants from reaching the olfactory cleft. Trauma leading to improper mucosal secretions can lead to rhinosinusitis and lead to olfactory loss. Rhinosinusitis can impair sinonasal secretions and block airflow, therefore, hindering odorant access to the olfactory receptors (Reiter et al., 2004). This mechanism of OD most often results in unilateral hyposmia, and rarely anosmia and bilateral symptoms. Midface fractures and deceleration injuries, as seen in MVA and falls, can result in shearing of the olfactory bulb fibers across the cribriform plate. This mechanism of injury results in bilateral anosmia or severe hyposmia (Zusho, 1982). Lastly, damage to central components of the olfactory pathway can result in OD. Contusions to the temporal lobe and fronto-orbital brain region can be exceptionally vulnerable during OD related trauma (Levin et al., 1982). Contusions to these areas rarely result in complete anosmia, instead they typicall lead to olfactory recognition impairments.

Recent studies indicate that 15-30% of cases of anosmia are linked to head trauma and can occur even without definite cribriform plate fractures. Depending on the nature and severity of traumatic brain injury, damage to the connections between axons and the olfactory bulb can occur, leading to decreased sensory input and a reduction in the total number of cells in the olfactory bulb. Individuals with olfactory dysfunction have been observed to exhibit reduced gray matter volume in both primary and secondary olfactory cortex regions compared to healthy controls, impacting sensory input and white matter connectivity (Erb et al., 2012; Erb et al.,

2014). Moreover, scar formation and fibrosis in the olfactory bulb have been identified in cases of OD following head trauma (Cho, 2014). Recovery of olfactory function occurs in only 10-30% of cases, while 20% of patients experience worsening symptoms. If improvement is not observed within 6 months to 1 year following TBI, recovery becomes unlikely. Despite being a relatively common consequence of TBI, olfactory impairments often remain undetected initially for days or even weeks, as neurological and orthopedic injuries typically receive priority attention. Currently, there are no effective treatments available for patients suffering from post-traumatic olfactory dysfunction.

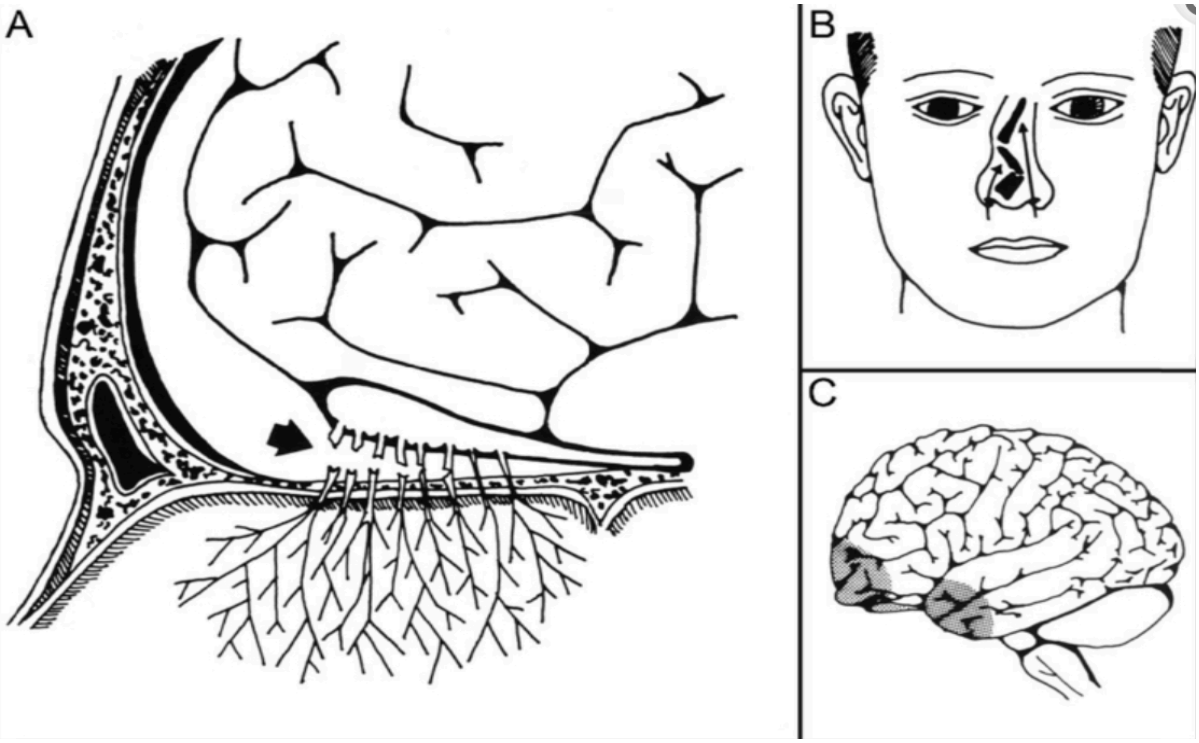

Figure 1.2.2 Post-Traumatic Olfactory Dysfunction Mechanisms A) Direct shearing of olfactory nerve fibers at the cribriform plate B) sinonasal tract disruption C) olfactory cortex focal contusion or hemorrhage. Image adapted from Costanzo and Zasler.

1.2.3 Anatomy of the Olfactory Bulb

The olfactory bulb, one of the earliest structures of the vertebrae forebrain to develop, plays a crucial role in the processing of olfactory information from the nose to the brain (Yan et al., 2022). It is one of the few places in the brain where neurogenesis continues throughout life, which plays an essential role in synaptic plasticity and structure of the olfactory bulb. In most vertebrates, such as rats, the olfactory bulb is located on the most rostral part of the brain; however, in humans, it is on the inferior side of the brain. The olfactory bulb is located on the upper part of the cribriform plate, a perforated section of the ethmoid bone that separates the frontal lobe of the cerebrum with from the olfactory epithelium of the nasal cavity containing cranial nerve I axons (Branigan, 2023). Axons from the olfactory receptor neurons of the olfactory epithelium carry sensory input to the mitral cell axons to relay information to higher processing structures of the brain. The bulb is divided into two distinct structures: the main olfactory bulb and the accessory olfactory bulb (Branigan, 2023). The main olfactory bulb directly connects the amygdala via the piriform cortex of the primary olfactory cortex and contains the main layers of the olfactory bulb; it is the main focal region of this project. The accessory bulbs reside on the dorsal-posterior region of the main olfactory bulb and constitutes a parallel pathway separate from the primary olfactory bulb, serving as the second processing stage in the accessory olfactory system (Mucignant-Caretta et al., 2012). This structure receives axonal input from the vomeronasal organ, responsible for detecting pheromones and chemical stimuli, which contains sensory epithelium distinct from the primary olfactory epithelium (Mucignant-Caretta et al., 2012).

Layers of the Olfactory Bulb

The main olfactory bulb is organized into seven layers, each with distinct functions. From superficial to deep, the layers are **(Figure 1.2.3.1):**

1) Olfactory Nerve Layer (ONL): The ONL is the outermost layer of the olfactory bulb, where initial synaptic connections occur between the olfactory receptor neurons and the neurons in the olfactory bulb (Sharma et a., 2023). The ONL comprises of unmyelinated olfactory axons that converge at the ONL after traversing through the cribriform plate of the ethmoid bone and penetrate into the glomeruli of the Glomerular layer.

2). Glomerular Layer (GL): The GL is the second layer and contains structures called glomeruli. Glomeruli are uniquely packed neutrophil-rich spheroid structures, where terminals of the olfactory neuron synapse with dendritic tufts of mitral, tufted, and other interneurons (Sharma et al, 2023). Glomeruli are important for detecting and responding to different odorant receptors.

3). External Plexiform Layer (EPL): The EPL is the third layer where axons of olfactory nerve form synapses with apical dendrites of mitral and tufted cells. In rats and animals, the EPL contains a significant number of interneurons, several different types of tufted cells, and astrocytes (Hamilton et al., 2005). The EPL is important for processing of olfactory signals.

4). Mitral Cell Layer (MCL): The MCL is a thin layer comprised of large somas of mitral cells, the primary projection neurons in the olfactory bulb, and small somas of interneurons. The mitral cells receive and process olfactory input from the GL before transmitting it to higher brain regions (Sharma et al, 2023).

5). Internal Plexiform Layer (IPL): The IPL is a thin, cell-free thin that is involved in the processing and integration of olfactory information (Sharma et al, 2023). In this layer, inhibitory

circuit contribute in the distinguishing of distinct odors, and the transmission of olfactory signals to higher brain regions.

6). Granule Cell Layer (GCL): The GCL contains several layers of granule cell somas and larger somas of deep-short axon cells. Granule cells are axon less inhibitory interneurons that constate the majority of the olfactory bulb in vertebrates and receive the majority of the cortical feedback in the olfactory bulb (Egger et al., 2003). GCs modulate the activity between principal excitatory neurons, mitral, and tufted cells. Additionally, they provide a spatial contrast mechanism of sharpening mitral and tufted cells odorant receptors, similar to the role of lateral inhibition of the visual system.

7). Subependymal Layer: The subependymal layer is the innermost region of the olfactory bulb, located adjacent to the lateral ventricle of the SVZ. Newly generated cells of the olfactory bulb generate from the subependymal layer, contributing to the ongoing neurogenesis observed in the olfactory bulb throughout life. Additionally, this layer contains neuronal precursors that continuously divide while undergoing migration and contains multipotent stem cells, making it an important site of plasticity and repair.

Cells of the Olfactory Bulb

Olfactory Receptor Neurons (ORNs): ORNs are bipolar transduction cells in the olfactory epithelium that transmit olfactory information to the brain. The axons of ORNs traverse through the cribriform plate of the ethmoid bone and terminate in the GL, synapsing with mitral cells in other interneurons. Each ORN axon innervates only a single glomerulus and is responsible for detecting specific odorants by converting chemical signals of the odor into electrical signals for the brain to interpret.

Mitral Cells: Mitral cells **(Figure 1.2.3.2)** are a major output channel of the olfactory bulb. Axons from ORNs synapse with the dendrites of mitral cells in the GL. The mitral cells transmit information about odorants to the olfactory cortex, where olfactory information is further processed ad integrated.

Tufted Cells: Similar to mitral cells, tufted cells **(Figure 1.2.3.2)** are also a major output channel for the olfactory bulb. They receive olfactory input in the GL where they first process odor signals in the glomerulus. Next, they further process information in the EPL and relay the information to the olfactory cortex.

Granule Cells (GCs): Granule cells **(Figure 1.2.3.2)** are the most abundant neuronal population in the olfactory bulb. They form reciprocal dendritic synapses with Mitral and Tufted cell and receive gluatermgic input. They also receive inhibitory input from short axon cells, which enables them to discriminate between chemically similar odorants (Walter and Freeman, 1983). GCs are continuously renewed throughout life and are essential for the maintenance of mitral and tufted cells. They inhibit mitral cells at their basal dendrites and are known to generate the oscillatory pattern on an EEG in response to odorant detection.

Periglomerular Cells (PGCs): Periglomerular cells **(Figure 1.2.3.2)** is an interneuron cell located around the glomeruli in the GL and projects its axons and dendrites into the glomeruli. Within the glomerulus, PGCs form reciprocal synapses with the mitral, tufted, and interneuron cells, and are essential for the maintenance and proliferation. They mediate lateral inhibition of mitral and tufted cells, which is important for odor discrimination; they act on the mitral cell apical dendrites (Walter and Freeman, 1983).

Short Axon Cells: Short axon cells, located in the plexiform and granule cell layers of the olfactory bulb, make local connections with the lateral dendrites of the mitral/tufted cells. They

are GABAergic interneurons and contribute to the shaping and modulating of neuronal activity in the olfactory bulb (Ashwell, 2012). They release inhibitory signals to mitral and tufted cells, contributing to the fine-tuning and modulation of olfactory signals, as well as regulating odor discrimination.

Sustentacular (Supporting Cells): Sustentacular support cells are non-neuronal cells that provide nourishment to the ORNS in the olfactory epithelium. They have processes that extend onto the epithelial surface and penetrate the mucus layer. Supporting cells play and important role is discerning between odorants from the air and mucus (Ashwell, 2012).

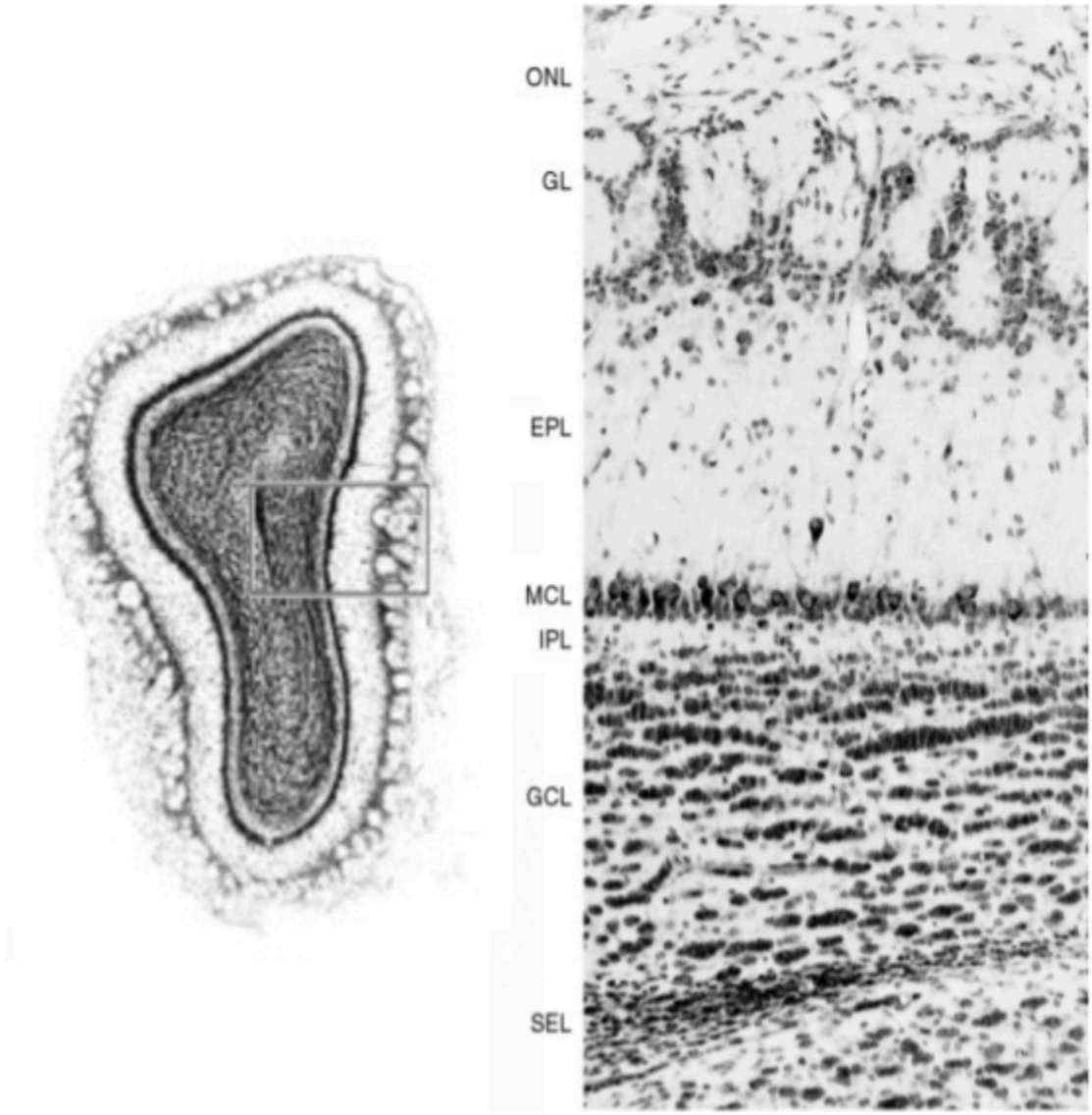

Figure 1.2.3.1 Layers of the Olfactory Bulb The image on the left is a mouse OB image taken on the confocal laser scanning microscope. From the most superficial to deep, the OB layers are: Olfactory Nerve Layer (ONL), Glomerular Layer (GL), External Plexiform Layer (EPL), Mitral Cell Layer (MCL), Internal Plexiform Layer (IPL), Granule Cell Layer (GCL), and Subependymal Layer (SEL). Image taken from Kasoka, 2009.

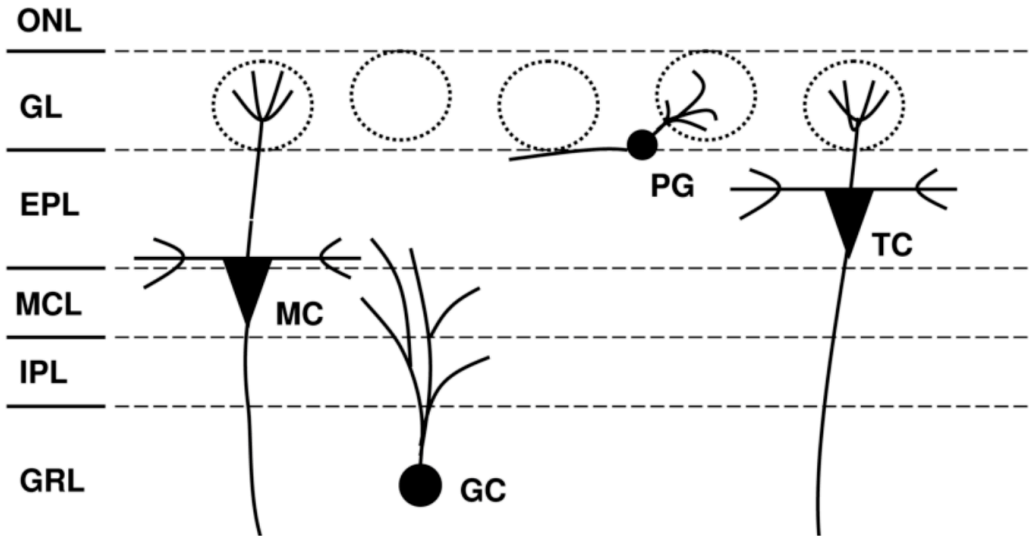

Figure 1.2.3.2 Cells in the OB The image illustrates the most common cell types found in the main layers of the OB. Granule cells (GC), Mitral Cells (MC), Tufted Cells (TC), and Periglomerular Cells (PGCs). Image taken from Sandström, 2010.

1.2.4 Adult Neurogenesis and Plasticity in the Olfactory Bulb

Research indicates that neurogenesis continues throughout the lifespan in mammalian brains, occurring primarily in two regions: the dentate gyrus of the hippocampus and the subventricular zone (SVZ) of the lateral ventricles (Zhao et al., 2008; Ming and Song, 2011). Around 2-3 weeks after their formation, approximately 50-60% of neural stem cells (NSCs) undergo apoptosis, while the surviving NSCs begin expressing the mature neuronal marker Neun. These NSCs then undergo further division and develop into fully mature and functional neurons by approximately 8 weeks.

Neural stem cells in the SVZ give rise to adult olfactory bulb interneurons, which continuously integrate into the neural circuitry of the olfactory bulb (Pass et al., 2020). Although

mechanisms of neurogenesis and plasticity have been largely investigated in rodents, the exact mechanism remains unclear in humans and further research is needed.

In rodents, there are two pathways for cell generation in OB. The first is continuous renewal of ORNs in the olfactory neuroepithelium and the synaptogenesis between the axons of ORNs and mitral cells in the GL. The olfactory epithelium comprises of proliferating progenitor cells that continuously produce ORNs throughout life that form new synapses with the dendrites of mitral and tufted cells at the GL (Huart et al., 2013). The regeneration of ORNs is essential since the olfactory epithelium is in direct contact with the environment, making it susceptible to potential environmental damage such as toxins and trauma (Huart et al., 2013). The second pathway, endogenous neurogenesis, and the focus of this research project, is the continuous neurogenesis of neuroblasts from the SVZ of the lateral ventricle which differentiate into mature neurons in the OB.

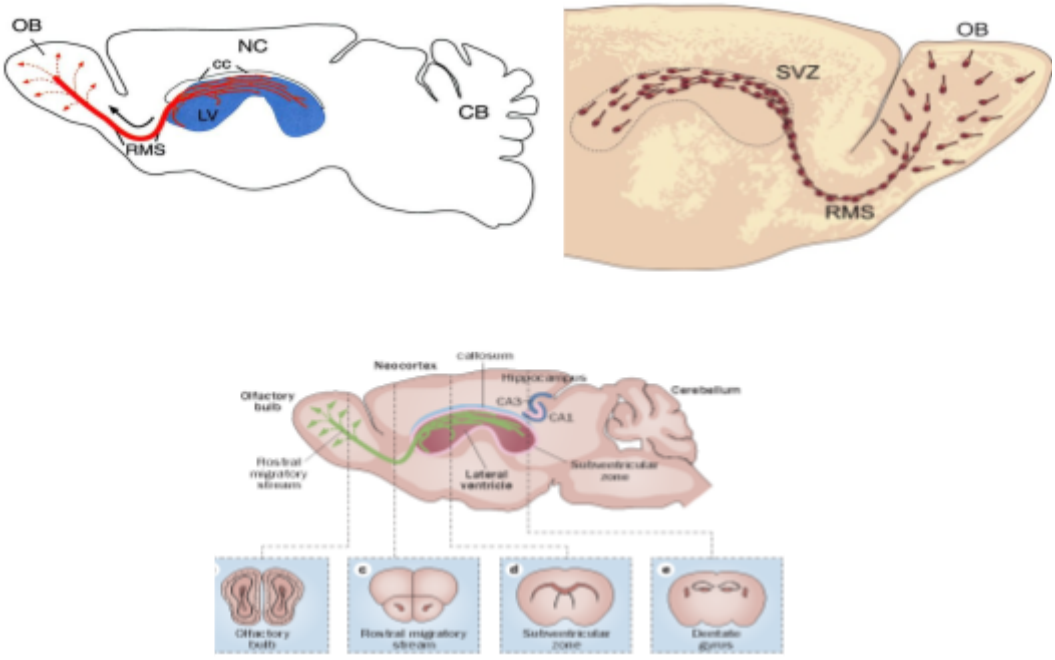

Figure 1.2.4 Neurogenesis Pathway in the Olfactory Bulb Top images illustrates the pathway of the newly generated NSCs that originate in the SVZ (blue) and migrate along the rostral migratory stream (red) to become olfactory bulb neurons. Bottom image illustrates the different structures of the OB relative to the hippocampus.

The SVZ of the lateral ventricles contains the most extensive populations of NSCs. The adult neural stem cells (aNSCs) persist in a quiescent state to prevent their exhaustion, consistently producing neurons throughout an individual's lifespan (Huart et al., 2013). Upon activation, aNSCs generate neural precursor cells (NPCs), which then undergo differentiation into neuroblasts. Neuroblasts migrate to the OB via the rostral migratory stream (RMS) within 5-9 days **(Figure 1.2.4)**. Within the OB, neuroblasts migrate to the superficial layers of the OB, where they differentiate into interneurons of the OB. The majority of newly generated cells become granule cells (~94%) in the granular cell layer (GCL) and periglomerular cells (4%) in the GL (Huart et al., 2013). The continuous generation of interneurons in the OB via subventricular zone (SVZ) is pivotal for olfactory function, odor discrimination, and social interactions. These interneurons form synapses with OB projection neurons, which, in turn, receive signals from olfactory sensory neurons in the olfactory epithelium. Any changes in SVZ neurogenesis can potentially impact the overall function of the OB (Marin et al, 2020; Azargoonjahromi, 2023).

For humans, the process of neurogenesis from the SVZ as observed in rodents would require two perquisites: 1) existence of an RMS, 2) migrating neuroblasts. Although controversial, Curtis et al. have proposed a ventral extension of the lateral ventricle, indicating the possible existence of an RMS in humans. In the fetal brain, an RMS system from the lateral ventricle to the OB have been implicated and a substantial number of proliferating cells are evident in the SVZ. However, this population significantly diminishes by the age of 2.

1.2.5 TBI Induced Neurogenesis in the Olfactory Bulb

Olfactory dysfunction is observed in approximately 20-68% of individuals with TBI, which not only adversely affects their quality of life but also impacts cognitive and neurological functions. Following a TBI, endogenous neurogenesis is upregulated in the SVZ as observed in many rodent SVZ in various experimental models of LFPI cortical impact, and stroke, suggesting a therapeutic management of TBI using endogenous NSCs and NPs (O'Donnel1 et al., 2021). Despite the high frequency and severity of olfactory dysfunction post TBI, there is limited research on the pathophysiological mechanisms underlying endogenous recovery of olfactory function.

Following fluid percussive injury, recent studies have indicated increases in cell proliferation, neurogenesis, and size of the SVZ. In a study conducted by Marin et al., an increase in the number of olfactory bulb interneurons and an increase in SVZ neurogenesis was observed indicating a role of OB glomerular dopaminergic interneurons in the recovery of olfactory function (2020). Furthermore, the increase in OB dopaminergic interneurons may be attributed to an upregulation of SIRT-1 and SIRT-4 proteins, which are associated with synaptic plasticity and olfactory abilities (Marin et al., 2020)

While existing data has shown human SVZ proliferation within the first 2 years after birth, research on human SVZ proliferation following traumatic brain injury remains limited. Further comprehensive research is needed to enhance our understanding of the proliferative potential of the human SVZ and to explore ways to leverage endogenous stem cell proliferation (Marin et al., 2020).

1.3 Notch1 Signaling

Notch signaling is a highly conserved evolutionary pathway that plays a pivotal role in many cellular and developmental processes. Although initially discovered as a neurogenic gene in Drosophila, research has shown that Notch is essential for embryonic and postnatal development in mammals (Borggrefe and Liefke, 2012). Research in our laboratory and others have illustrated the significant role of Notch signaling in neurogenesis, cell proliferation, cell differentiation, cell survival, synaptic plasticity, and apoptosis (Kopan, 2012; Borggrefe and Liefke, 2012). In our lab's preliminary studies, it was discovered that the expression levels of Notch proteins in neurogenic regions was elevated which was correlated to an increase in NSC proliferation and neurogenesis (Weston and Sun, 2018). Additionally, it exerts regulatory control over stem cell differentiation in the hematopoietic system, gut, skin, and nervous system (Mitzutani et al., 2007). The Notch pathway has been associated with functions in learning and memory, social behavior, addiction, and has played a modulatory role in various neurodegenerative disorders, including Alzheimer's.

At the molecular level, Notch signaling occurs directly between the Notch transmembrane receptors and its ligand on neighboring cells **(Figure 1.3**). Upon Jagged or Delta-Serrate ligand binding, proteolytic cleavage of the Notch receptor by a gamma(γ)-secretase complex, releases the intracellular domain of Notch (NICD). Subsequently, NICD migrates into the nucleus and forms a ternary complex with the central DNA binding transcription factor RBP-J and Mastermind like-1 (MAML) to activate transcription (Borggrefe and Liefke, 2012). In the central nervous system, the NICD/RBP-J/MAML complex activates target genes such as Hes1 and Hes5 (Mitzutani et al., 2007). Transcriptional activity discontinues when NICD

becomes heavily phosphorylated and subsequently ubiquinated, resulting in a proteasome dependent degradation (Borggrefe and Liefke, 2012) .

In mammals, there are four different Notch receptors (Notch1-4) and five Notch ligands (Delta-like1, -3, -4 and Jagged1, -2) (Borggrefe and Liefke, 2012). Notch1 and Notch2 serve essential functions in embryonic development and lethality, while Notch4, a divergent member of the Notch family, plays a pivotal role in angiogenesis and the maintenance of vasculature (James et al., 2014; Aburjania et al., 2018). Notch3 has been implicated in oncogenesis, tumor maintenance, vascular smooth muscle, and thymocytes (Aburjania et al., 2018). Expression cells that contain Notch receptors include neural stem cells, microglia, immune cells, and epithelial cells.

Notch signaling exhibits a dual role in apoptosis depending on the cellular context, and abnormalities in Notch1 signaling have been associated with cancer development. In certain contexts, Notch signaling promotes cell survival by upregulating anti-apoptotic genes such as the Bcl-2 family and inhibitors of apoptosis proteins, which inhibit caspase activation and promote cell survival (Yu, 2022). Conversely, Notch signaling can suppress apoptosis by downregulating pro-apoptotic factors like p53.

Notch signaling is also pivotal in cancer progression, invasion, and metastasis, with Notch1 signaling dysregulation observed in various solid tumors including breast, ovarian, liver, colorectal, pancreatic, and prostate cancers (Yu, 2022). Despite its significance in tumorigenesis, the specific mechanisms underlying Notch1's role remain poorly understood.

Studies indicate that Notch1 protects against oxidative stress-induced cell death by inhibiting apoptosis signal-regulating kinase 1 (ASK1), a crucial regulator of programmed cell death pathways. Notch1 prevents H2O2-induced ASK1 activation and downstream p38 MAPK

signaling, acting as a negative regulator in ASK1 pathways (Mo et al., 2013). Enhanced Notch1 expression shields cells from apoptosis, whereas Notch1 knockdown increases apoptotic cell populations.

Notch Signaling in the Olfactory Bulb

Notch signaling is known to play a crucial role in stem cell proliferation and differentiation in various tissues; however, its involvement in the olfactory bulb has not been extensively investigated. In a study by Brai et al., mice lacking notch1 (notch1cKO) showed reduced aversion to propionic acid compared to control mice, indicating the regulatory function of Notch1 signaling in olfactory processing and behavior. Furthermore, the study revealed that olfactory stimulation activated a specific subset of mitral cells, suggesting odor-dependent and localized Notch signaling within the mitral cells of the olfactory bulb. The absence of Notch1 was associated with decreased responsiveness of mitral cells to specific odors. These findings underscore the regulatory role of Notch1 in the olfactory bulb and suggest that disruptions in Notch1 signaling could impair olfactory discrimination and odor perception.

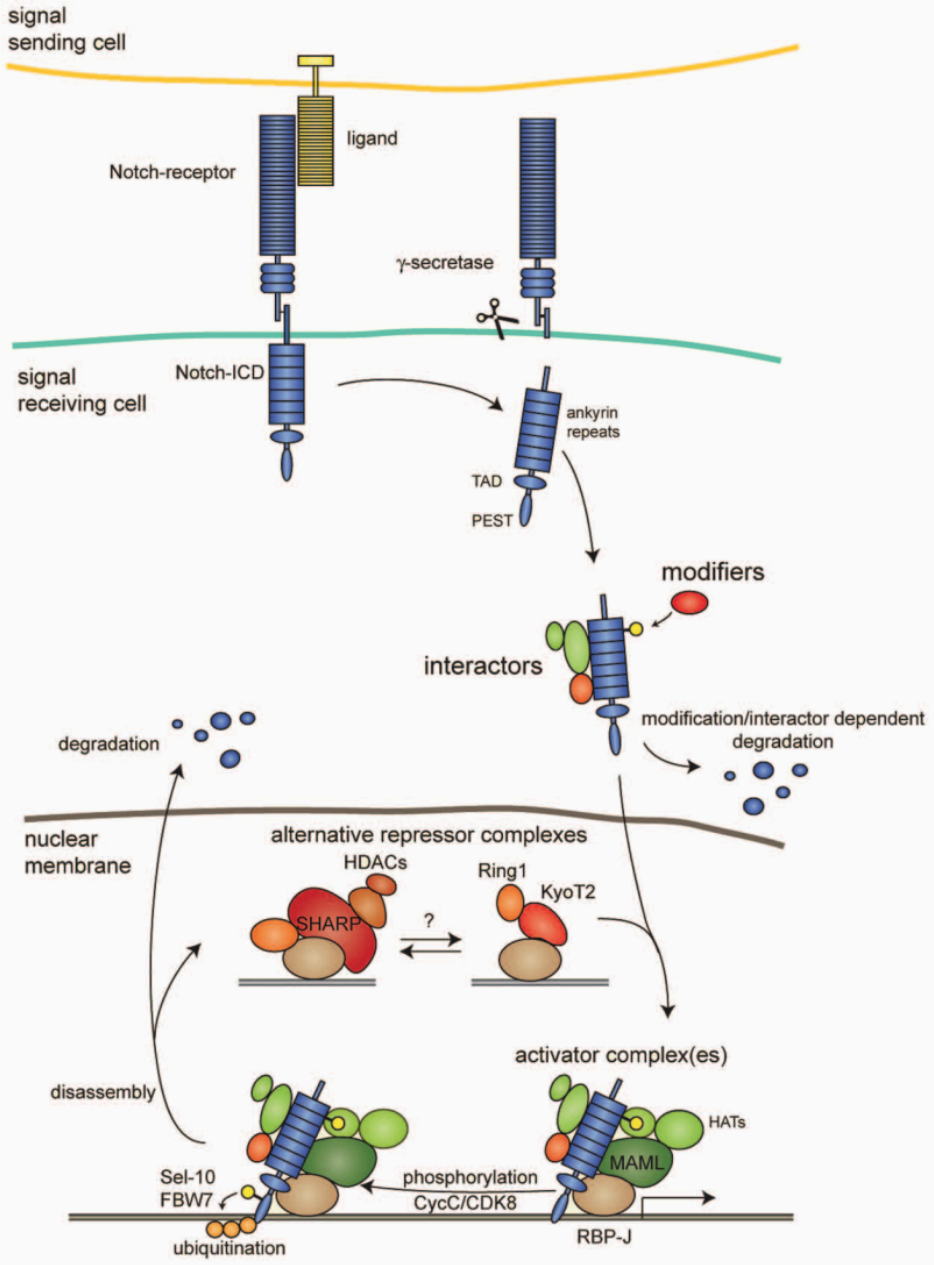

Figure 1.3 Notch Signaling Pathway Image adapted from Borggrefe and Liefke, 2012. Upon ligand binding, γ-secretase cleaves the Notch receptor, NICD, which translocates to the nucleus and forms a ternay complex with RBP-J and MAML to activate transcription.

1.4 Dissertation objectives/Hypothesis

The objective of this study is to examine how traumatic brain injury (TBI) affects neurogenesis in the olfactory bulb (OB) and to assess the role of Notch1 in controlling this response. We hypothesized that TBI disrupts the developmental process of newly generated neurons in the olfactory bulb, with Notch1 playing a significant role in regulating this process.

To test this hypothesis, we utilized transgenic NC-Y (control) and NC-NKO-Y (Notch1 conditional knockout) mice. The animals underwent either sham surgery or moderate lateral fluid percussion injury. Animals received intraperitoneal injections of bromodeoxyuridine (BrdU) daily (50 mg/kg) from 1 to 7 days post-injury (DPI) to label injury induced cells and were sacrificed at either 4 WPI or 8 WPI. Olfactory bulb sections were subjected to triple immunofluorescent staining with GFP+, BrdU+, and NeuN+, followed by imaging using a confocal laser scanning microscope. The total number of GFP+, BrdU+, GFP+/BrdU+, BrdU+/Neun+, GFP+/BrdU+/NeuN+ triple-labeled cells were quantified using the ImageJ FIJI software.

Chapter 2: Materials and Methods

2.1 Experimental Subjects

A combination of 32 adult male and female transgenic NC-Y and NC-NKO-Y mice that did not undergo behavior testing were used in this study **(Table 2.1)**. Animals received either sham surgery or a moderate LFPI and were sacrificed at 4 WPI or 8 WPI. Both 4 WPI and 8 WPI animals received i.p. BrdU injection single daily (50mg/kg) at 1-7 DPI to study the survival of BrdU-labeled new cells at these two time points.

All experimental mice were maintained in a Plexiglass cage in an animal facility with ad libitum access to food and water, 12-hour light-dark cycle, controlled temperature and humidity,

pathogen-free conditions, and weekly cage changes. All mice were bred and genotyped by Virginia Commonwealth University's Transgenic/Knockout Mouse Core. All procedures followed the ethical care guidelines of the NIH and were approved by the Virginia Commonwealth University Institutional Animal Care and Use Committee (IACUC) and the Department of Animal Research.

Group	4 WPI	8 WPI
NC-Y Sham	4	4
NC-Y LFPI	4	4
NC-NKO-Y Sham	4	4
NC-NKO-Y LFPI	4	4

Table 2.1 Total Animals Used in 4 WPI and 8 WPI IHC

2.2 Transgenic Mice Strain

In this study, Tamoxifen (TAM) inducible Cre-Lox system transgenic mouse lines were genotyped (Figure 2.2) and transferred from VCU Transgenic/Knockout Mouse Core (Weston, 2022). Once received, the mice began receiving i.p TAM injections (180mg/kg in 10% 141 EtOH/sunflower oil) for six consecutive days, and subsequently started receiving surgery two weeks post last i.p TAM injection.

The Cre-LoxP recombinase system is powerful gene editing tool that uses site-specific conditional gene inactivation for phenotypic analysis of specific cells (spatial control) and temporal control (Lepper & Fan, 2012). To achieve the TAM inducible Cre-Lox system, the Cre protein is fused with an estrogen receptor containing a mutated ligand binding domain (ER-LBD), creating a Cre-ER recombinase enzyme (Kim et al., 2018). Normally, Cre-ER is sequestered in the cytoplasm by the HSP90 shock protein, however, upon TAM injection, the

Cre-ER disassociates from the HSP90 chaperone and translocates to the nucleus to express site-specific recombination between flanking loxP sites in a time specific manner. This creates a tamoxifen-dependent Cre recombinase enzyme, Cre-ER^{T}, that is activated by tamoxifen and not estrogen (Indra et al., 1999). Additionally, TAM injections ablated the Notch1 exon and promoter, along with the stop codon for R26R-YFP resulting in the elimination of Notch1 and Nestin+ YFP expressing cells **(Figure 2.2)** (Ables et al., 2010). Two mouse lines were created for the experiment from three mouse strains **(Figure 2.2).** The control line (NC-Y) derived from nestin-CreER (Jax. Stock No: 012906) and R26R-EYFP (Jax. Stock No:006148) to produce eYFP expression in cells (Weston, 2022). The R26-stop-EYFP mutant mice have a loxP-flanked STOP sequence followed by the Enhanced Yellow Fluorescent Protein gene (EYFP) inserted and when bred with Cre recombinase, the STOP sequence is deleted and EYFP expression is observed in the cre-expressing tissues (What Does This Nomenclature Mean, 2022). eYFP expression, the enhanced version of the Yellow Fluorescent Protein was used to detect Nestin+ cells and their progeny in the SVZ (Srinivas et al., 2001). Nestin is a cytoskeletal intermediate filament that is expressed in neural progenitor cells (Bernal & Arranz, 2018). Additionally, the Notch1 conditional knockout (NC-NKO-Y) was made from Notch1flox (Jax. Stock No:007181), the nestin-CreER, and R26R-EYFP lines to produce both eYFP expression and knockout of Notch1 in Nestin+ cells (Weston, 2022).

2.3 Surgical Procedure

All animals received either a sham surgery or LFPI. LFPI is the most used injury model to analyze focal and diffuse brain injury since it closely replicates TBI in humans (Alder et al., 2011). It reproduces the cognitive, behavioral, and motor deficits seen with TBI, as well as impairments in working memory and prefrontal cortex function (Smith et al., 2015). For the

purpose of this study, the LFPI model enables evaluation of olfactory impairment seen in TBI patients (Howell et al., 2018).

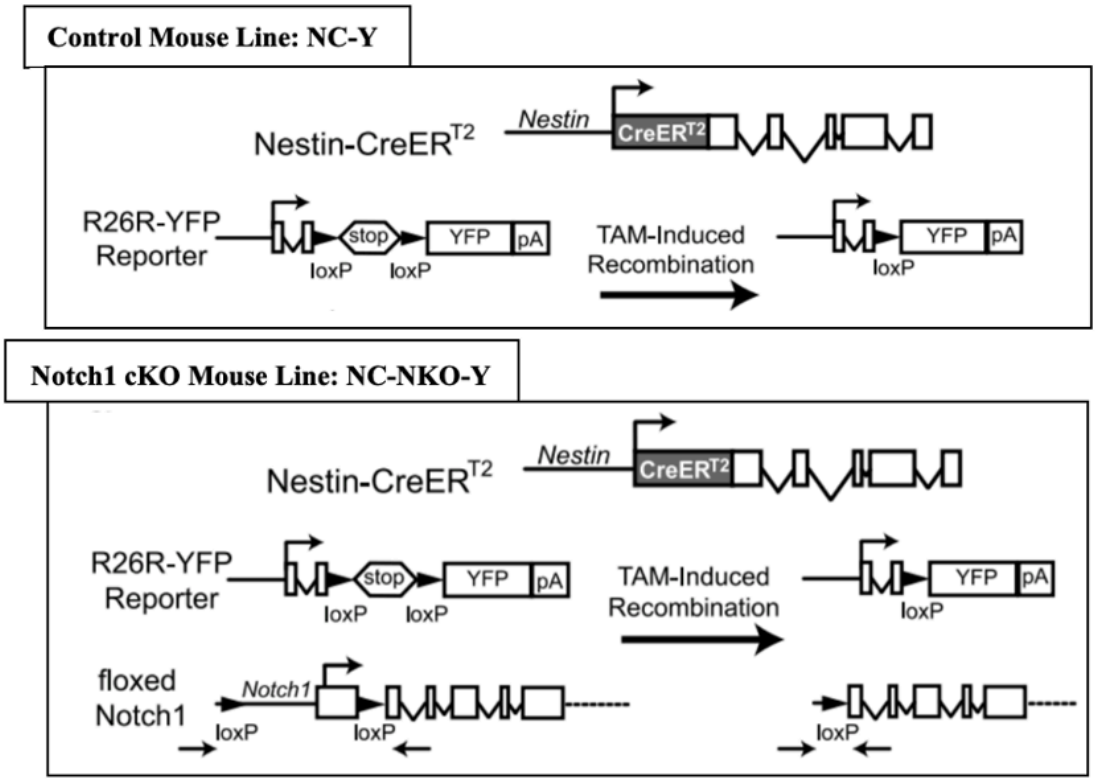

Ables et al. (2010). [Image].

Figure 2.2 Transgenic Mice Strains Diagram of the derivation of the Control and Notch1 cKO mouse lines for this experiment. Nestin-CreER^{T2} and R26R-YFP were crossed with floxed Notch1 to produce Notch1 cKO mice. TAM injections remove the promoter and first exon of Notch1 and the stop signal for R26R-YFP, leading to the elimination of Notch1 gene and Nestin+ YFP expressing cells and their progeny (Ables et al., 2010).

All materials used in the surgical procedure were sterilized and followed aseptic protocol as per IACUC and VCU DAR regulations. Initially, mice were weighed and anesthetized in an acrylic glass chamber using 4% isoflurane until unconscious and significant reduction in breathing and pulse rate (approximately 4 minutes). After the animal's head shaved, the animal

was fixed on a stereotaxic frame to stabilize their heads and ventilated continuously with 2.5% isoflurane in a 30% O2 gas mixture to keep the mice anesthetized during the procedure. To prevent hypothermia and regulate the mice's body temperature, a continuously heated Gaymar water pad was placed underneath the mice throughout the duration of the surgery. To sterilize the incision site on the mice's head and prevent their eyes from drying, Betadine and Paralube were applied respectively. In both Sham and LFPI animals, a midline incision was made using a scapula to expose the skull and a hemostat was used to retract the skin and prepare the LFPI mice for craniotomy. For the LFPI animals, a 2.7 mm trephine was used to perform a craniectomy midway between the Bregma and Lambda sutures, laterally **(Figure 2.3.1).** The trephined skull flap was carefully lifted to prevent breaching of the dura. Next, a 20-gauge circumference Luer needle hub cap was secured over the craniectomy window with cyanoacrylate glue and reinforced with dental acrylic. All mice had a minimum of one hour rest between surgery and injury (or sham procedure) where anesthesia was turned off and mice were placed on a heating pad with access to food and water. After the recovery period, mice were anesthetized with 4% isoflurane and O2 with Luer head cap already installed. In order to create an injury that mimics a moderate severity TBI, the Luer hub cap was filled with 0.9% saline and a calibrated fluid percussion device administered a pulse target of 1.83 ATM as demonstrated in **Figure 2.3.2** (Weston, 2022). Sham animals received the same sterilized procedures without the craniectomy and moderate fluid percussion injury (Weston, 2022). After injury, the righting time of when the mice returned from a supine to upright position was recorded as an acute marker of TBI severity (Grin'kina et al., 2016). Following the measurement of righting time, mice were anesthetized using 4% isoflurane, and the Luer hub cap was removed. The incision site was sutured, and the animal was placed in a recovery cage with a heating pad. Subsequently, the mice were returned

to their cages with a hydrogel supplement to aid hydration and then transferred back to the animal vivarium (Weston, 2022).

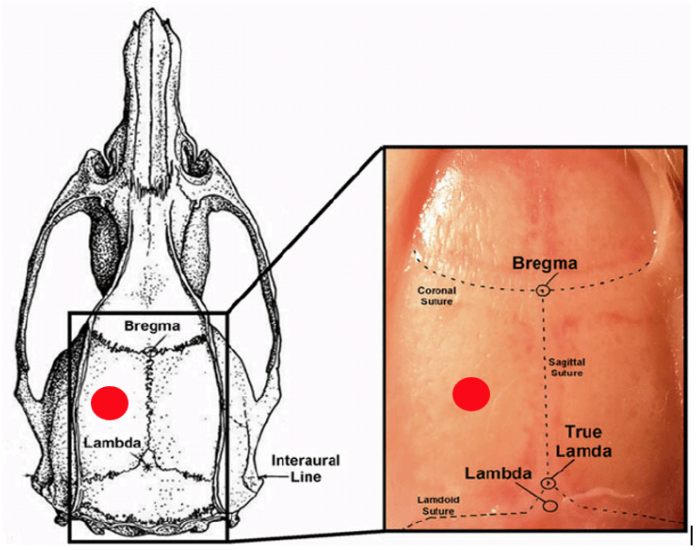

Benskey et al. (2016). [Image].

Figure 2.3.1 LFPI Model The red circles demonstrate the lateral Luer hub placement between the Bregma and Lambda sutures.

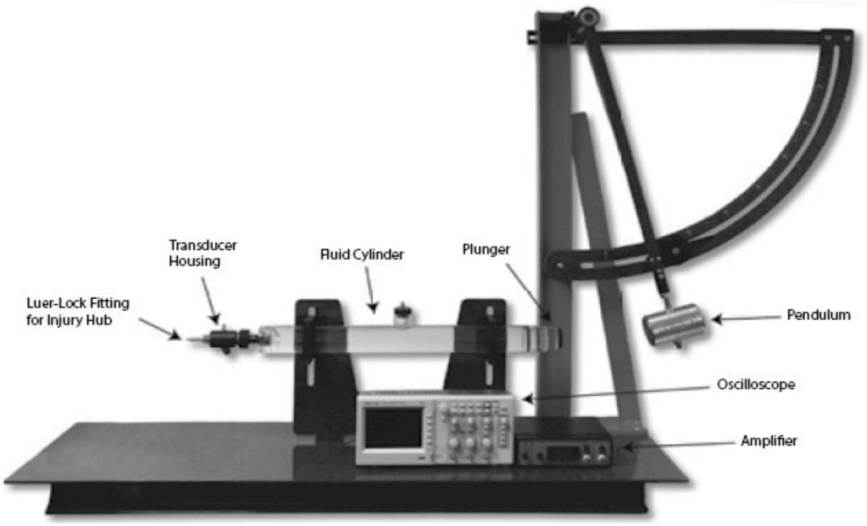

Pignatelli & Belluzzi. (2010). [Image].

Figure 2.3.2 FPI Percussion Device Fluid Percussion Injury device used to administer 1.83 ATM injury at craniectomy site

2.4. Tissue Processing

2.4.1 Transcardial Perfusion

At 4 or 8 weeks post TBI, mice were deeply anesthetized with 4% isoflurane and transcardially perfused as a means of euthanasia and maximize the health of brain slices by minimizing excitotoxicity (Carrick, 2023). During transcardial perfusion, the thoracic cavity was exposed, and a needle was inserted into the left ventricle to replace blood in the rodent brain with saline followed by 4% PFA. The PFA fixative preserves brain tissue for immunostaining by breaking down into formaldehyde, which covalently cross-links protein and DNA molecules into an insoluble mesh (Kim et al., 2017). Rodent brains and intact olfactory bulbs were dissected from the skull and fixed for 48 hours in 4% paraformaldehyde, then stored at 4°C in PBS (phosphate-buffered saline) with 0.05% sodium azide until processed for experiments.

2.4.2 Tissue Embedding in Agarose

All mice olfactory bulbs were dissected from the brain using a blade and subsequently embedded in agarose to maintain tissue integrity due to their small size and fragile nature. The olfactory bulbs were observed under a light microscope to ensure correct distinction between the left and right olfactory bulb **(Figure 2.4.2)**. In a clear beaker, powdered agarose was dissolved in PBS+0.05% sodium azide and sporadically heated in the microwave for 2 minutes or until the mixture was clear and the agarose was completely dissolved. A 1:20 ratio of agarose and PBS+0.05% sodium azide was used for

optimal results. The agarose and PBS+0.05% sodium azide mixture was poured into a weighing boat and allowed to slightly congeal prior to positioning the separated left and right olfactory bulbs posteriorly into the agar. The weighing boats containing the olfactory bulbs were covered in parafilm and kept in 4°C until further processing.

a)

Matsumoto et al. (2006). [Image].

b)

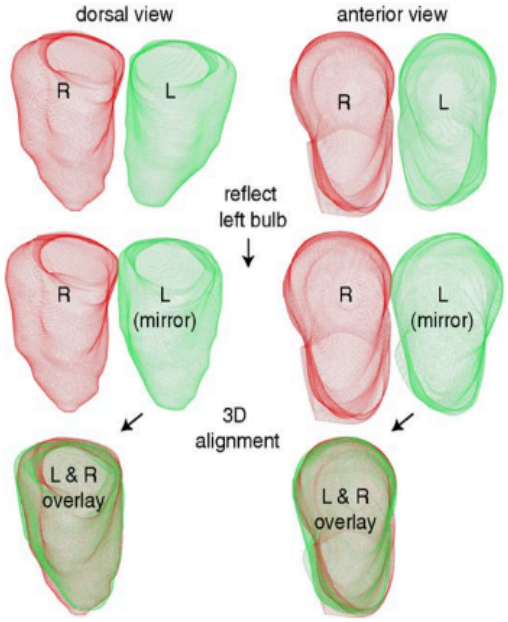

Zapiec & Mombaerts. (2015). [Image].

Figure 2.4.2 Dorsal View of Olfactory Bulb a) Rodent brains were placed dorsally to distinguish between left and right olfactory bulbs prior to slicing. **b)** illustration of the dorsal, anterior, and overlay of left and right olfactory bulbs.

2.4.3 Tissue Preparation and Collection

Left and right olfactory bulbs embedded in agarose were mounted with super glue onto the stage and sliced into 50 µm sections with a Leica VT1000 S vibrating microtome and collected sequentially in alternating rows of a different 48-well plate containing

PBS+0.05% sodium azide at 4ºC until further use **(Figure 2.4.3).** For the experiments (4 WPI and 8 WPI), sections were collected in sequence within a span of 850µm of the olfactory bulbs. Starting with the 5th well, every 4th free floating section was collected for a total of 5 sections per animal. Only left olfactory bulbs sections were analyzed in this experiment since it was ipsilateral to the LFPI.

2.5

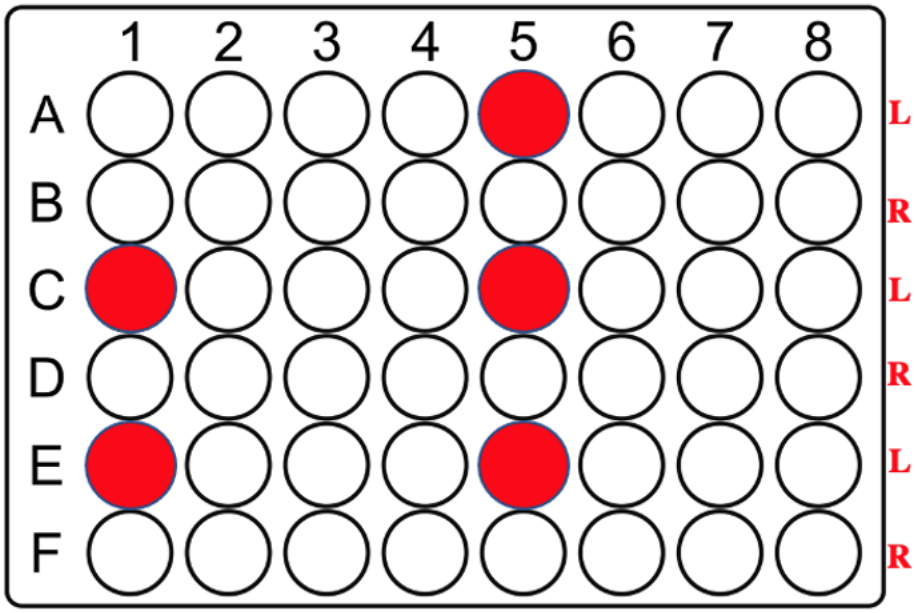

Figure 2.4.3 Tissue Collection A 48 well plate containing PBS+0.05% sodium azide was used to collect tissues. The left and right olfactory bulb tissues were collected sequentially within a span of 850µm and placed in designated alternating rows, Left (L) and Right (R). For the experiments, starting from the 5th well, every 4th free floating section was collected for a total of 5 sections per animal for the left olfactory bulb only.

Immunohistochemistry

A 5-day protocol of triple immunofluorescence staining was followed in which the primary antibodies used were anti-GFP (1:2000; Invitrogen A11122), anti-BrdU (1:1500; Abcam

AB6326), and anti-NeuN (1:100; Millipore MAB377). Secondary antibodies used were biotinylated anti-rabbit (1:400; Vector Biolabs BA-1000), AlexaFluor 568 anti-rat (1:400; Invitrogen A11077), and AlexaFluor 647 anti-mouse (1:200; Invitrogen A21235),

In brief, on day 1, sections were washed with 1xPBS, placed in a blocking solution, and incubated in the GFP and NeuN primary overnight (~16 hours) at 4ºC. On day 2, sections were washed with 1xPBS, incubated in 1% hydrogen peroxide (H_20_2), rinsed with 1xPBS, and incubated in fluorescent secondary antibody of NeuN and biotinylated GFP overnight in tin foil (~16 hours) at 4ºC. On day 3, after ABC Elite kit incubation, TSA™ Fluorescein Tyramide Reagent kit (1:50; 42 AKOYA Biosciences SAT701001EA) was applied to amplify the GFP signal. Next, the sections were denatured in 2N HCl at 37ºC for 30 minutes, and subsequently stained for BrdU primary, and fluorescent secondary on day 4. On day 5, the sections were mounted with antifade medium and stored in a slide box at -20ºC until needed for experiments.

2.6 Confocal microscopy

Slides containing GFP+/BrdU+/NeuN+ olfactory bulb sections were imaged with a ZEISS confocal laser scanning microscope (LSM 880) at the VCU Microscopy Facility. First, the 10x and 20x dry objectives were used to focus the image to obtain a clear resolution of each section prior to using the 25x oil lens. Next, a small amount of oil is placed on the 25x oil lens and using the z-control and fine adjust knob, the desired focal plane and region is chosen. The Zeiss Zen microscope software was used to capture a 1x3 tile scan made up of 3 adjacent images for each of the average 5 sections per animal slide **(Figure 3.1).** The images covered the GCL, EPL, and GL of the olfactory bulbs. The pinhole was set to 2.6μm for each image.

2.7 Quantification and Stereology

The 1x3 tiled images were put into the FIJI software and viewed in a hyperstack with split channels. The images were then oriented in the same way and the brightness/contrast were adjusted. The number of GFP+, BrdU+, GFP+/BrdU+, BrdU+/Neun+, GFP+/BrdU+/NeuN+ cells in the GCL, EPL, and GL of each section was counted using the FIJI plugin Cell Counter and data was recorded in an excel spreadsheet. The presence of BrdU+ ensures that the measured cell originated directly from the injury-induced population, GFP+ enables the visualization of cell morphology, and NeuN+ verifies that the measured cell is a mature neuron (Weston, 2023).

Stereology was used to calculate the total number of cells within the defined OB area (1x3 tile scan) using the equation: $N = \Sigma Q^{-} \cdot t/h \cdot 1/asf \cdot 1/ssf$ where Q^{-} is total particles counted, t is measured section thickness, h is counting frame height, asf is area sampling fraction, and ssf is section sampling fraction (Zhao & van Praag, 2020). For this experiment, the section thickness (t) of 29μm was acquired by averaging random parts of 5 different tissues across multiple fields of view using the MICA Microhub. The dissector height was set to the size of the pinhole which was set to 2.6μm. The average sampling fraction (asf) was set to 1 because the entire region was quantified in these samples, and the sample sampling fraction (ssf) was set to 0.25 due to 5 sections representing 1/4th of the left olfactory bulb within a span of 850μm thickness of the olfactory bulb.

2.8 Statistical Analysis

All stereologically calculated cell numbers were run through GraphPad's online Outlier Calculator, which performs Grubb's test also called the ESD method (Extreme studentized

deviation), to determine any significant outliers. Grubb's test is based on a normal distribution and the Z test statistic is calculated from the most extreme data point. None of the data in this study contained outliers. The total stereologically calculated total number of cells for GFP+, BrdU+, GFP+/BrdU+, BrdU+/Neun+, and GFP+/BrdU+/Neun+ were analyzed between each of the 3 olfactory bulb cell layers: the granule cell layer (GCL), external plexiform layer (EPL), and the glomerular layer (GL). All data was then analyzed using GraphPad Prism 9 software to determine the statistical significance of genotype and injury. An ordinary one-way analysis of variance (ANOVA) test was performed combined with Tukey HSD post hoc tests with multiple comparisons initially. Next, a Two-Way ANOVA test was conducted along with Tukey HSD post hoc tests with multiple comparisons. This analysis aimed to assess differences in the total number of cells between the 4-week and 8-week time points across the four groups, and to evaluate potential effects of injury or genotype on the survival of newly generated cells. The significance level was set to $\alpha=0.05$ for all analyses performed and all data was plotted in a column bar graph with the standard error bars expressed as mean ± SEM.

Chapter 3: Results

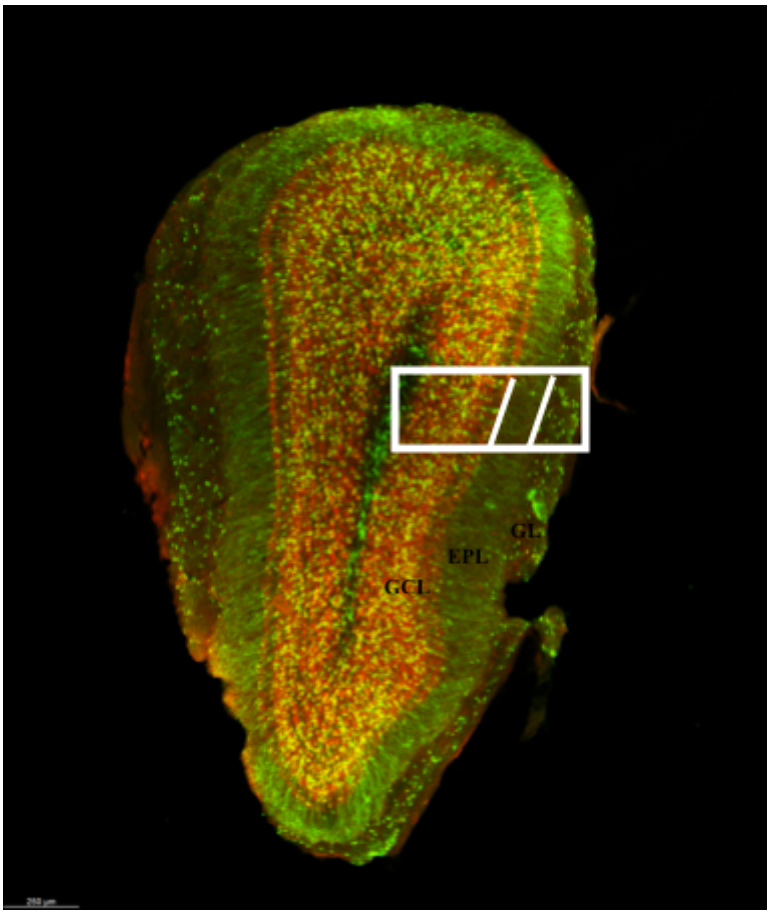

Figure 3.1 Olfactory Bulb Staining The figure illustrates the left olfactory bulb of a Control LFPI 8 WPI sample ipsilateral to injury. GFP+ staining is in green, BrdU+ staining is in red, and double labeled staining of GFP+/BrdU+ is in yellow. The layers of the OB that were quantified were the Granule Cell Layer (innermost), External Plexiform Layer (middle), and Glomerular Layer (outermost). The white box delineates the specific 1x3 tile scan region used for cell quantification

3.1 Influence of TBI and Notch1 cKO on Survival and Neuronal Differentiation of Injury-Induced Newly Generated Cells in the OB

To assess the survival of newly generated cells post-injury, cells labeled with BrdU were imaged using the LSM 880 confocal microscope and stereologically quantified. BrdU+ cells are newly generated cells occurring at 1-7 days post-injury. Our study time points are at 4 or 8 weeks post-injury that mark the survival of these newly generated cells in the OB originated from SVZ. NeuN is a marker for mature neurons, differentiating it from proliferating or glial cells. Cells labelled with GFP+ originated from the nestin+ NSCs with a fluorescent reporter and Notch1 successfully knocked out. Double labeling of BrdU/NeuN tracks the fate of newly generated cells post-TBI differentiating into adult-born mature neurons. Cells double labeled with GFP/BrdU identify NSCs which became active dividing cells at 1-7 days post-TBI. Triple labeling of GFP+/BrdU+/and NeuN+ identifies newly generated cells originating from nestin+ NSCs during the 1-7 days post-injury period, which have differentiated into mature neurons within the olfactory bulb.

Cells in the GCL, EPL, and GL of the olfactory bulb were imaged using a 25x oil lens, and quantitatively assessed through stereological analysis of cell counts across the three cell layers **(Figure 3.1).** The GCL layer is the innermost layer of the OB that primarily contains newly generated granule cells, including those labeled with GFP+, BrdU+, and NeuN+. The EPL is located between the GCL and GL and comprises of the dendrites and axons of mitral and tufted cells. It plays a crucial role in synaptic connections and processing of olfactory information. Some NeuN positive cells, primarily their dendrites, maybe present in the EPL. The GL is the outermost layer of the OB and contain glomeruli which facilitate the connection

between olfactory sensory neurons and mitral cells. All post-hoc ANOVA analysis results are listed in **Table 3.1** for 4 WPI and **Table 3.2** for 8 WPI.

At four weeks post-injury, cells labeled with NeuN and BrdU were evident. The typical pattern of BrdU+ cells in four study groups was demonstrated in **Figure 3.2**, with a greater number of **BrdU+** cells observed in the injured control and Notch1 cKO groups **(Figure 3.2 b, d).** ANOVA analysis revealed no statistical significance of **BrdU+** cells in the GCL, EPL, or GL across the different groups **(Figure 3.3).** The pattern of BrdU/NeuN labeled cells in four study groups was shown in **Figure 3.4**. Similarly, more **BrdU/NeuN** double labeled cells were observed in the injured control groups and Notch1 cKO mice **(Figure 3.4 b, d),** however, ANOVA analysis revealed no statistical significance of double labeled BrdU+/NeuN+ in the GCL, EPL, or GL across the different treatment groups (**Figure 3.5**).

At eight weeks post injury, the staining pattern of BrdU+ cells is demonstrated in **Figure 3.6**, with more **BrdU+** cells observed in the GCL of Notch1 cKO LFPI group compared to other groups **(Figure 3.6 d).** Post-hoc ANOVA analysis revealed a genotype-related difference with a statistically significant higher number of **BrdU+** cells in the GCL of the Notch1 cKO mice in both injured and sham groups as compared to the matched control groups, i.e. injured Notch1 cKO group vs. injured control group ($p=0.0142$), and Notch1 cKO sham vs control sham ($p<0.0352$) **(Figure 3.7).** No statistical significance found between groups in the EPL or GL. A similar staining pattern was found in Brdu+/NeuN+ double labeling with more **BrdU+/NeuN+** cells found in the GCL of Notch1 cKO LFP group **(Figure 3.8 d)**. Post-hoc ANOVA analysis revealed a genotype-related difference in the number of BrdU/neuN double-labeled cells in the GCL showing statistically significant higher number of **Brdu+/NeuN+** cells in injured Notch1 cKO group compared to control LFPI group ($p = 0.0064$), Notch1 cKO Sham compared to

Control Sham (p = 0.0364) **(Figure 3.9).** No statistical significance was observed in the EPL or GL.

In summary, cell quantification data of BrdU+ cells and BrdU+/NeuN+ cells suggest that at 8 weeks post-injury, there is a Notch1 cKO associated differences in survival (BrdU+ cells) and neuronal differentiation (BrdU+/NeuN+ cells) of post-injury generated OB GCL cells, with higher number of new cells survived and becoming mature GCL neurons in Notch1 cKO mice in both sham and following injury when compared to the Control Sham at the same experimental condition. This genotype related difference is not significant at 4 weeks post-injury.

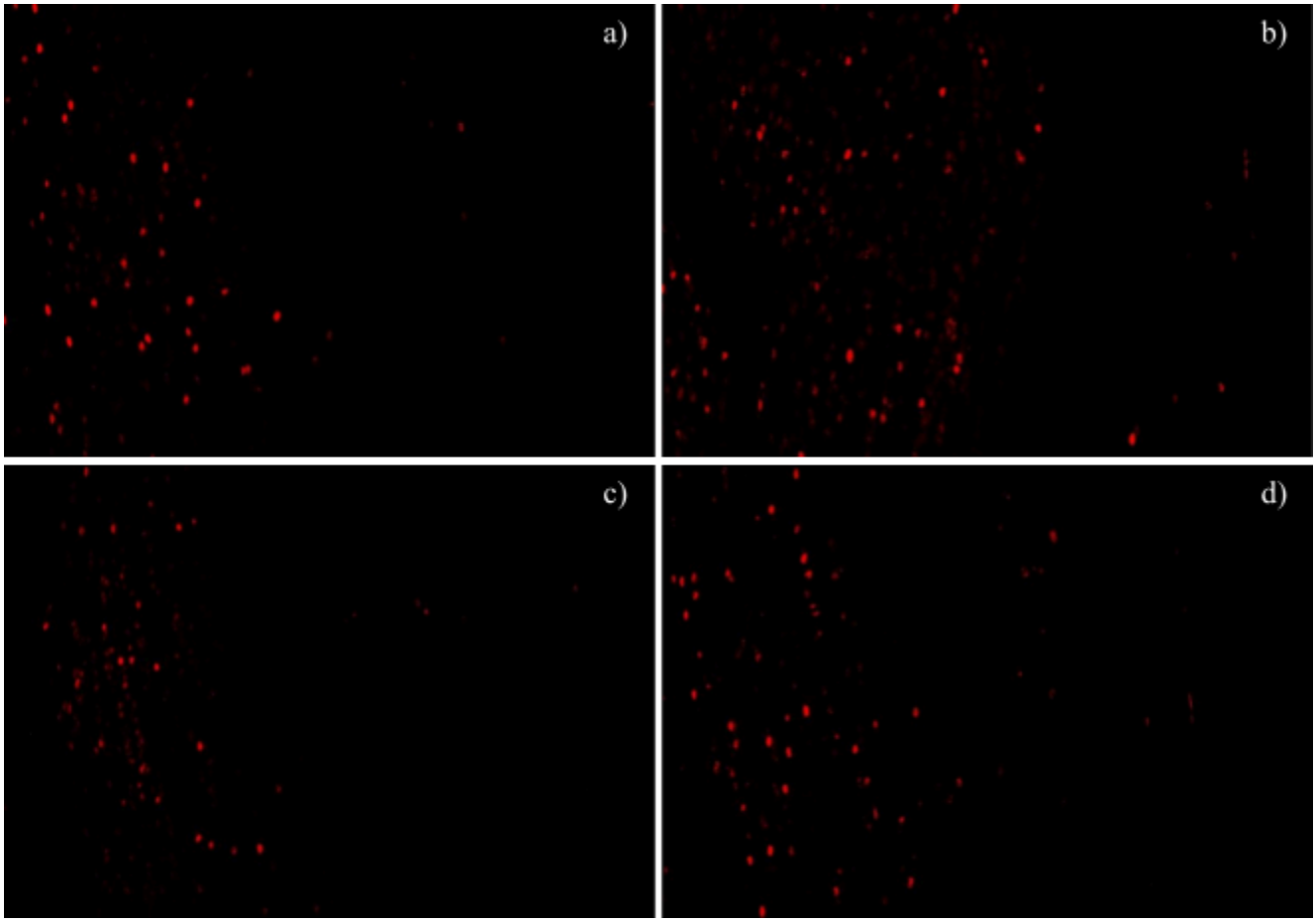

Figure 3.2 BrdU+ Staining Pattern at 4WPI. Representative image of BrdU staining at a region of coronal sections of ipsilateral olfactory bulb tissue visualized under a 25x oil lens of a confocal microscope. **a)** Control-Sham **b)** Control-LFPI **c)** Notch1 cKO Sham **d)** Notch1 cKO LFPI.

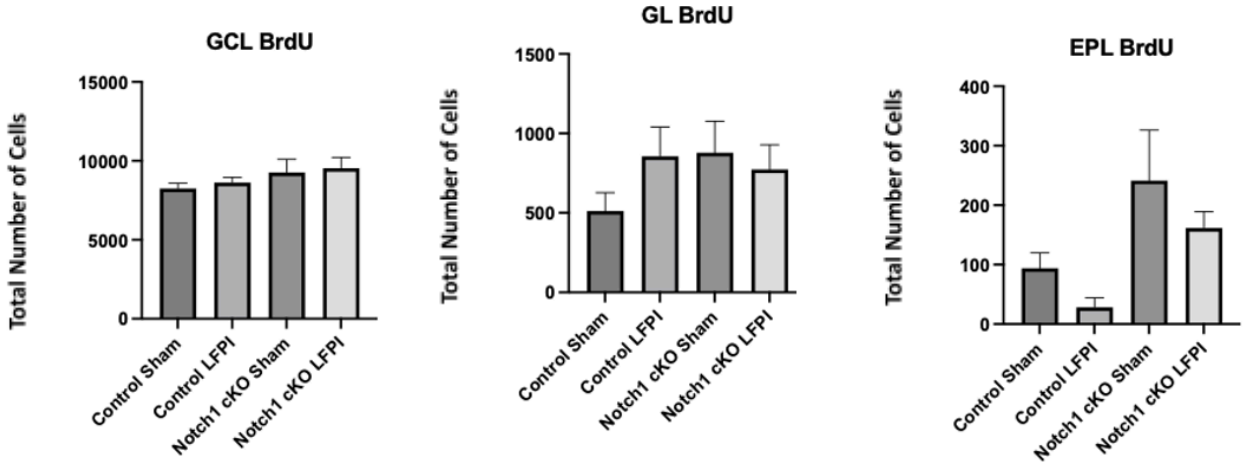

Figure 3.3 Quantification of BrdU+ Cells in the GCL, EPL, and GL of the Olfactory Bulb at 4WPI. Stereologically calculated total BrdU+ cell counts in the GCL, EPL, and GL of 4 WPI mice. No statistically significant differences were observed between groups in all three regions.

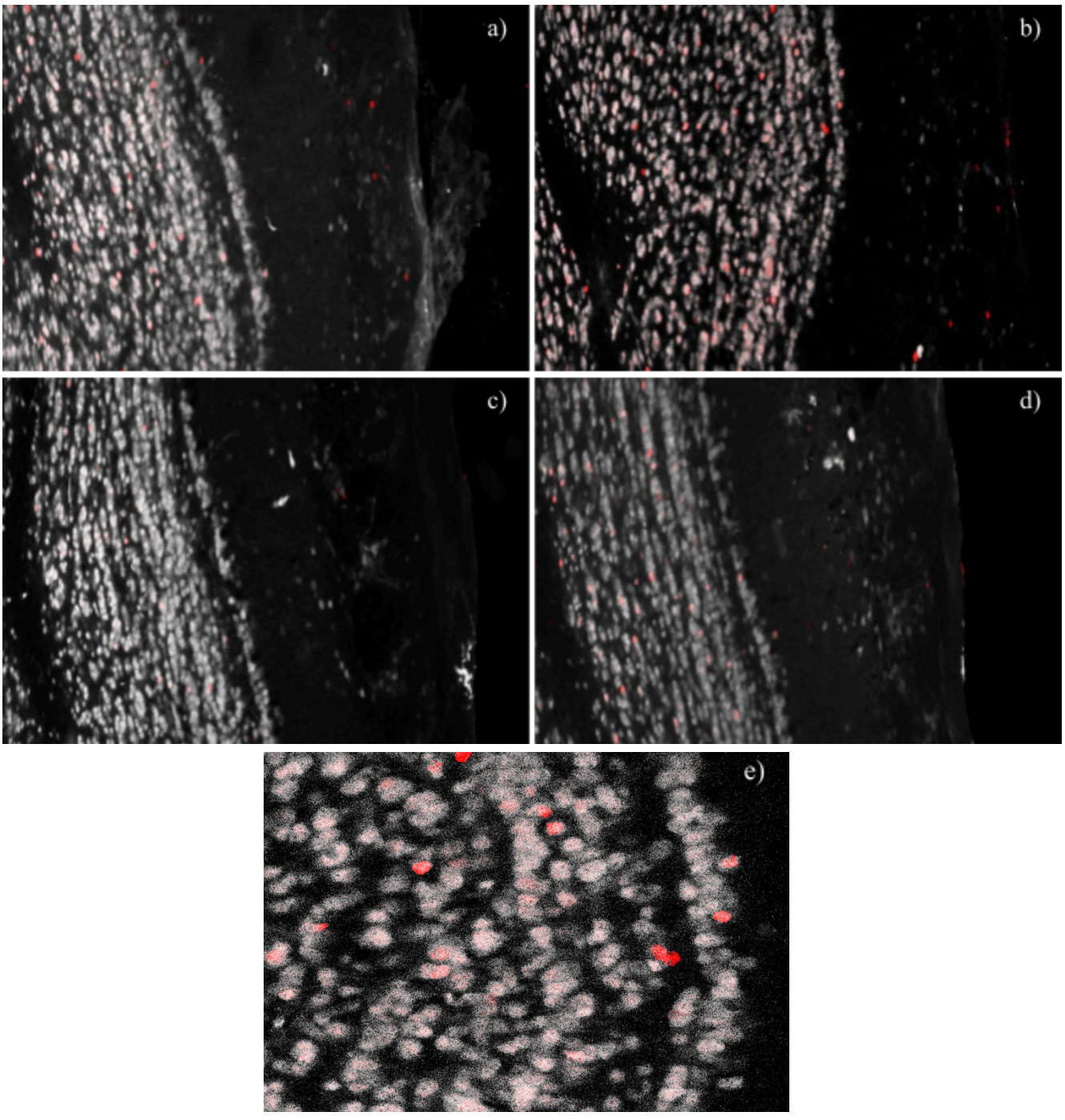
a)
b)
c)
d)
e)

Figure 3.4 BrdU+/Neun+ Staining Pattern at 4WPI. Representative image of BrdU/NeuN double-labeling at a region of coronal sections of ipsilateral olfactory bulb tissue visualized under a 25x oil lens of a confocal microscope. **a)** Control-Sham **b)** Control-LFPI **c)** Notch1 cKO Sham **d)** Notch1 cKO LFPI.

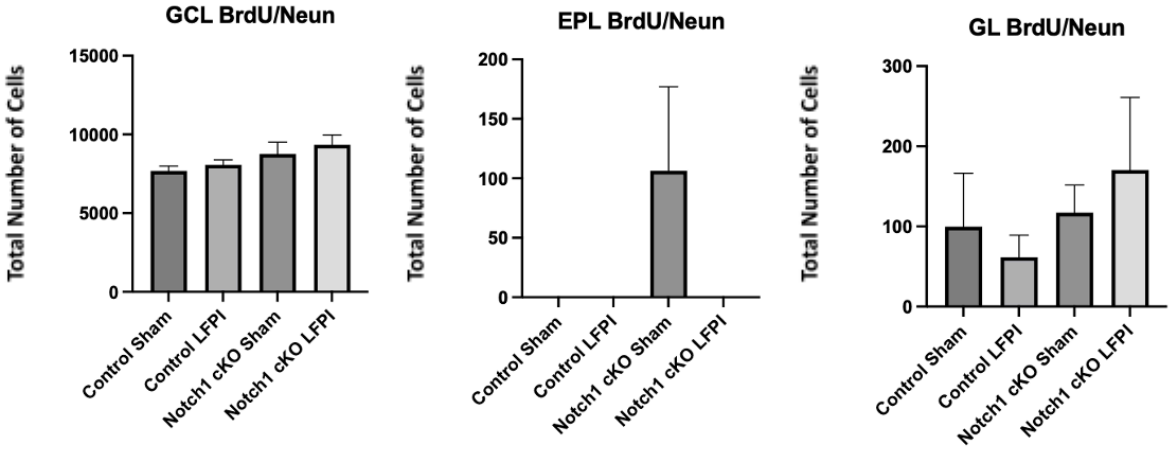

Figure 3.5 Quantification of BrdU+/NeuN+ Cells in the GCL, EPL, and GL of the Olfactory Bulb at 4 WPI. Stereologically calculated total BrdU+/NeuN+ cell counts in the GCL, EPL, and GL of 4 WPI mice. No statistically significant differences were observed between groups.

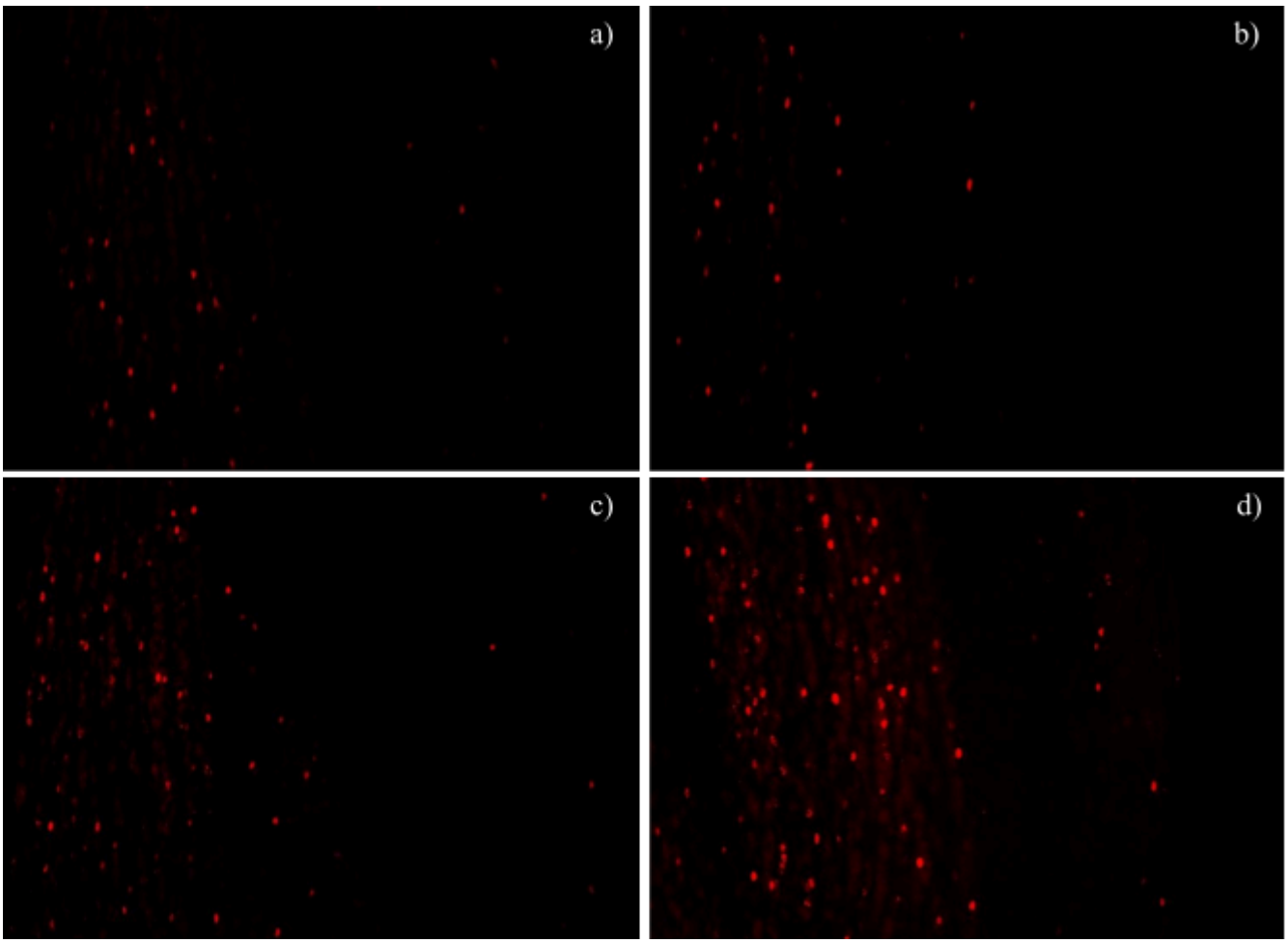

Figure 3.6 BrdU+ Staining Pattern at 8 WPI. Representative image of BrdU staining at a region of coronal sections of ipsilateral olfactory bulb tissue visualized under a 25x oil lens of a confocal microscope. **a)** Control-Sham **b)** Control-LFPI **c)** Notch1 cKO Sham **d)** Notch1 cKO LFPI.

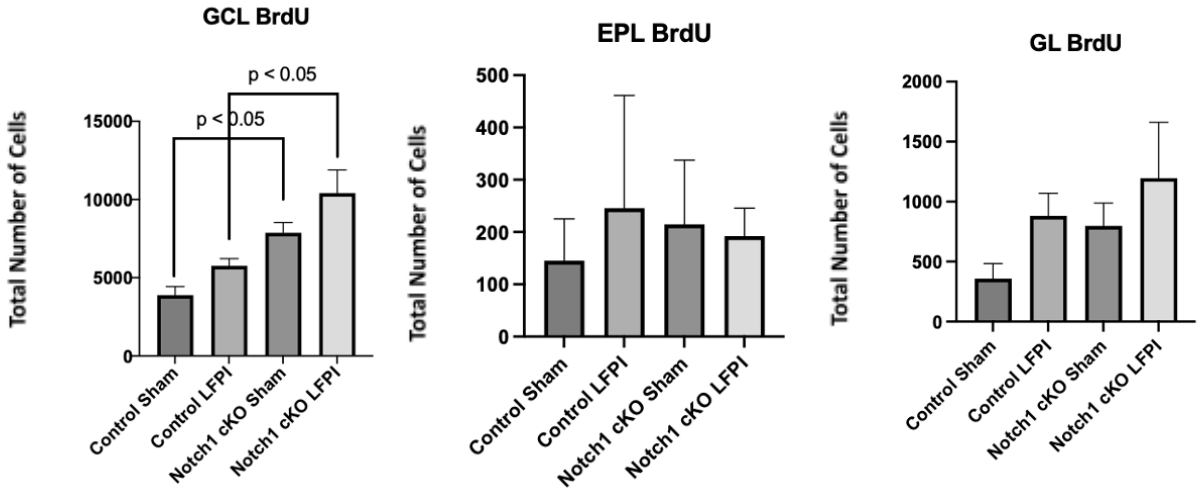

Figure 3.7 Quantification of BrdU+ in the GCL, EPL, and GL of the Olfactory Bulb at 8 WPI. Stereologically calculated total BrdU+ cell counts in the three different OB layers are plotted. In the GCL, a statistically significant higher number of BrdU+ cells were observed in Notch1 cKO LFPI as compared to Control-LFPI group ($p<0.05$). In Sham groups, a statistically significant higher number of BrdU+ cells were observed in Notch1 cKO Sham compared to Control-Sham ($p<0.05$). No statistical significance was observed in the EPL or GL between groups.

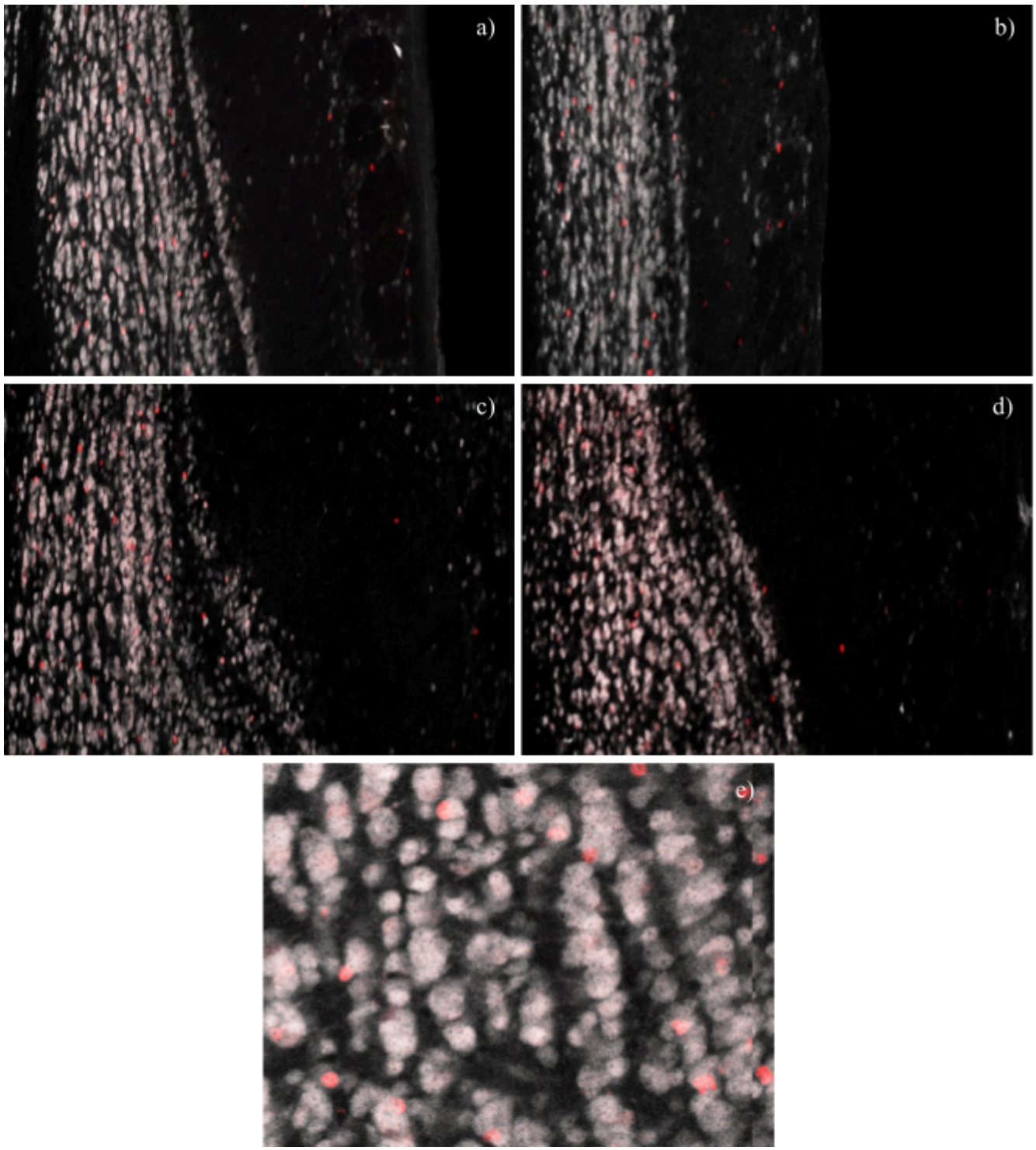
a)
b)
c)
d)
e)

Figure 3.8 BrdU+/Neun+ Staining Pattern at 8 WPI. Representative image of BrdU staining at a region of coronal sections of ipsilateral olfactory bulb tissue visualized under a 25x oil lens of a confocal microscope. **a)** Control-Sham **b)** Control-LFPI **c)** Notch1 cKO Sham **d)** Notch1 cKO LFPI.

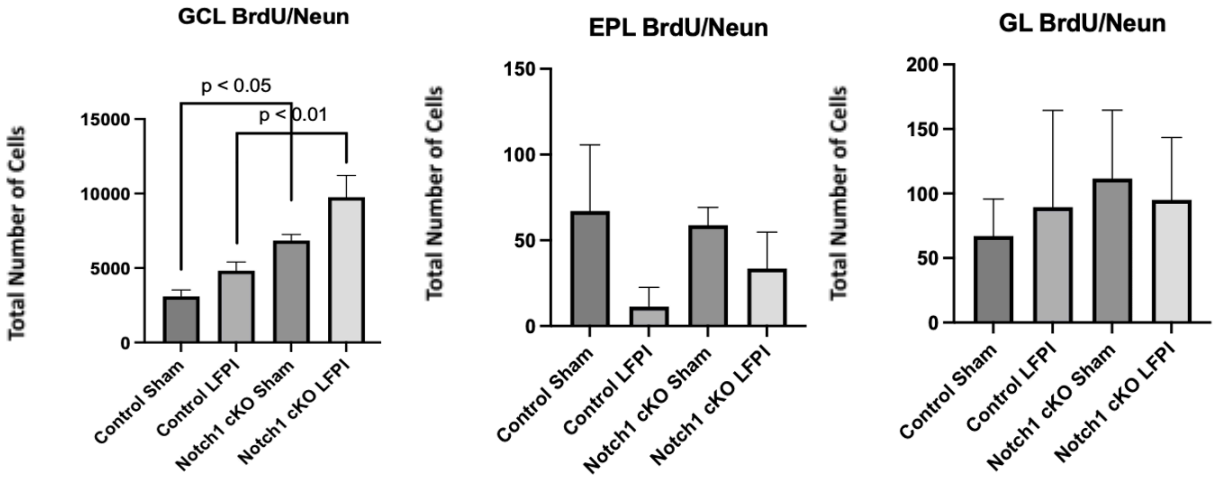

Figure 3.9 Quantification of BrdU+/NeuN in the GCL, EPL, and GL of the Olfactory Bulb at 8 WPI. Stereologically calculated BrdU+/NeuN+ cell counts in the three different OB layers are plotted. In the GCL, a statistically significant higher number of BrdU+/NeuN+ cells was observed in Notch1 cKO LFPI group compared to Control-LFPI group($p<0.01$). In sham groups, a statistically significant higher number of BrdU+/NeuN+ cells was observed in Notch1

cKO Sham compared to Control-Sham ($p<0.05$). No statistical significance was observed in the EPL or GL between groups.

3.2 Changes of GFP+ Cell Populations with Increased Time from Injury

In our animals, cells expressing the fluorescent GFP marker originate from the Nestin+ cells in the neurogenic regions. Monitoring GFP+ cells enables the tracking of the long-term fate and survival of cells derived from the nestin+ NSC population.

In the OB at four weeks post injury, extensive GFP+ cells were observed in the GCL of all four study groups **(Figure 3.10 b).** Quantification analysis with ANOVA analysis revealed no statistical significance of **GFP+** cells in the GCL, EPL or GL of the OB across the different treatment groups (**Figure 3.11).** At eight weeks post-injury, a different pattern of GFP+ cells was found with more GFP+ cells observed in the GCL of Notch1 cKO LFPI group (**Figure 3.12)**. Quantification analysis revealed a statistically significant higher number of **GFP+** cells in the GCL in the injured Notch1 cKO group compared to injured Control group **(Figure 3.13, p=0.0015).** No statistical significance was identified in the EPL or GL across the different groups.

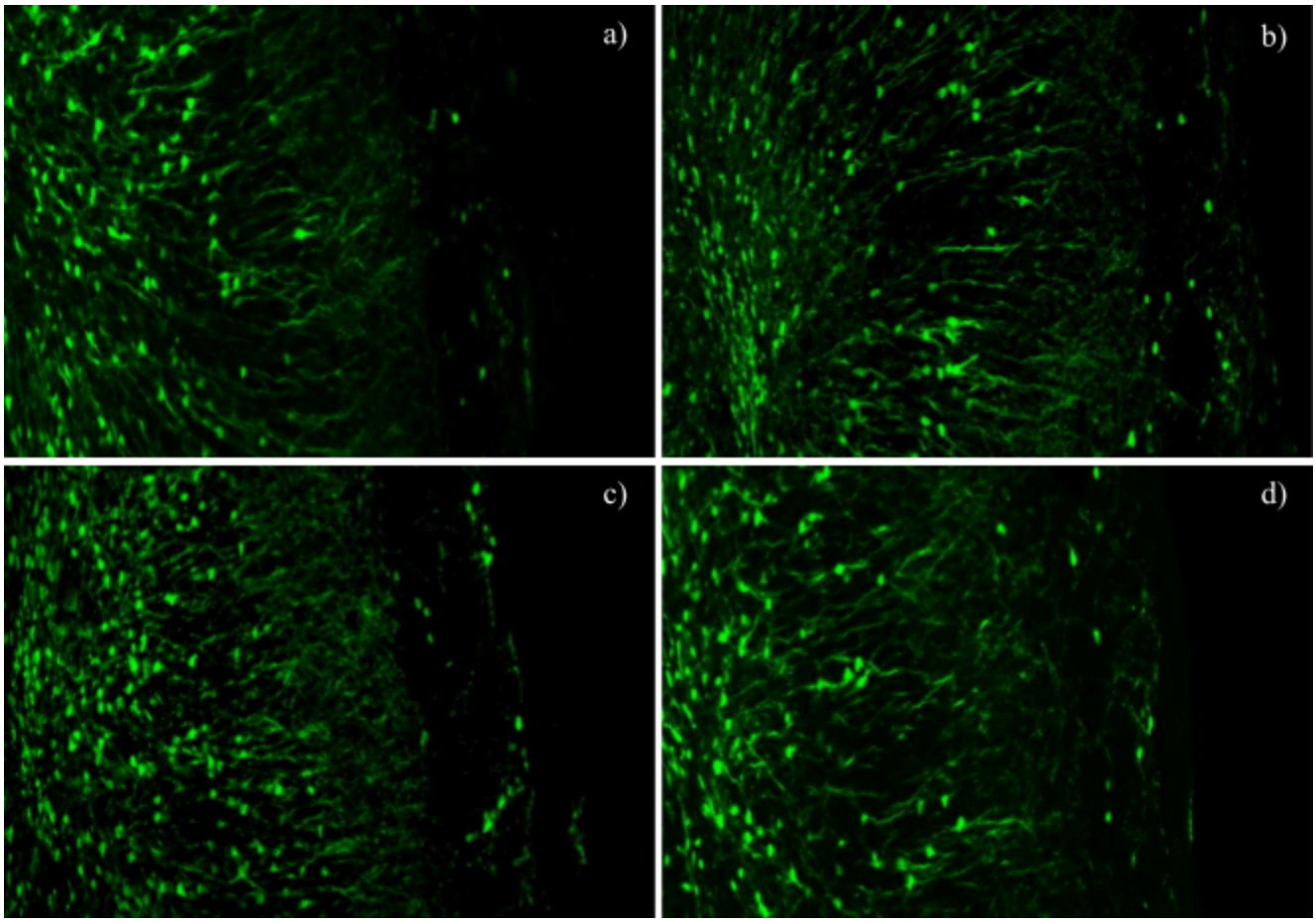

Figure 3.10 GFP Staining Pattern at 4 WPI. Representative image of GFP staining at a region of coronal sections of ipsilateral olfactory bulb tissue visualized under a 25x oil lens of a confocal microscope. **a)** Control-Sham **b)** Control-LFPI **c)** Notch1 cKO Sham **d)** Notch1 cKO LFPI.

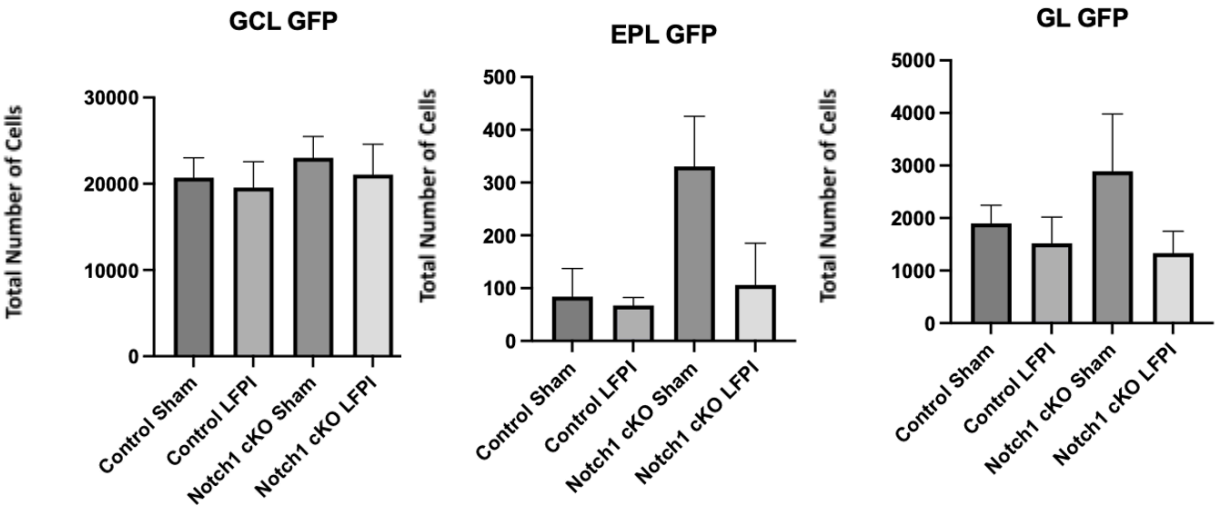

Figure 3.11. Quantification of GFP+ Cells in the GCL, EPL, and GL of the Olfactory Bulb at 4 WPI. Stereologically calculated total GFP+ cell counts in the GCL, EPL, and GL of 4 WPI mice. No statistically significant differences were observed between groups.

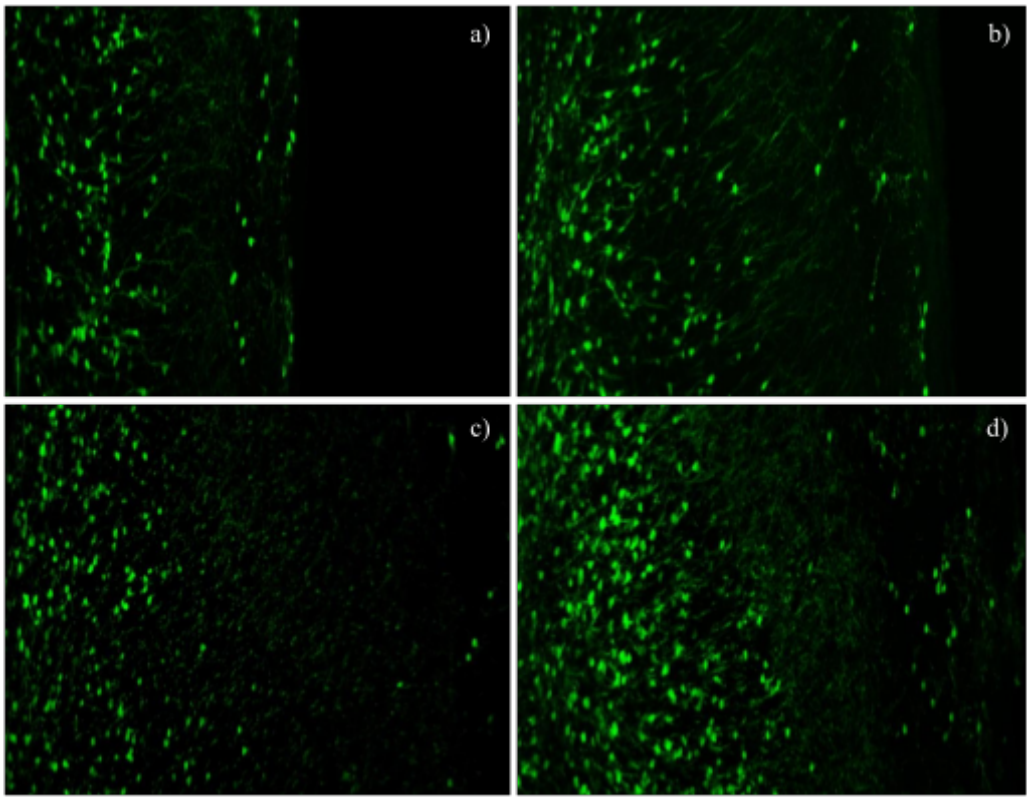

Figure 3.12. GFP Staining Pattern at 8 WPI. Representative image of GFP staining at a region of coronal sections of ipsilateral olfactory bulb tissue visualized under a 25x oil lens of a confocal microscope. **a)** Control-Sham **b)** Control-LFPI **c)** Notch1 cKO Sham **d)** Notch1 cKO LFPI.

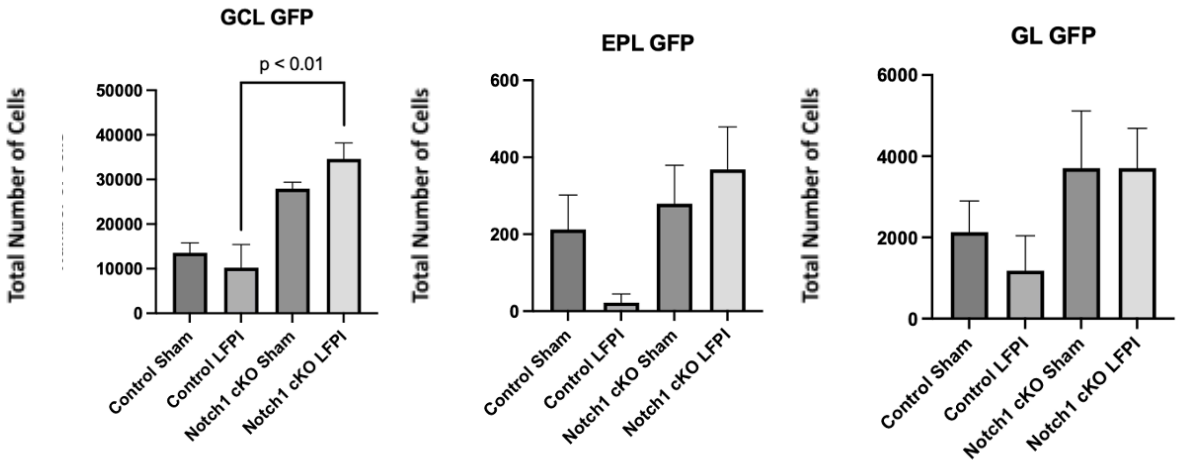

Figure 3.13. Quantification of GFP+ in the GCL, EPL, and GL of the Olfactory Bulb at 8 WPI. Stereologically calculated total GFP+ cell counts in the three different OB layers are plotted. In the GCL, compared to Control LFPI, a statistically significant higher number of GFP+ cells was observed in Notch1 cKO LFPI compared to Control LFPI group ($p<0.01$). No statistical significance was observed in the EPL or GL.

3.3 Loss of Notch1 Results in an Increase of Neuronal Differentiation and Proliferation Dependent on GCL

In our study, cells with GFP+/BrdU+ double-labeling are NSCs in the SVZ activated at 1-7 days post-injury and migrated to the OB. At four weeks post-injury, the staining pattern of GFP/BrdU doubling labeling is demonstrated in **Figure 3.14**. Quantification analysis revealed no statistical significance of cells double labeled with **GFP/BrdU** in the GCL, EPL, or GL across the different groups for this study time point **(Figure 3.15).** At 8 weeks post-injury, the pattern of **GFP+/BrdU** double-labeled cells was changed with visually more cells seen in the GCL of Notch1 cKO LFPI group **(Figure 3.18)**. Quantification analysis revealed a statistical significant higher number of **GFP+/BrdU+** cells in the GCL in Notch1 cKO LFPI compared to control LFPI ($p < 0.0001$) and Notch 1 cKO Sham ($p = 0.0081$) **(Figure 3.19).** No statistical significance was observed in the EPL or GL across the groups.

In this study, cells triple labeled with **GFP/BrdU/NeuN** are NSCs in the SVZ activated at 1-7 days post-injury and migrated to the OB becoming mature neurons at the study time points. At 4 weeks post-injury, the staining pattern of **GFP/BrdU/NeuN** is shown in **Figure 3.16**. Quantification analysis revealed no statistical significance of cells with **GFP/BrdU/NeuN** triple-labeling in the GCL, EPL, or GL across the different groups for this study time point **(Figure 3.17).** At 8 weeks post-injury, the staining pattern of **GFP+/BrdU/NeuN** triple-labeled cells is shown in Figure 3.20, visually more cells was seen in the GCL of Notch1 cKO LFPI group **(Figure 3.20)**. Quantification analysis revealed a statistical significant higher number of **GFP/BrdU/NeuN** triple-labeled cells in the GCL in Notch1 cKO LFPI compared to control LFPI ($p < 0.0001$) and Notch 1 cKO Sham ($p = 0.0042$) **(Figure 3.21).** No statistical significance was observed in the EPL or GL across the groups.

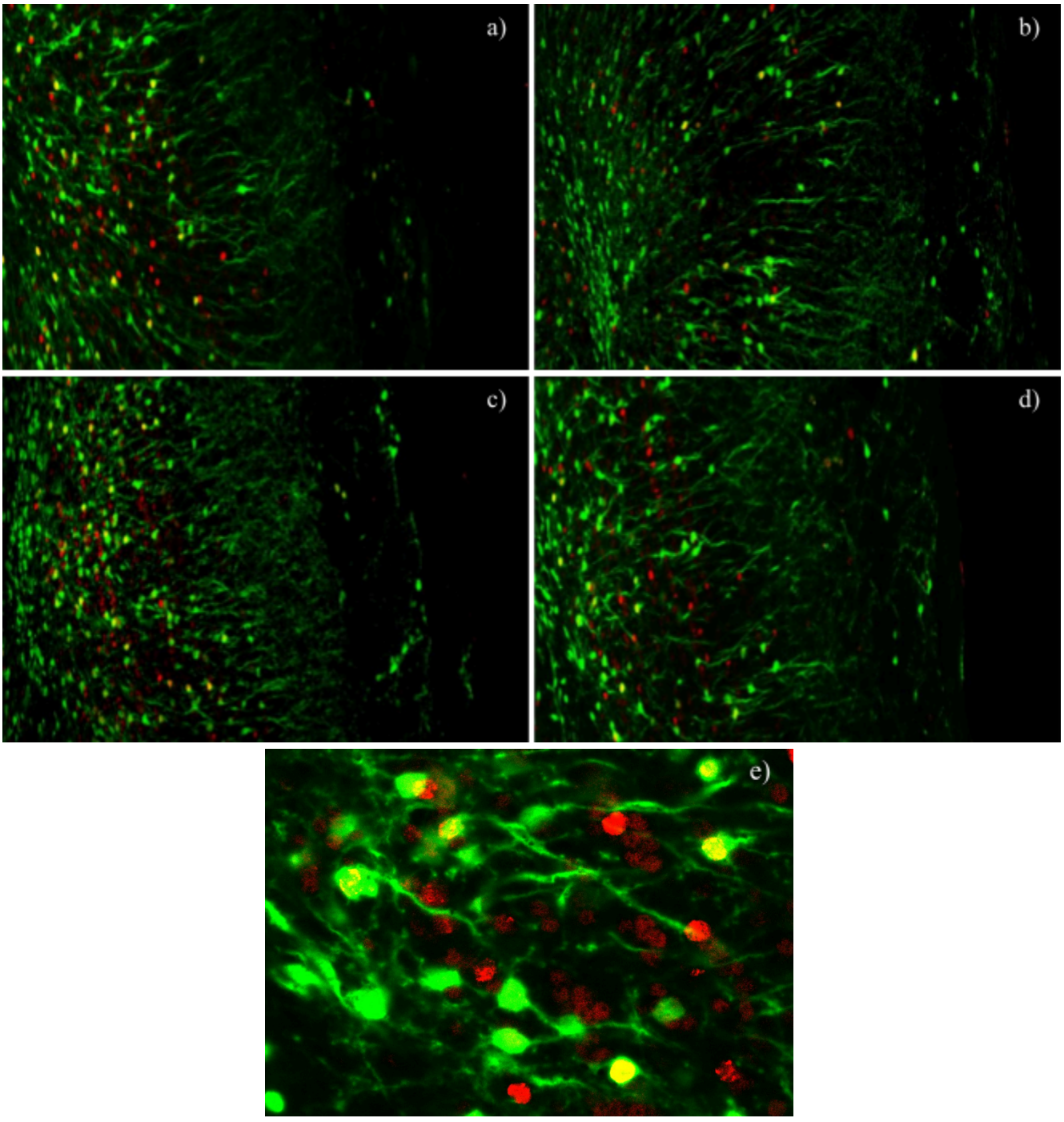
a)
b)
c)
d)
e)

Figure 3.14 GFP/BrdU Double-Labeling Staining Pattern at 4 WPI. Representative images of GFP/BrdU staining at a region of coronal sections of ipsilateral olfactory bulb tissue visualized under a 25x oil lens of a confocal microscope. **a)** Control-Sham **b)** Control-LFPI **c)** Notch1 cKO Sham **d)** Notch1 cKO LFPI.

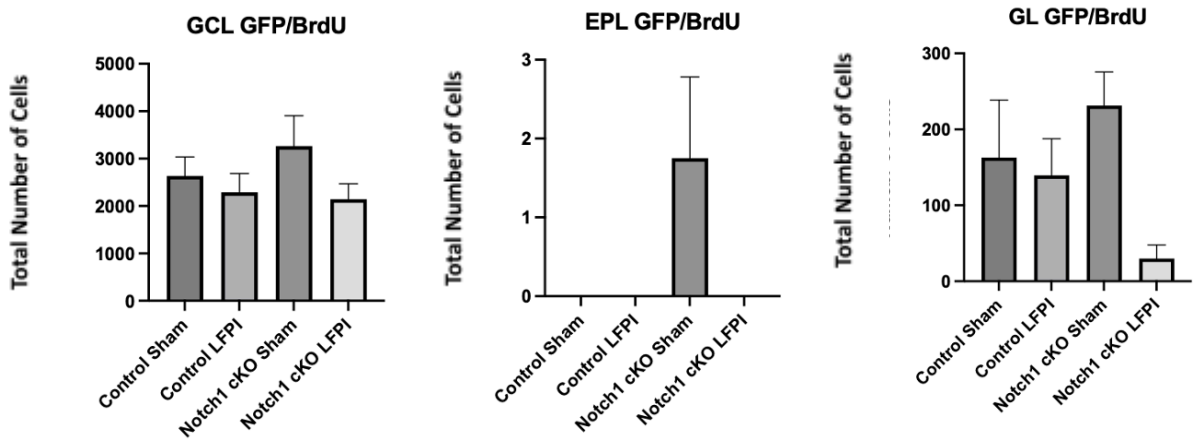

Figure 3.15 Quantification of GFP+ /BrdU+ Cells in the GCL, EPL, and GL of the Olfactory Bulb at 4 WPI. Stereologically calculated total GFP+/BrdU+ cell counts in the GCL, EPL, and GL of 4 WPI mice. No statistically significant differences were observed between 4 groups.

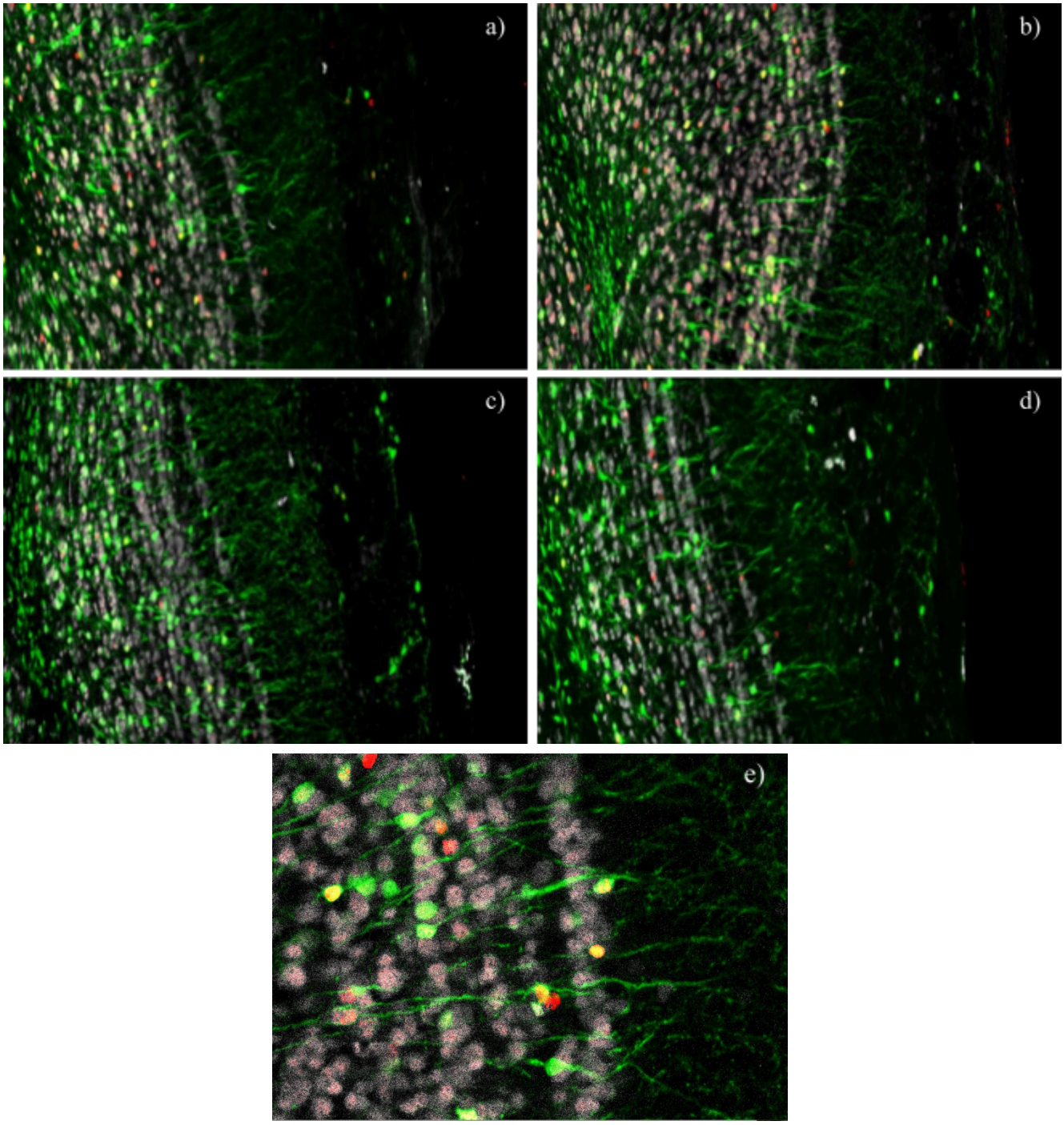
a)
b)
c)
d)
e)

Figure 3.16 GFP/BrdU/NeuN Triple-Labeling Staining Pattern at 4 WPI. Representative images of GFP/BrdU?NeuN staining at a region of coronal sections of ipsilateral olfactory bulb tissue visualized under a 25x oil lens of a confocal microscope. **a)** Control-Sham **b)** Control-LFPI **c)** Notch1 cKO Sham **d)** Notch1 cKO LFPI.

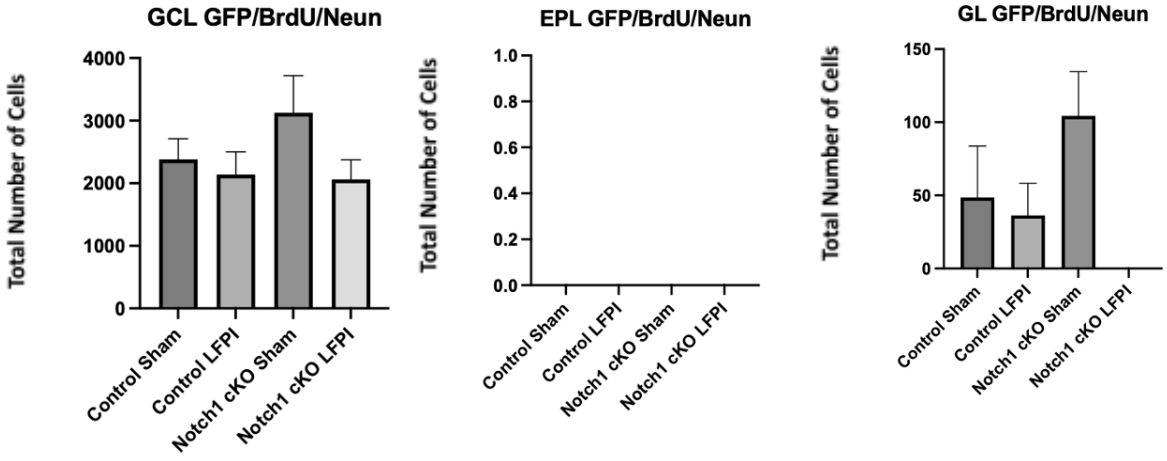

Figure 3.17 Quantification of GFP+ /BrdU+/NeuN Cells in the GCL, EPL, and GL of the Olfactory Bulb at 4 WPI Stereologically calculated total GFP+/BrdU+/NeuN cell counts in the GCL, EPL, and GL of 4 WPI mice. No statistically significant differences were observed between 4 groups.

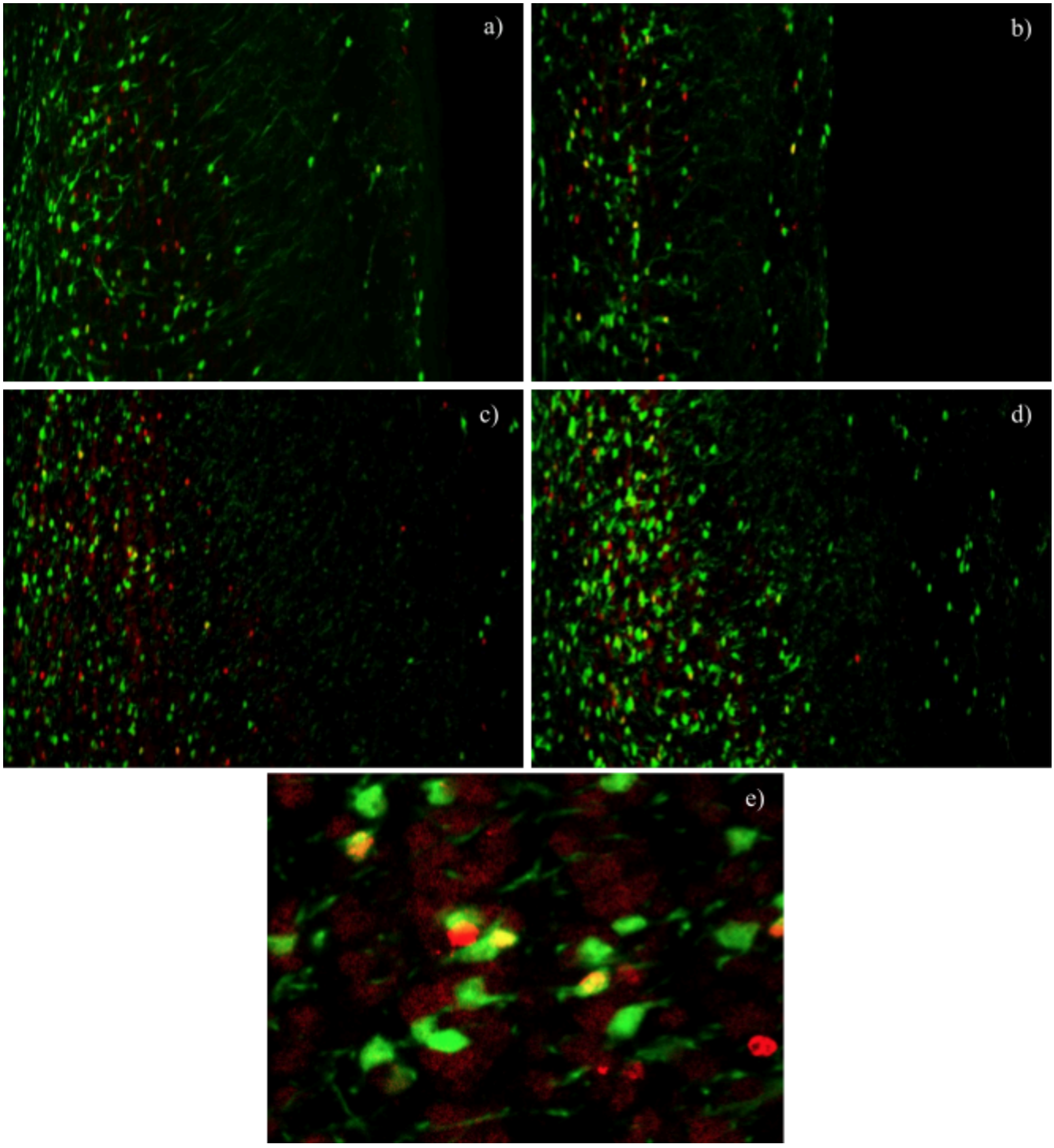
a)
b)
c)
d)
e)

Figure 3.18 GFP/BrdU Double-Labeling Staining Pattern at 8 WPI. Representative images of GFP/BrdU staining at a region of coronal sections of ipsilateral olfactory bulb tissue visualized under a 25x oil lens of a confocal microscope. **a)** Control-Sham **b)** Control-LFPI **c)** Notch1 cKO Sham **d)** Notch1 cKO LFPI.

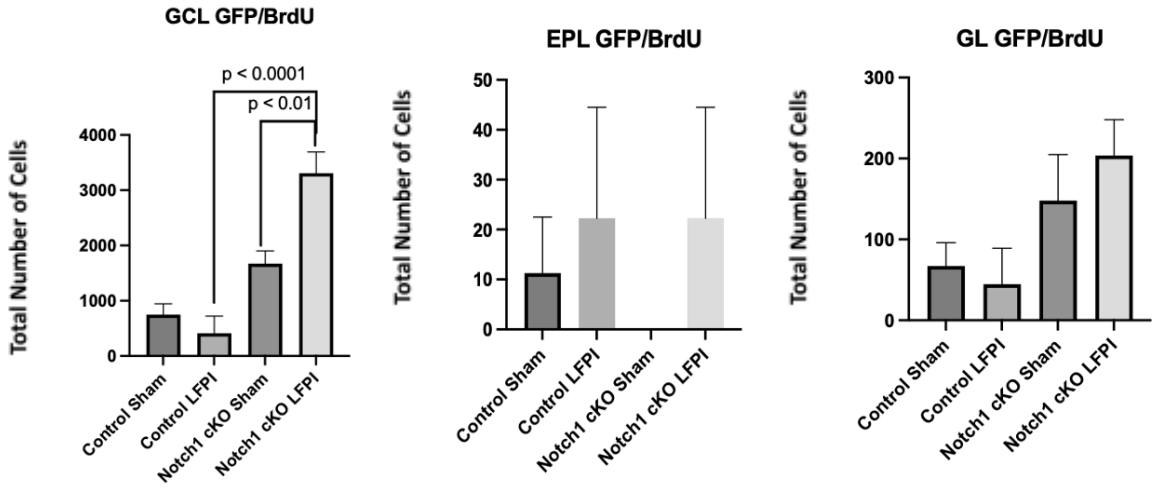

Figure 3.19 Quantification of GFP+/BrdU+ in the GCL, EPL, and GL of the Olfactory Bulb at 8 WPI. Stereologically calculated total double labeled GFP+/BrdU+ cell counts in the three different OB layers are plotted. In the GCL, Compared to Control LFPI, a statistically significant increase in GFP+/BrdU+ cells were observed in Notch1 cKO LFPI ($p<0.0001$). Compared to Notch1 cKO Sham, a statistically significant increase in GFP+/BrdU+ cells were observed in Notch1 cKO LFPI ($p<0.01$). No statistical significance was observed in the EPL or GL.

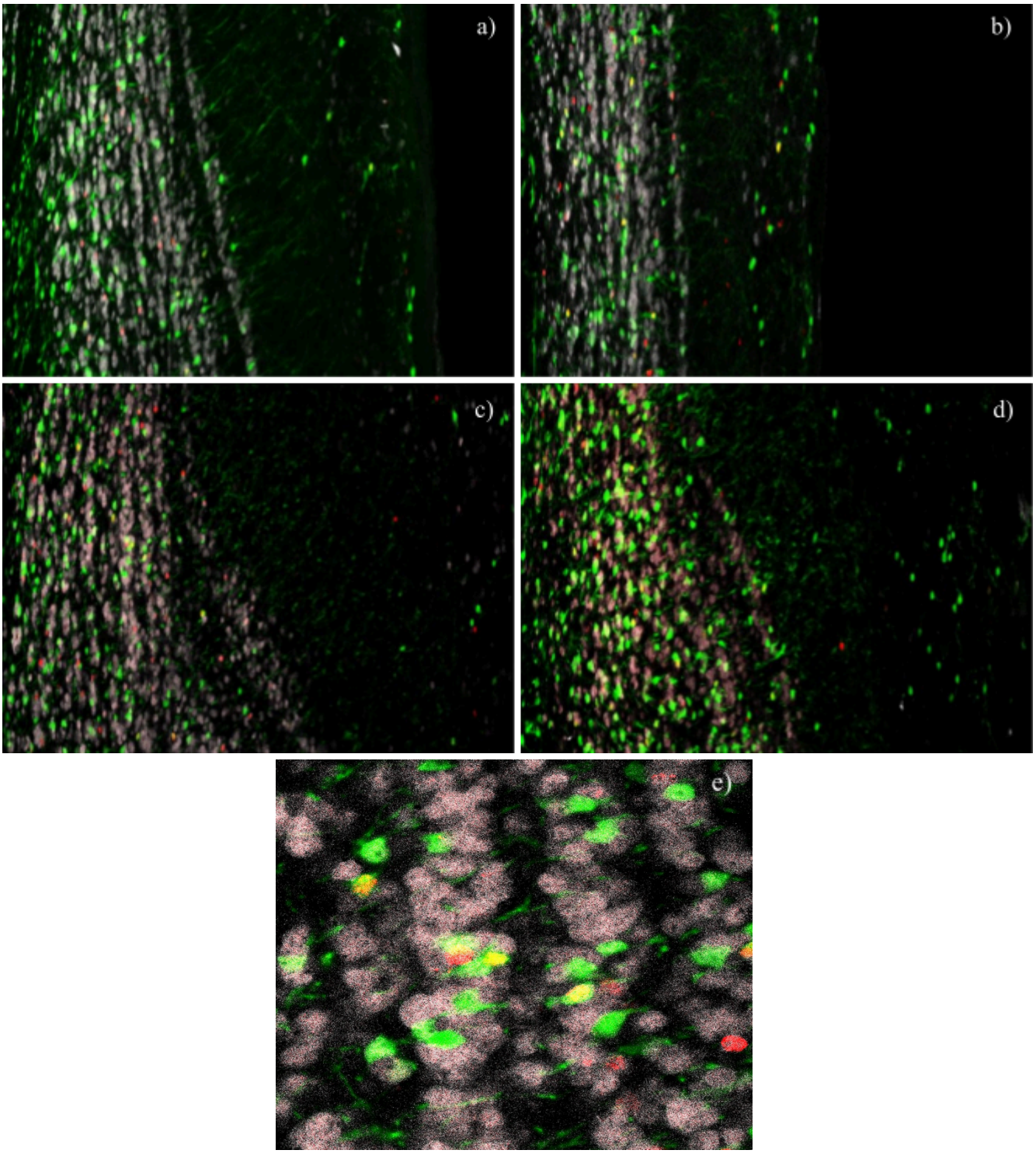
a)
b)
c)
d)
e)

Figure 3.20 GFP/BrdU Triple-Labeling Staining Pattern at 8 WPI. Representative images of GFP/BrdU staining at a region of coronal sections of ipsilateral olfactory bulb tissue visualized under a 25x oil lens of a confocal microscope. **a)** Control-Sham **b)** Control-LFPI **c)** Notch1 cKO Sham **d)** Notch1 cKO LFPI.

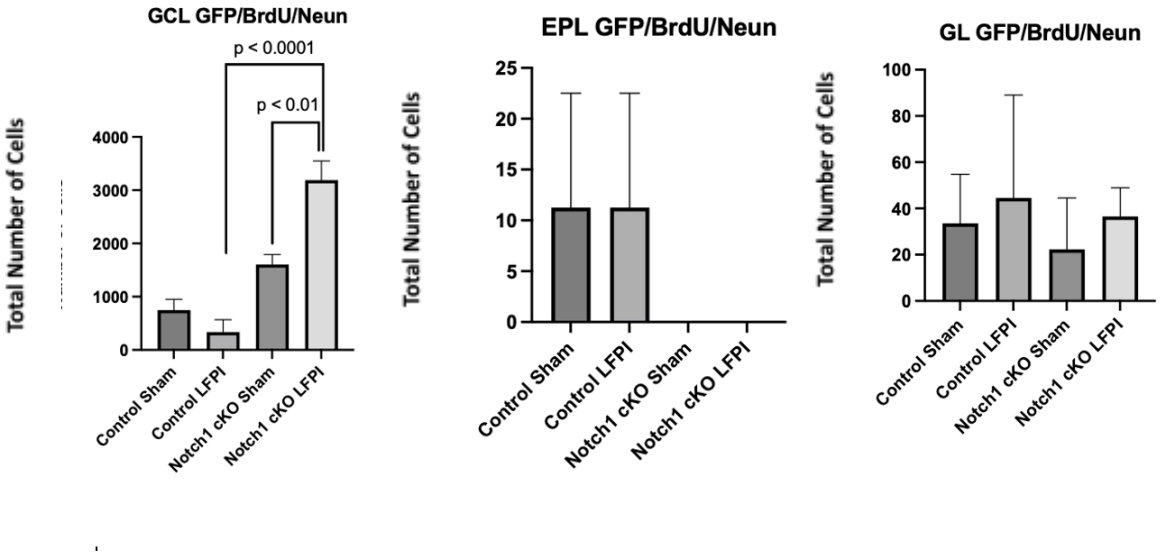

Figure 3.21 Quantification of GFP+/BrdU+/NeuN in the GCL, EPL, and GL of the Olfactory Bulb at 8 WPI. Stereologically calculated total triple labeled GFP+/BrdU+/NeuN cell counts in the three different OB layers are plotted. In the GCL, compared to Control LFPI, a statistically significant increase in GFP+/BrdU+/NeuN cells were observed in Notch1 cKO LFPI ($p<0.0001$). Compared to Notch1 cKO Sham, a statistically significant increase in GFP+/BrdU+/NeuN cells were observed in Notch1 cKO LFPI ($p<0.01$). No statistical significance was observed in the EPL or GL.

Table 3.1: P values of Two-Way ANOVA Post-hoc Test at 4 WPI.

Cell Phenotype	Control Sham vs Control LFPI	Notch1 cKO Sham vs Notch1 cKO LFPI	Control Sham vs Notch1 cKO Sham	Control LFPI vs Notch1 cKO LFPI
4 WPI				
GCL				
GFP+	p = 0.9939	p = 0.9721	p = 0.9547	p = 0.9863
BrdU+	p = 0.9867	p > 0.9999	p = 0.8007	p = 0.9381
GFP+/BrdU+	p = 0.9180	p = 0.1914	p = 0.6554	p = 0.9931
BrdU+/NeuN+	p = 0.9848	p = 0.9998	p = 0.7612	p = 0.8924
GFP+/BrdU+/NeuN+	p = 0.9584	p = 0.1568	p = 0.4400	p = 0.9985
EPL				
GFP+	p = 0.9988	p = 0.2093	p = 0.1469	p = 0.9851
BrdU+	p = 0.9659	p = 0.9421	p = 0.7268	p = 0.7812
GFP+/BrdU+	p > 0.9999	p = 0.8796	p = 0.08796	p > 0.9999
BrdU+/NeuN+	p > 0.9999	p = 0.1459	p = 0.0880	p = 0.9934
GFP+/BrdU+/NeuN+	p > 0.9999	p > 0.9999	p > 0.9999	p > 0.9999
GL				
GFP+	p = 0.9897	p = 0.5881	p = 0.8484	p = 0.9986
BrdU+	p = 0.7112	p = 0.9874	p = 0.6697	p = 0.9938
GFP+/BrdU+	p = 0.9854	p = 0.0317*	p = 0.7458	p = 0.3906
BrdU+/NeuN+	p = 0.6288	p = 0.9605	p = 0.8978	p = 0.7499
GFP+/BrdU+/NeuN+	p = 0.9880	p = 0.0502	p = 0.4680	p = 0.7738

Table 3.2: P values of Two-Way ANOVA Post-hoc Test at 8 WPI.

Cell Phenotype	Control Sham vs Control LFPI	Notch1 cKO Sham vs Notch1 cKO LFPI	Control Sham vs Notch1 cKO Sham	Control LFPI vs Notch1 cKO LFPI
8 WPI				
GCL				
GFP+	p = 0.8771	p = 0.4628	P = 0.0184*	p = <0.0001***
BrdU+	p = 0.3601	p = 0.1378	p = 0.0080**	p = 0.0019**
GFP+/BrdU+	p = 0.9248	p = 0.0277*	p = 0.3396	p <0.0001**
BrdU+/NeuN+	p = 0.4107	p = 0.0618	P = 0.0113*	p = 0.0008**
GFP+/BrdU+/NeuN+	p = 0.8318	p = 0.0168*	p = 0.3160	p < 0.0001**
EPL				
GFP+	p = 0.3426	p = 0.2093	p = 0.1469	p = 0.9851
BrdU+	p = 0.8916	p = 0.9985	p = 0.9597	p = 0.9813
GFP+/BrdU+	p = 0.9224	p = 0.5912	p = 0.9176	p > 0.9999
BrdU+/NeuN+	p = 0.5693	p = 0.9339	p = 0.9974	p = 0.9533
GFP+/BrdU+/NeuN+	p > 0.9999	p > 0.9999	p = 0.5030	p = 0.5030
GL				
GFP+	p = 0.5795	p > 0.9999	p = 0.5809	p = 0.1955
BrdU+	p = 0.3818	p = 0.6089	p = 0.5291	p = 0.7618
GFP+/BrdU+	p = 0.9871	p = 0.8439	p = 0.6392	p = 0.1165
BrdU+/NeuN+	p = 0.9969	p = 0.9987	p = 0.9762	p > 0.9999
GFP+/BrdU+/NeuN+	p = 0.9912	p = 0.9813	p = 0.9906	p = 0.9966

Table 3.3: P values of Two-Way ANOVA Post-hoc Test comparing 4 WPI vs. 8 WPI

4 WPI vs. 8 WPI				
Cell Phenotype	**Control Sham**	**Control LFPI**	**Notch1 cKO Sham**	**Notch1 cKO LFPI**
GCL				
GFP+	p = 0.1248	p = 0.0483*	p = 0.2813	p = 0.0059**
BrdU+	p = 0.0007***	p = 0.0176*	p =0.2299	p = 0.3191
GFP+/BrdU+	p = 0.0019**	p = 0.0020**	p = 0.0071**	p = 0.0413*
BrdU+/NeuN+	p = 0.0003***	p = 0.0068**	p = 0.0928	p = 0.4154
GFP+/BrdU+/NeuN+	p = 0.0026**	p = 0.0011**	p = 0.0047**	p = 0.0294*
EPL				
GFP+	p = 0.2603	p = 0.6894	p = 0.6475	p = 0.0270*
BrdU+	p = 0.7200	p = 0.1368	p = 0.8542	p = 0.8296
GFP+/BrdU+	p = 0.5274	p = 0.2169	p = 0.4659	p = 0.2169
BrdU+/NeuN+	p = 0.1302	p = 0.7947	p = 0.2775	p = 0.6075
GFP+/BrdU+/NeuN+	p = 0.1701	p = 0.1701	p = >0.9999	p = >0.9999
GL				
GFP+	p = 0.8503	p = 0.7853	p = 0.5113	p = 0.0645
BrdU+	p = 0.6336	p = 0.9387	p = 0.8039	p = 0.2003
GFP+/BrdU+	p = 0.1713	p = 0.1756	p = 0.2307	p = 0.0172*
BrdU+/NeuN+	p = 0.2591	p = 0.8005	p = 0.9600	p = 0.4949
GFP+/BrdU+/NeuN+	p = 0.6952	p = 0.8292	p = 0.0403*	p = 0.3441

3.4 Two-Way ANOVA Analysis Revealed Time Difference Between Cells in OB

A Two-Way ANOVA test was performed combined with Tukey HSD post hoc tests with multiple comparisons to compute the difference in the total number of cells between 4 and 8 weeks in the four groups and to see if there any injury or genotype effect on survival of newly generated cells **(Table 3.3).** The significance level was set to $\alpha=0.05$ for all analyses performed and all data was plotted in a column bar graph with the standard error bars expressed as mean ± SEM. The analysis revealed a statistically significant difference between 4 WPI and 8 WPI, predominantly in the GCL of the OB. For GFP+ cells, the Control LFPI ($p=0.0483$) had a greater total number of cells at the 4 WPI time point compared to the 8 WPI, while the Notch 1 ckO LFPI ($p=0.0059$) had a greater total number of cells at 8 WPI. For BrdU+ cells, the Control Sham ($p = 0.0007$) and Control LFPI ($p = 0.0176$) had a greater number of cells at 4 WPI. For double labeled GFP+/BrdU+ cells, the Control Sham ($p=0.0019$), Control LFPI ($p=0.0020$), and Notch1 cKO Sham ($p=0.0071$) groups had a greater number of cells at 4 WPI, however, the Notch1 cKO LFPI ($p =0.0413$) had a greater number of cells at 8 WPI. For double labeled BrdU+/NeuN+ cells, Control Sham ($p=0.0019$) and Control LFPI ($p=0.0020$) had a greater number of cells at 4 WPI. For triple labeled GFP+/BrdU+/NeuN+, the Control Sham ($p=0.0026$), Control LFPI ($p=0.0011$), and Notch1 cKO Sham ($p=0.0047$) groups had a greater number of cells at 4 WPI, however, the Notch1 cKO LFPI ($p =0.0294$) had a greater total number of cells at 8 WPI.

In the EPL, the Notch1 cKO LFPI ($p=0.0270$) group had a greater number of GFP+ cells at 8 WPI, however, no other significant results were found between the two time points across the different groups. In the GL, Notch1 cKO LFPI ($p=0.0172$) had a greater number of

GFP+/BrdU+ cells at 8 WPI, and a greater number of triple labeled GFP+/BrdU+/NeuN+ at 4 WPI in the Notch1 cKO Sham condition ($p=0.0403$)

Two-Way ANOVA analysis at 4 WPI **(Table 3.1)** did not reveal any statistically significant differences across the treatment groups, except for the total number of double-labeled GFP+/BrdU+ cells in the GL layer between the Notch1 cKO Sham and Notch1 cKO LFPI conditions. Specifically, the Notch1 cKO Sham group exhibited a significantly higher number of double-labeled GFP+/BrdU+ cells compared to the Notch1 cKO LFPI condition.

At 8 WPI **(Table 3.2)** the ANOVA analysis showed statistically significant increases in the total number of cells for all markers within the Notch1 cKO LFPI group compared to the Control LFPI group, particularly in the GCL layer. Similarly, a significantly higher number of GFP+, BrdU+, and double-labeled BrdU+/NeuN+ cells were observed in the Notch1 cKO Sham group compared to the Control Sham group in the GL layer. Furthermore, within the GL layer, the Notch1 cKO LFPI group exhibited higher numbers of GFP+/BrdU+ and GFP+/BrdU+/NeuN+ cells compared to the Notch1 cKO Sham group.

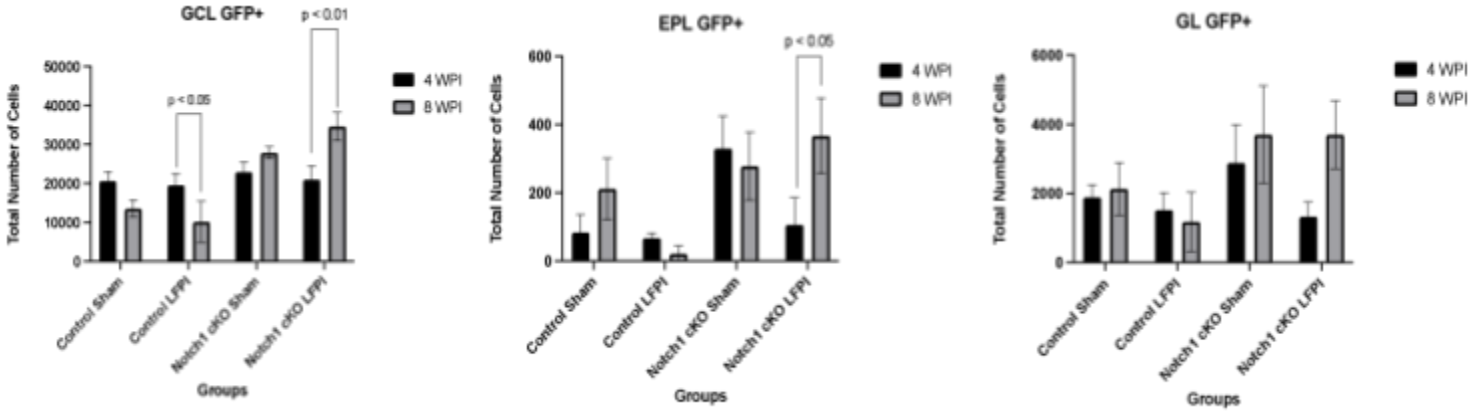

Figure 3.22 Comparison of the number of GFP+ cells between 4 and 8 weeks WPI. For GFP+ cells, in the GCL there is a significant reduction of cells number in the Control LFPI group from 4 WPI to 8 WPI. While in the Notch1 cKO LFPI, there is significant increase in cells from 4 WPI to 8 WPI. In the EPL, there is a significant increase in cells from 4 WPI to 8 WPI. No differences in the GL were not observed.

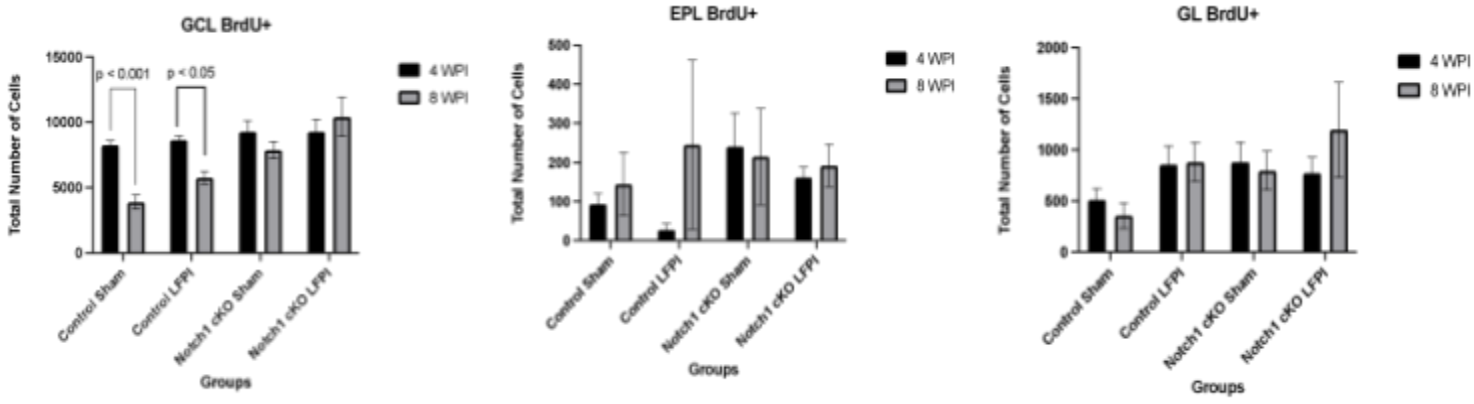

Figure 3.23 Comparison of the number of BrdU+ cells between 4 and 8 weeks WPI. For BrdU+ cells, in the GCL there is a significant reduction of cells in the Control Sham and Control LFPI groups from 4 WPI and 8 WPI. No differences were observed in the EPL or GL.

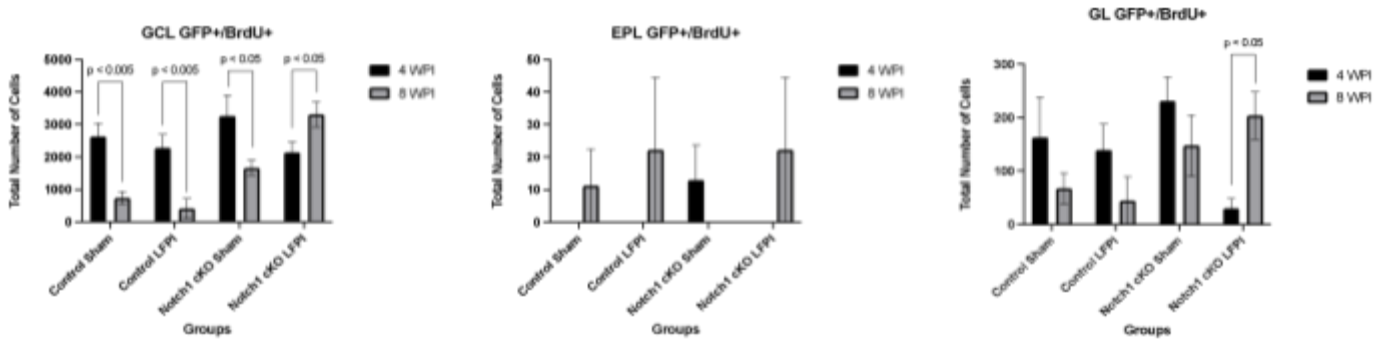

Figure 3.24 Comparison of the number of GFP+/BrdU+ cells between 4 and 8 weeks WPI. For GFP+/BrdU+ cells, in the GCL there is a significant reduction of cells in the Control Sham, Control LFPI, and Notch1 cKO Sham from 4 WPI to 8 WPI. In the Notch1 CKO LFPI group, there is a significant increase in total number of cells from 4 WPI to 8 WPI. In the GL, there is a significant increase in the number of cells in the Notch1 cKO LFPI group from 4 WPI to 8 WPI. No differences were observed in the EPL.

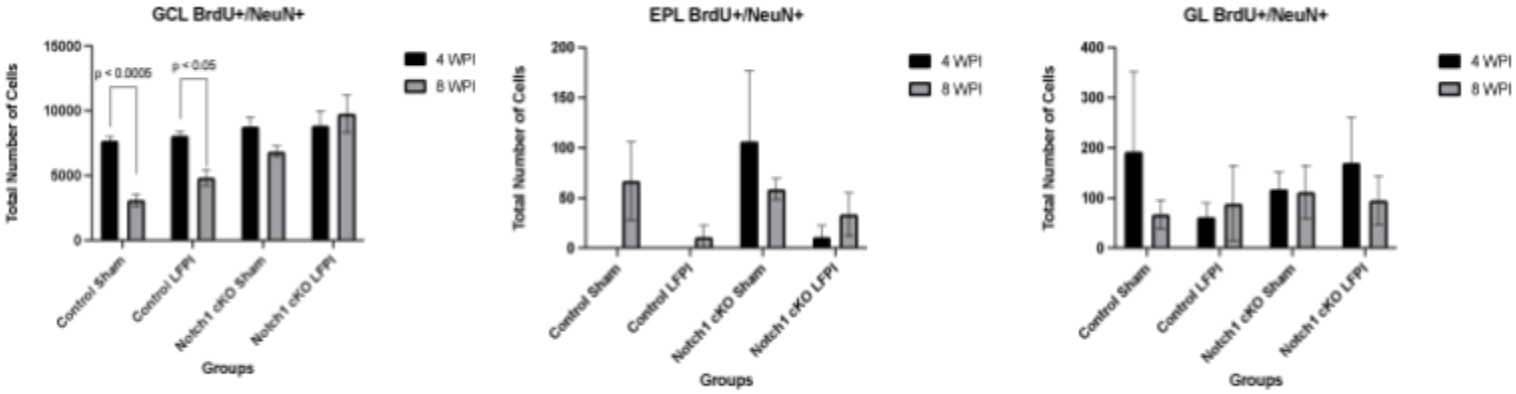

Figure 3.25 Comparison of the number of BrdU+/NeuN+ cells between 4 and 8 weeks WPI. For BrdU+/NeuN+ cells, in the GCL there is a significant reduction of cell number in the Control Sham and Control LFPI group from 4 WPI to 8 WPI. No differences were observed in the EPL or GL.

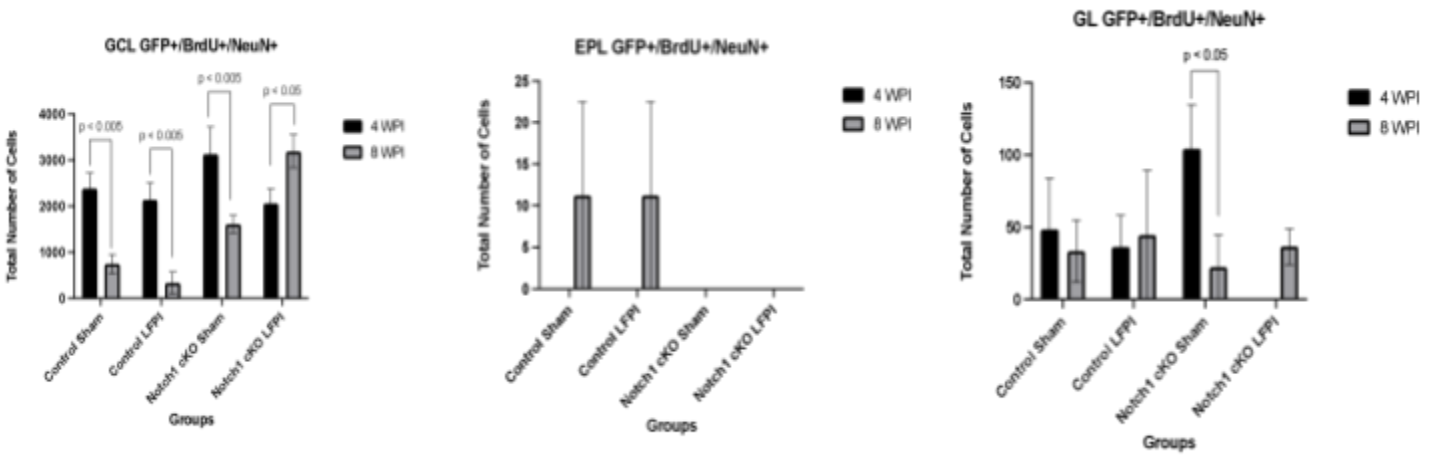

Figure 3.26 Comparison of the number of GFP+/BrdU+/NeuN+ cells between 4 and 8 weeks WPI. For GFP+/BrdU+/NeuN+ cells, in the GCL there is a significant reduction in the number of cells in the Control Sham, Control LFPI, Notch1 cKO Sham from 4 WPI to 8 WPI. In the Notch1 cKO LFPI group, there is a significant increase in the number of cells. In the GL, there is a significant reduction in the number of cells in the Notch1 cKO Sham group. No differences were observed in the EPL.

Chapter 4: Discussion

Following TBI in the adult mammalian brain, there is an endogenous neurogenic response in the SVZ and DG of the CNS, suggesting the role of neurogenesis in the brain's regenerative ability after injury (Sun, 2015). The majority of the new neurons in the SVZ travel via the rostral migratory stream and integrate into the olfactory circuitry (Sun, 2015). Although olfactory dysfunction is a common sequela of TBI, affecting 20-68% of TBI patients, there is limited research on the endogenous neurogenesis capacity of the OB post injury (Liu et al, 2023). In this study, we investigated the role of Notch1 in the injury-induced neurogenic response in the olfactory bulb. Research indicates that Notch1 plays a significant role in the proliferation and differentiation of NSCs, however, its regulatory role on NSCs in olfactory bulb following TBI remains unclear. Transgenic NC-Y (control) and NC-NKO-Y (Notch1 cKO) mice that had no prior exposure to behavior tests were used in this study.

In this study, the mice underwent either sham surgery or a moderate LFPI and were sacrificed at 4 WPI or 8 WPI. In both the 4 WPI and 8 WPI groups, animals received a daily intraperitoneal injection of BrdU (50mg/kg) from 1 to 7 days post-injury (DPI) to label active dividing cells at these specified time points. We examined the number of cells labeled by BrdU or GFP alone, or double and triple labeled with mature neuronal marker NeuN to assess the survival and neuronal differentiation/maturation of NSCs derived from the SVZ that were migrated to the OB at 4 or 8 weeks post-injury. The study time points of 4 or 8 weeks were selected as published studies have shown that adult generated new neurons in the hippocampus begin to express mature neuronal marker NeuN that become fully functional mature neurons around 8 weeks (Zhao et al., 2008). In our study, we compared injury and genotype effect on the number of newly generated cells (BrdU+), new cells became mature neurons (BrdU+/NeuN+),

dividing NSCs at 1-7 days post-TBI (GFP+/BrdU+) and dividing NSCs at 1-7 days post-TBI becoming mature neurons (GFP+/BrdU+/NeuN+) at 4 or 8 weeks post-injury. We found no statistical significance across all markers in any of the three layers of OB among the study groups at 4 WPI. However, differences were found at the 8 WPI study time with the injured Notch1 cKO mice showing increased number of cells with all markers in the GCL layer of the OB in comparison to Control LFPI group, suggesting a genotype effect on the generation of SVZ nestin+ NSC derived OB new neurons post-injury, with Notch1 cKO positively affecting these cells. Injured Notch1 cKO mice also showed increased number of GFP+/BrdU+ and GFP+/BrdU+/NeuN+ cells in the GCL of the OB in comparison to Notch1 cKO sham group, suggesting an injury effect in activating NSCs in Notch1 cKO mice, but not in the Control mice.

Influence of TBI on adult neurogenesis in the hippocampus has been extensively studied in varying TBI models (Sun 2016), whereas research on SVZ has been comparatively limited. Our lab has previously reported injury-enhanced cell proliferation in the SVZ at 2 and 7 days post-injury in the rat LFPI model (Chirumamilla et al., 2002; Sun et al., 2005). New cells generated from the SVZ constantly migrate to the OB which make the study of examining the fate of SVZ derived cells more complicated. It is known that OB cells are constantly replaced by SVZ generated new cells in the lifespan of the animals (Imayoshi et al., 2008); however, there is no report about injury effect on this process.

In our study, we examined the number of BrdU+, BrdU+/NeuN+, GFP+/BrdU+, GFP/BrdU+/NeuN+ in the OB at 4 or 8 weeks to assess survival and differentiation of cells generated at the window of 1-7 days post-injury. At 4 weeks, the absolute cell counts for all markers across all four groups were comparable and notably higher than those observed at 8 weeks post-injury, indicating a decline in cell counts during the time span between 4 and 8 weeks

post-TBI. The reduction of new cells in the OB over time is anticipated due to the ongoing turnover of OB cell replacement. However, our study revealed a notably higher count of cells expressing all markers at 8 weeks post-injury in the injured Notch1 cKO mice compared to Control LFPI mice, suggesting the involvement of Notch1 in the survival and neuronal differentiation of neural stem cells following injury. Interestingly, our data showed no discernible injury or genotype disparity among groups at 4 weeks post-injury. This could imply that the severity of injury in the animals at 4 weeks post-injury may not significantly affect SVZ neurogenesis. Additionally, it is plausible that the OB we evaluated may comprise a mix of the ipsilateral and contralateral sides, as the LFPI model primarily impacts the ipsilateral side.

The regions of the OB that were analyzed were the GCL, EPL, and GL. The GCL is the innermost layer of the OB containing newly generated GCs. The EPL is between the GCL and GL and is important for synaptic connections, and the GL is the outermost layer that facilitates connections between the OB neurons. The GCL continually receives newly generated neurons originating from the SVZ and undergoes continuous replacement throughout lifetime. In contrast, the GL does not exhibit significant neurogenesis in the adult brain. After injury, it is expected that there is an aberrant migration of NPCs to the outer layers beyond the GCL (Ibrahim et al., 2016). However, this was not observed in our study. While the 4 WPI group did not exhibit statistical significance in any of the layers of the OB, mice at 8 WPI showed a notable increase in BrdU+ cells in the GCL, suggesting that the GCL is an important site for injury-induced proliferation and survival of newly generated cells.

Cells labeled with BrdU allow for the tracking of the fate of proliferating NSCs and newly generated cells from the injury-induced response. The survival of these cells and how they integrate into the neural circuitry are important for understanding the endogenous recovery

mechanism post-injury. At 4 WPI, there was no difference in BrdU or double labeling of BrdU/Neun proliferation across the different treatment groups. At 8 WPI, statistically significance was found for BrdU+ cell only in the GCL, suggesting a significant increase in cells in this layer due to injury. For both Brdu+ and double lableed BrdU/NeuN cells, Notch1 cKO Sham had a greater number of cells than Control Sham and Notch1 cKO LFPI had a greater number compared to Control LFPI. The results support our hypothesis that the injury group had a greater number of BrdU cells due to the neurogenic response. The significant number of double labeled BrdU/NeuN indicate that a significant number of cells originally part of the injury-induced population had survived to maturity and differentiated into mature neurons, which supports our hypothesis. The results suggest that the Notch1 cKO may enhance the survival of newly generated cells post injury in the GCL at 8 WPI. This did not support our hypothesis or established literature of the role of Notch1 in regulating neurogenesis and stem cell proliferation.

GFP+ cells are important for tracking the fate of NSCs originating from the Nestin+ population prior to injury. At 4 WPI, there were no statistically significant differences between the different treatment groups in any of the layers for GFP+, double labeled GFP/BrdU, nor triple labeled GFP/BrdU/NeuN. However, by 8 WPI there was a large genotype difference between Notch1 cKO LFPI having the highest number of GFP+ cells compared to Control LFPI. This did not support our hypothesis, rather suggesting that Notch1 cKO increases the neurogenic response in the GCL of the OB 8 WPI. For double labeled GFP/Brdu and triple labeled GFP/BrdU/Neun, Notch1 cKO LFPI had a greater number than both Control LFPI and Notch1 cKO Sham. This suggests that the Notch1 conditional knockout in combination with LFPI may lead to enhanced survival and maturation of cells originally part of the injury-induced population in the GCL of OB.

Research conducted in our lab, as well as previously published studies, have highlighted the significant regulatory role of Notch1 in both stem cell proliferation and neurogenesis. However, the outcome of this project did not support these findings. There exists limited understanding regarding the molecular mechanisms orchestrating neural differentiation subsequent to the inactivation of the Notch1 pathway. A pivotal aspect contributing to the augmentation of neurogenesis following Notch1 cKO is the disruption of the delicate balance between the proliferation and differentiation of neural progenitor cells (NPCs). This disruption, occurring particularly during specific embryonic stages, paradoxically results in increased neural differentiation and subsequent neurogenesis into mature neurons (Randen et al., 2010).

In instances such as traumatic brain injury (TBI), where there is a heightened necessity for neurogenesis to replenish damaged neurons, Notch signaling tends to impede differentiation while prioritizing the maintenance of neural stem cells (NSCs) in a quiescent state. Consequently, the conditional knockout of Notch1 alleviates this inhibition, thereby augmenting neurogenesis and stem cell proliferation to facilitate the replenishment of damaged cellular populations. Moreover, emerging research suggests a notable interplay between Notch1 signaling and the expression of Hes1 and Hes5, prominent transcriptional repressors pivotal in modulating the downstream effects of the Notch1 pathway (Ohtsuka and Kageyama, 2021). These factors not only encourage stem cell differentiation but also exert inhibitory effects on neuronal differentiation. Consequently, the knockout of Notch1 would engender an increase in neuronal differentiation, a phenomenon observed in our investigation.

Two Way ANOVA analysis revealed a statically significant temporal difference in the total number of cells in the 3 OB layers of stained cells between 4 WPI and 8 WPI, particularly in the GCL of the Olfactory Bulb. Notably, Control LFPI showed a higher total number of GFP+

cells at 4 WPI compared to 8 WPI, while the Notch1 cKO LFPI group exhibited a higher total number of cells of GFP+ cells at 8 WPI. Similarly, for other cell types (BrdU+, double labeled GFP+/BrdU+, double labeled BrdU+/NeuN+, triple labeled GFP+/BrdU+/NeuN+), significant differences in total number of cells were observed between 4 WPI and 8 WPI across different groups. The results indicate that the 8 WPI is critical for the survival of newly generated cells post injury.

At 8 WPI, the Notch1 cKO LFPI group consistently showed higher total number of stained cells at 8 WPI, highlighting the potential impact of Notch1 deficiency combined with injury on cell survival. These findings highlight that Notch1 plays a crucial role in regulating cell proliferation and maintaining the NSC pool. Notch1 signaling typically keeps cells in a proliferative state by inhibiting their exit from the cell cycle, thus reducing the number of cells that mature into neurons. However, when Notch1 is knocked out, it leads to the depletion of the proliferative pool as cells are driven towards neuronal differentiation. In the short term, this may increase cell survival, but in the long term, it could deplete the NSC pool, leading to potential exhaustion of neural stem cells.

Notch1 signaling supports cell survival by inhibiting apoptotic pathways and encouraging cell differentiation and viability. However, in the absence of Notch1, cells lack the protective mechanisms against apoptosis, potentially leading to cell death. Paradoxically, when Notch1 is knocked out, this loss of protection from pro-apoptotic signals may initially result in increased cell survival potentially due to the surviving cells developing better resistance to signals that would normally trigger cell death.

As indicated in **Tables 3.1** and **3.2**, both the Control LFPI and Control Sham groups exhibited significant decreases in various cell types from 4 WPI to 8 WPI, including BrdU+,

GFP+/BrdU+, BrdU+/NeuN+, and GFP+/BrdU+/NeuN+ cells. Similarly, the Notch1 cKO Sham group showed a comparable reduction in GFP+/BrdU+ and GFP+/BrdU+/NeuN+ cells from 4 WPI to 8 WPI. In contrast, the Notch1 cKO LFPI group demonstrated a significant increase in the numbers of GFP+, GFP+/BrdU+, and GFP+/BrdU+/NeuN+ cells from 4 WPI to 8 WPI. These results highlight that injury in the Control mouse line does not markedly influence the observed outcomes when compared to uninjured animals. One plausible interpretation of these findings is that the moderate LFPI might not be sufficiently severe to produce measurable outcomes. Moreover, the absence of Notch1 in the same conditions resulted in a pattern similar to the Control LFPI and Control Sham groups. However, the Notch1 cKO LFPI group exhibited a substantial increase in cell survival. This suggests that Notch1 knockout alone does not significantly affect the survival of newly generated neurons post-injury compared to the control mouse lines. Conversely, when Notch1 cKO is combined with LFPI, there is a notable increase in the total number of cells surviving from 4 WPI to 8 WPI, particularly in the GCL of the OB.

The regulation of cell proliferation and neurogenesis by Notch signaling is influenced by specific contexts, demonstrating both tumor suppressor and oncogenic functions. Zou et al. (2018) revealed that Notch1 acts as an oncogene, promoting tumor initiation, while Notch2 functions as a tumor suppressor during lung carcinogenesis. Overexpressing Notch1 in adenocarcinoma cells inhibited cell growth and induced apoptosis, and indirect inhibition of Notch1 reduced cell proliferation and induced apoptosis (Zou et al., 2018). Additionally, another study by Chet et al. demonstrated that increasing the expression of Notch1 Intracellular Domain (N1ICD) in adenocarcinoma cells suppressed cell growth and triggered apoptosis, whereas reducing Notch1 expression led to increased cell proliferation and apoptosis (Zou et al., 2018).

Our data indicates that the absence of Notch1 combined with injury leads to increased cell survival in the olfactory bulb following injury. One plausible explanation for this finding is that increased Notch signaling inhibits proliferation and promotes apoptosis, whereas Notch1 knockdown leads to increased cellular proliferation and reduced apoptosis. Further studies are needed to explore the role of Notch1 in regulating cell survival in the olfactory bulb following injury.

Conclusion and Future Direction

In conclusion, our data failed to show injury effect in neurogenesis in OB, however, we found that loss of Notch1 in nestin+ cells significantly affect survival of cells in OB GCL at 8 weeks post-injury in the injured animals. Our data demonstrated that Notch1 cKO when combined with LFPI resulted in an increased in cell survival from 4 WPI to 8 WPI, indicating the unique role of Notch1 in apoptosis. To better understand the injury and genotype effect in the olfactory bulb following TBI, future studies are needed. Given the lack of statistically significant findings at 4 WPI, a more severe injury model could be beneficial resulting in more pronounced and measurable outcomes following injury. Additionally, incorporating a functional assessment of olfaction, such as an odor discrimination or sensitivity task, would be valuable for comparing behavioral outcomes related to olfactory functioning following traumatic brain injury (TBI). Finally, assessing more acute time points would be beneficial given the high cell turnover rate and ongoing neurogenesis in the olfactory bulb.

Vita

Sarah graduated from the University of Virginia with her Bachelor of Arts in Biology and Psychology and a Minor in South Asian Studies in 2019. After graduation, Sarah went on to complete the premedical certification postbaccalaureate program at Virginia Commonwealth University School of Medicine (VCU SOM) and subsequently her Master of Science in Anatomy and Neurobiology from VCU SOM in 2024. During her interim, she has worked as an analyst for Deloitte.

References

Ables, J. L., DeCarolis, N. A., Johnson, M. A., Rivera, P. D., Gao, Z., Cooper, D. C., Radtke, F., Hsieh, J., & Eisch, A. J. (2010). Notch1 Is Required for Maintenance of the Reservoir of Adult Hippocampal Stem Cells. Journal of Neuroscience. https://doi.org/10.1523/JNEUROSCI.4721-09.2010

Aburjania Z, Jang S, Whitt J, Jaskula-Stzul R, Chen H, Rose JB. The Role of Notch3 in Cancer. Oncologist. 2018 Aug;23(8):900-911. doi: 10.1634/theoncologist.2017-0677. Epub 2018 Apr 5. PMID: 29622701; PMCID: PMC6156186.

Alder, J., Fujioka, W., Lifshitz, J., Crockett, D. P., & Thakker-Varia, S. (2011). Lateral fluid percussion: model of traumatic brain injury in mice. Journal of visualized experiments : JoVE, (54), 3063. https://doi.org/10.3791/3063

Allaire, A., Picard-Jean, F., & Bisaillon, M. (2015). Immunofluorescence to Monitor the Cellular Uptake of Human Lactoferrin and its Associated Antiviral Activity Against the Hepatitis C Virus. Journal of visualized experiments: JoVE, (104), 53053. https://doi.org/10.3791/53053

Alao, T., & Waseem, M. (2022). Penetrating Head Trauma. National Library of Medicine. https://www.ncbi.nlm.nih.gov/books/NBK459254/

Alvarez-Buylla A, Nottebohm F. Migration of young neurons in adult avian brain. Nature. 1988;335:353–354.

Andriessen, T. M., Jacobs, B., & Vos, P. E. (2010). Clinical characteristics and pathophysiological mechanisms of focal and diffuse traumatic brain injury. Journal of cellular and molecular medicine, 14(10), 2381–2392. https://doi.org/10.1111/j.1582-4934.2010.01164.x

Ashwell, K. (2012). The Olfactory System. In C. Watson, G. Paxinos, & L. Puelles (Eds.), The Mouse Nervous System (pp. 653-660). Academic Press. https://doi.org/10.1016/B978-0-12-369497-3.10026-3.

Azargoonjahromi A. A systematic review of the association between zinc and anxiety. Nutr Rev. 2023. Online ahead of print. https://doi.org/10.1093/nutrit/nuad076.

Baracaldo-Santamaría, D., Ariza-Salamanca, D. F., Corrales-Hernández, M. G., Pachón-Londoño, M. J., Hernandez-Duarte, I., & Calderon-Ospina, C. A. (2022). Revisiting Excitotoxicity in Traumatic Brain Injury: From Bench to Bedside. Pharmaceutics, 14(1), 152. https://doi.org/10.3390/pharmaceutics14010152

Brai, E., Marathe, S., Zentilin, L., Giacca, M., Nimpf, J., Kretz, R., Scotti, A., & Alberi, L. (2014). Notch1 activity in the olfactory bulb is odour-dependent and contributes to olfactory behaviour. European Journal of Neuroscience, 40(11), 3436-3448. https://doi.org/10.1111/ejn.12719

Bramlett, H. M., & Dietrich, W. D. (2015). Long-Term Consequences of Traumatic Brain Injury: Current Status of Potential Mechanisms of Injury and Neurological Outcomes. Journal of neurotrauma, 32(23), 1834–1848. https://doi.org/10.1089/neu.2014.3352

Benskey, Matthew & Manfredsson, Fredric. (2016). Intraparenchymal Stereotaxic Delivery of rAAV and Special Considerations in Vector Handling. 10.1007/978-1-4939-3271-9_14.

Bernal, A., & Arranz, L. (2018). Nestin-expressing progenitor cells: function, identity and therapeutic implications. Cellular and molecular life sciences : CMLS, 75(12), 2177–2195. https://doi.org/10.1007/s00018-018-2794-z

Branigan B, Tadi P. Physiology, Olfactory. [Updated 2023 May 1]. In: StatPearls [Internet]. Treasure Island (FL): StatPearls Publishing; 2023 Jan-. Available from: https://www.ncbi.nlm.nih.gov/books/NBK542239/

Bratthauer G. L. (2010). The avidin-biotin complex (ABC) method and other avidin-biotin binding methods. Methods in molecular biology (Clifton, N.J.), 588, 257–270. https://doi.org/10.1007/978-1-59745-324-0_26

Brdu Alternative: Thermo Fisher Scientific - US. Click-iT EdU Assays-A Superior BrdU Alternative | Thermo Fisher Scientific - US. (n.d.). https://www.thermofisher.com/us/en/home/life-science/cell-analysis/cell-viability-and-regulation/cell-proliferation/click-it-edu-assays.html

Bryden, D. W., Tilghman, J. I., & Hinds, S. R., 2nd (2019). Blast-Related Traumatic Brain Injury: Current Concepts and Research Considerations. Journal of experimental neuroscience, 13, 1179069519872213. https://doi.org/10.1177/1179069519872213

Buchwalow, I., Samoilova, V., Boecker, W., & Tiemann, M. (2011). Non-specific binding of antibodies in immunohistochemistry: fallacies and facts. Scientific reports, 1, 28. https://doi.org/10.1038/srep00028

Carrick, K. (2023). Rodent brain perfusion. Rodent Brain Perfusion. https://www.umt.edu/laboratory-animal-resources/sops/sop-perfusion.php

Centers for Disease Control and Prevention. (2023, April 20). Get the facts about TBI. Centers for Disease Control and Prevention. https://www.cdc.gov/traumaticbraininjury/get_the_facts.html

Cernak, I., & Noble-Haeusslein, L. J. (2010). Traumatic brain injury: an overview of pathobiology with emphasis on military populations. Journal of cerebral blood flow and metabolism : official journal of the International Society of Cerebral Blood Flow and Metabolism, 30(2), 255–266. https://doi.org/10.1038/jcbfm.2009.203

Chang EH, Adorjan I, Mundim MV, Sun B, Dizon ML, Szele FG. Traumatic Brain Injury Activation of the Adult Subventricular Zone Neurogenic Niche. Front Neurosci. 2016 Aug 2;10:332. doi: 10.3389/fnins.2016.00332. PMID: 27531972; PMCID: PMC4969304.

Cho, S. H. (2014, July 3). Clinical Diagnosis and Treatment of Olfactory Dysfunction . Department of Otorhinolaryngology: Head and Neck Surgery. https://synapse.koreamed.org/upload/SynapseData/PDFData/0130hmr/hmr-34-107.pdf

Chung HJ, Lim HS, Lee K, et al. Incidence of Olfactory Dysfunction and Associated Factors: A Nationwide Cohort Study From South Korea. Ear, Nose & Throat Journal. 2021;0(0). doi:10.1177/01455613211012906

Ciurleo, Rosella & De Salvo, Simona & Bonanno, Lilla & Marino, Silvia & Bramanti, Alessia & Caminiti, Fabrizia. (2020). Parosmia and Neurological Disorders: A Neglected Association. Frontiers in Neurology. 11. 10.3389/fneur.2020.543275.

Costanzo, R. M., Becker, D. P., Meiselman, H. L., & Rivlin, R. S. (1986). Clinical measurements of taste and smell.

Costanzo R.M., DiNardo L.J., Reiter E.R. Head injury and olfaction. In: Doty R.L., editor. Handbook of Olfaction and Gustation. 2nd ed. Marcel Dekker; New York, NY: 2003. pp. 629–638

Costanzo R.M., Reiter R.J., Yelverton J.C. Smell and taste. In: Zasler N.D., Katz D.I., Zafonte R.D., editors. Brain Injury Medicine: Principles and Practice. Demos; New York, NY: 2012. pp. 794–808

Costanzo R.M., Zasler N.D. Head trauma. In: Getchell T.V., Doty R.L., Bartoshuk L.M., Snow J.B. Jr., editors. Smell and Taste in Health and Disease. Raven Press; New York, NY: 1991. pp. 711–730.

Damm, M., Temmel, A., Welge-Lüssen, A., Eckel, H. E., Kreft, M. P., Klussmann, J. P., Gudziol, H., Hüttenbrink, K. B., & Hummel, T. (2004). Riechstörungen. Epidemiologie und Therapie in Deutschland, Osterreich und der Schweiz [Olfactory dysfunctions. Epidemiology and therapy in Germany, Austria and Switzerland]. HNO, 52(2), 112–120. https://doi.org/10.1007/s00106-003-0877-z

Douaud, G., Lee, S., Alfaro-Almagro, F., Arthofer, C., Wang, C., McCarthy, P., et al. (2022).
SARS-CoV-2 is associated with changes in brain structure in UK Biobank. Nature 604, 697–707. doi: 10.1038/s41586-022-04569-5

Direct vs Indirect Immunofluorescence. Abcam. (2023, May 17). https://www.abcam.com/secondary-antibodies/direct-vs-indirect-immunofluorescence

Egger V, Svoboda K, Mainen ZF. Mechanisms of lateral inhibition in the olfactory bulb: efficiency and modulation of spike-evoked calcium influx into granule cells. J Neurosci. 2003 Aug 20;23(20):7551-8. doi: 10.1523/JNEUROSCI.23-20-07551.2003. PMID: 12930793; PMCID: PMC6740749.

Erb, K., Bohner, G., Harms, L., Goektas, O., Fleiner, F., Dommes, E., et al. (2012). Olfactory function in patients with multiple sclerosis: A diffusion tensor imaging study. J. Neurol. Sci. 316, 56–60. doi: 10.1016/J.JNS.2012.01.031

Erb-Eigner, K., Bohner, G., Goektas, O., Harms, L., Holinski, F., Schmidt, F. A., et al. (2014). Tract-based spatial statistics of the olfactory brain in patients with multiple sclerosis. J. Neurol. Sci. 346, 235–240. doi: 10.1016/J.JNS.2014.08.039

Esposito, R. (2022, January 24). What are the different detection methods for IHC?. Enzo Life Sciences. https://www.enzolifesciences.com/science-center/technotes/2019/august/what-are-the-different-detection-methods-for-ihc?%2F

Faget, L., & Hnasko, T. S. (2015). Tyramide Signal Amplification for Immunofluorescent Enhancement. Methods in molecular biology (Clifton, N.J.), 1318, 161–172. https://doi.org/10.1007/978-1-4939-2742-5_16

Finkelstein E, Corso P, Miller T and associates. The Incidence and Economic Burden of Injuries in the United States. New York (NY): Oxford University Press; 2006.

Gentleman, S. M., Leclercq, P. D., Moyes, L., Graham, D. I., Smith, C., Griffin, W. S. T., et al. (2004). Long-term intracerebral inflammatory response after traumatic brain injury. Forensic Sci. Int. 146, 97–104. doi: 10.1016/j.forsciint.2004.06.027

Ginsburg, J., & Huff, S. (2023). Closed Head Trauma. National Library of Medicine. https://www.ncbi.nlm.nih.gov/books/NBK557861/

Gopinath, B., Sue, C. M., Kifley, A., & Mitchell, P. (2012). The association between olfactory impairment and total mortality in older adults. The journals of gerontology. Series A, Biological sciences and medical sciences, 67(2), 204–209. https://doi.org/10.1093/gerona/glr165

Graham DI, Gennarelli TA, McIntosh TK. Trauma. In: Graham DI, Lantos PL, editors. Greenfield's Neuropathology. Arnold; London: 2002. pp. 823–898

Grin'kina, N. M., Li, Y., Haber, M., Sangobowale, M., Nikulina, E., Le'Pre, C., El Sehamy, A. M., Dugue, R., Ho, J. S., & Bergold, P. J. (2016). Righting Reflex Predicts Long-Term Histological and Behavioral Outcomes in a Closed Head Model of Traumatic Brain Injury. PloS one, 11(9), e0161053. https://doi.org/10.1371/journal.pone.0161053

Gudziol, V., Hoenck, I., Landis, B., Podlesek, D., Bayn, M., & Hummel, T. (2014). The impact and prospect of traumatic brain injury on olfactory function: a cross-sectional and prospective study. European archives of oto-rhino-laryngology: official journal of the European Federation of Oto-Rhino-Laryngological Societies (EUFOS) : affiliated with the German Society for Oto-Rhino-Laryngology - Head and Neck Surgery, 271(6), 1533–1540. https://doi.org/10.1007/s00405-013-2687-6

Hamilton KA, Heinbockel T, Ennis M, Szabó G, Erdélyi F, Hayar A. Properties of external plexiform layer interneurons in mouse olfactory bulb slices. Neuroscience. 2005;133(3):819-29. doi: 10.1016/j.neuroscience.2005.03.008. PMID: 15896912; PMCID: PMC2383877.

Hasegawa, Y., Ma, M., Sawa, A. et al. Olfactory impairment in psychiatric disorders: Does nasal inflammation impact disease psychophysiology? Transl Psychiatry **12**, 314 (2022). https://doi.org/10.1038/s41398-022-02081-y

Heywood P.G., Zasler N.D., Costanzo R.M. Proceedings of the 14th Annual Conference on Rehabilitation of the Brain Injured. Williamsburg, Virginia. 1990. Olfactory screening test for assessment of smell loss following traumatic brain injury.

Huart C, Rombaux P, Hummel T. Plasticity of the human olfactory system: the olfactory bulb. Molecules. 2013 Sep 17;18(9):11586-600. doi: 10.3390/molecules180911586. PMID: 24048289; PMCID: PMC6269828.

Hummel, T., Landis, B. N., & Hüttenbrink, K. B. (2011). Störungen des Riechens und Schmeckens [Dysfunction of the chemical senses smell and taste]. Laryngo- rhino-otologie, 90 Suppl 1, S44–S55. https://doi.org/10.1055/s-0030-1270445

Hoffman, H. J., Rawal, S., Li, C. M., & Duffy, V. B. (2016). New chemosensory component in the U.S. National Health and Nutrition Examination Survey (NHANES): first-year results for measured olfactory dysfunction. Reviews in endocrine & metabolic disorders, 17(2), 221–240. https://doi.org/10.1007/s11154-016-9364-1

Howell, J., Costanzo, R. M., & Reiter, E. R. (2018). Head trauma and olfactory function. World journal of otorhinolaryngology - head and neck surgery, 4(1), 39–45. https://doi.org/10.1016/j.wjorl.2018.02.001

Huart, C., Rombaux, P., & Hummel, T. (2013). Plasticity of the human olfactory system: the olfactory bulb. Molecules (Basel, Switzerland), 18(9), 11586–11600. https://doi.org/10.3390/molecules180911586

Ibrahim, S., Hu, W., Wang, X. et al. Traumatic Brain Injury Causes Aberrant Migration of Adult-Born Neurons in the Hippocampus. Sci Rep 6, 21793 (2016). https://doi.org/10.1038/srep21793

IHC Tips: Cell Permeabilization. IHC Tips: Cell Permeabilization. (n.d.). https://www.sinobiological.com/category/ihc-tips-cell-permeabilization

Im, K., Mareninov, S., Diaz, M. F. P., & Yong, W. H. (2019). An Introduction to Performing Immunofluorescence Staining. Methods in molecular biology (Clifton, N.J.), 1897, 299–311. https://doi.org/10.1007/978-1-4939-8935-5_26

Imamura, F., Ito, A., & LaFever, B. J. (2020). Subpopulations of Projection Neurons in the Olfactory Bulb. Frontiers in neural circuits, 14, 561822. https://doi.org/10.3389/fncir.2020.561822

Imayoshi I, Sakamoto M, Ohtsuka T, Takao K, Miyakawa T, Yamaguchi M, Mori K, Ikeda T, Itohara S, Kageyama R. Roles of continuous neurogenesis in the structural and functional integrity of the adult forebrain. Nat Neurosci. 2008 Oct;11(10):1153-61. doi: 10.1038/nn.2185. Epub 2008 Aug 31. PMID: 18758458.

Indra, A. K., Warot, X., Brocard, J., Bornert, J. M., Xiao, J. H., Chambon, P., & Metzger, D. (1999, November 15). Temporally-controlled site-specific mutagenesis in the basal layer of the epidermis: Comparison of the recombinase activity of the tamoxifen-inducible CRE-er(t) and Cre-er(T2) recombinases. Nucleic acids research. https://www.ncbi.nlm.nih.gov/pmc/articles/PMC148712/

James, A. C., Szot, J. O., Iyer, K., Major, J. A., Pursglove, S. E., Chapman, G., & Dunwoodie, S. L. (2014). Notch4 reveals a novel mechanism regulating Notch signal transduction. Biochimica et Biophysica Acta (BBA) - Molecular Cell Research, 1843(7), 1272-1284. https://doi.org/10.1016/j.bbamcr.2014.03.015

Johnson, M., & Villani, T. (2022, August 16). Understanding blocking buffers in immunofluorescence workflows. Visikol. https://visikol.com/blog/2022/08/16/blocking-buffers-immunofluorescence/

Johnson, V. E., Stewart, J. E., Begbie, F. D., Trojanowski, J. Q., Smith, D. H., and Stewart, W. (2013). Inflammation and white matter degeneration persist for years after a single traumatic brain injury. Brain 136, 28–42. doi: 10.1093/brain/aws322

Kabadi, S. V., Hilton, G. D., Stoica, B. A., Zapple, D. N., & Faden, A. I. (2010). Fluid-percussion-induced traumatic brain injury model in rats. Nature protocols, 5(9), 1552–1563. https://doi.org/10.1038/nprot.2010.112

Kosaka, T., & Kosaka, K. (2009). In Encyclopedia of Neuroscience.

Kaur, P., & Sharma, S. (2018). Recent Advances in Pathophysiology of Traumatic Brain Injury. Current neuropharmacology, 16(8), 1224–1238. https://doi.org/10.2174/1570159X15666170613083606

Keller, A., & Malaspina, D. (2013). Hidden consequences of olfactory dysfunction: a patient report series. BMC ear, nose, and throat disorders, 13(1), 8. https://doi.org/10.1186/1472-6815-13-8

Kirn JR, Fishman Y, Sasportas K, Alvarez-Buylla A, Nottebohm F. Fate of new neurons in adult canary high vocal center during the first 30 days after their formation. J Comp Neurol. 1999;411:487–494.

Kim, H., Kim, M., Im, S.-K., & Fang, S. (2018, December 31). Mouse Cre-LoxP system: General principles to determine tissue-specific roles of target genes. Laboratory Animal Research. https://synapse.koreamed.org/articles/1111441

Kim, S. O., Kim, J., Okajima, T., & Cho, N. J. (2017). Mechanical properties of paraformaldehyde-treated individual cells investigated by atomic force microscopy and scanning ion conductance microscopy. Nano convergence, 4(1), 5. https://doi.org/10.1186/s40580-017-0099-9

Kopan R. Notch signaling. Cold Spring Harb Perspect Biol. 2012 Oct 1;4(10):a011213. doi: 10.1101/cshperspect.a011213. PMID: 23028119; PMCID: PMC3475170.

Kureshi, N., Erdogan, M., Thibault-Halman, G. et al. Long-Term Trends in the Epidemiology of Major Traumatic Brain Injury. J Community Health 46, 1197–1203 (2021). https://doi.org/10.1007/s10900-021-01005-z

Landgren, H., & Curtis, M. A. (2010, October 26). Locating and Labeling Neural Stem Cells in the Brain. https://onlinelibrary.wiley.com/doi/10.1002/jcp.22319

Lepper, C., & Fan, C. M. (2012). Generating tamoxifen-inducible Cre alleles to investigate myogenesis in mice. Methods in molecular biology (Clifton, N.J.), 798, 297–308. https://doi.org/10.1007/978-1-61779-343-1_17

Levin, H. S., High, W. M., & Eisenberg, H. M. (1985). Impairment of olfactory recognition after closed head injury. Brain : a journal of neurology, 108 (Pt 3), 579–591. https://doi.org/10.1093/brain/108.3.579

Lifshitz, J., Sullivan, P. G., Hovda, D. A., Wieloch, T., and McIntosh, T. K. (2004). Mitochondrial damage and dysfunction in traumatic brain injury. Mitochondrion 4, 705–713. doi: 10.1016/j.mito.2004.07.021

Liu, G., Zong, G., Doty, R. L., & Sun, Q. (2016). Prevalence and risk factors of taste and smell impairment in a nationwide representative sample of the US population: a cross-sectional study. BMJ open, 6(11), e013246. https://doi.org/10.1136/bmjopen-2016-013246

Liu, X., Lei, Z., Gilhooly, D., He, J., Li, Y., Ritzel, R. M., Li, H., Wu, L.-J., Liu, S., & Wu, J. (2023). Traumatic brain injury-induced inflammatory changes in the olfactory bulb disrupt neuronal networks leading to olfactory dysfunction. Brain, Behavior, and Immunity, 114, 22-45. https://doi.org/10.1016/j.bbi.2023.08.004

Lotocki, G., de Rivero Vaccari, J. P., Perez, E. R., Sanchez-Molano, J., Furones-Alonso, O., Bramlett, H. M., et al. (2009). Alterations in blood-brain barrier permeability to large and small molecules and leukocyte accumulation after traumatic brain injury: effects of post-traumatic hypothermia. J. Neurotrauma 26, 1123–1134. doi: 10.1089/neu.2008.0802

Matsumoto, S. -i., Yamazaki, C., Masumoto, K. -h., Nagano, M., Naito, M., Soga, T., et al. (2006). Abnormal development of the olfactory bulb and reproductive system in mice lacking prokineticin receptor PKR2. Proc. Natl. Acad. Sci. U S A 103, 4140–4145. doi: 10.1073/pnas.0508881103

Marin C, Langdon C, Alobid I, Mullol J. Olfactory dysfunction in traumatic brain injury: the role of neurogenesis. Curr Allergy Asthma Rep. 2020:20(10):55–65.

Ming GL, Song H. Adult neurogenesis in the mammalian brain: significant answers and significant questions. Neuron. 2011;70:687–702.

Mizutani, Ki., Yoon, K., Dang, L. et al. Differential Notch signalling distinguishes neural stem cells from intermediate progenitors. Nature 449, 351–355 (2007). https://doi.org/10.1038/nature06090

Mo, J.-S., Yoon, J.-H., Ann, E.-J., Park, H.-S., & Greenwald, I. (2013). Notch1 modulates oxidative stress induced cell death through suppression of apoptosis signal-regulating kinase 1. *Proceedings of the National Academy of Sciences of the United States of America,* 110(17), 6865-6870. https://doi.org/10.1073/pnas.1209078110

Moreno, V., Smith, E. A., & Piña-Oviedo, S. (2022). Fluorescent Immunohistochemistry. Methods in molecular biology (Clifton, N.J.), 2422, 131–146. https://doi.org/10.1007/978-1-0716-1948-3_9

Morganti-Kossmann, M. C., Rancan, M., Stahel, P. F., and Kossmann, T. (2002). Inflammatory response in acute traumatic brain injury: a double-edged sword. Cur. Opin. Crit. Care 8, 101–105. doi: 10.1097/00075198-200204000-00002

Mucignat-Caretta C, Redaelli M, Caretta A. One nose, one brain: contribution of the main and accessory olfactory system to chemosensation. Front Neuroanat. 2012 Nov 9;6:46. doi: 10.3389/fnana.2012.00046. PMID: 23162438; PMCID: PMC3494019.

Ng, S. Y., & Lee, A. Y. W. (2019). Traumatic Brain Injuries: Pathophysiology and Potential Therapeutic Targets . Frontiers in Cellular Neuroscience. doi:10.3389/fncel.2019.00528 https://pubmed.ncbi.nlm.nih.gov/31827423/

O'Donnell, J.C., Purvis, E.M., Helm, K.V.T. et al. An implantable human stem cell-derived tissue-engineered rostral migratory stream for directed neuronal replacement. Commun Biol 4, 879 (2021). https://doi.org/10.1038/s42003-021-02392-8

Ohtsuka T., Kageyama R. (2021b). Hes1 overexpression leads to expansion of embryonic neural stem cell pool and stem cell reservoir in the postnatal brain. Development 148:dev189191. 10.1242/dev.189191

Parma, V., Ohla, K., Veldhuizen, M. G., Niv, M. Y., Kelly, C. E., Bakke, A. J., Cooper, K. W., Bouysset, C., Pirastu, N., Dibattista, M., Kaur, R., Liuzza, M. T., Pepino, M. Y., Schöpf, V., Pereda-Loth, V., Olsson, S. B., Gerkin, R. C., Rohlfs Domínguez, P., Albayay, J.,

Farruggia, M. C., … Hayes, J. E. (2020). More Than Smell-COVID-19 Is Associated With Severe Impairment of Smell, Taste, and Chemesthesis. Chemical senses, 45(7), 609–622. https://doi.org/10.1093/chemse/bjaa041

Pass T, Assfalg M, Tolve M, Blaess S, Rothermel M, Wiesner RJ, Ricke KM. The impact of mitochondrial dysfunction on dopaminergic neurons in the olfactory bulb and odor detection. Mol Neurobiol. 2020:57(9):3646–3657.

Pinto, J. M., Wroblewski, K. E., Kern, D. W., Schumm, L. P., & McClintock, M. K. (2015). The Rate of Age-Related Olfactory Decline Among the General Population of Older U.S. Adults. The journals of gerontology. Series A, Biological sciences and medical sciences, 70(11), 1435–1441. https://doi.org/10.1093/gerona/glv072

Paul, C. (2023, May 12). Confocal Laser Scanning Microscopy. Bitesize Bio. https://bitesizebio.com/19958/confocal-laser-scanning-microscopy/#:~:text=A%20confocal%20laser%20scanning%20microscope,the%20fluorophores%20in%20the%20sample.

Pignatelli, A., & Belluzzi, O. (2010). Modeling fluid percussion injury - brain neurotrauma - NCBI bookshelf. Neurogenesis in the Adult Olfactory Bulb. https://www.ncbi.nlm.nih.gov/books/NBK299213/

Randen R. Nelson, Byron H. Hartman, Sean A. Georgi, Michael S. Lan, & Thomas A. Reh. (2007). Transient inactivation of Notch signaling synchronizes differentiation of neural progenitor cells. Developmental Biology, 304(2), 479-498. https://doi.org/10.1016/j.ydbio.2007.01.001

Ray, S. K., Dixon, C. E., and Banik, N. L. (2002). Molecular mechanisms in the pathogenesis of traumatic brain injury. Histol. Histopathol. 17, 1137–1152. doi: 10.14670/HH-17.1137

Reiter, E. R., DiNardo, L. J., & Costanzo, R. M. (2004). Effects of head injury on olfaction and taste. Otolaryngologic clinics of North America, 37(6), 1167–1184. https://doi.org/10.1016/j.otc.2004.06.005

Salic, A., & Mitchison, T. J. (2007, December 26). A Chemical Method for Fast and Sensitive Detection of DNA Synthesis In Vivo. https://www.pnas.org/doi/10.1073/pnas.0712168105

Sandström, Malin. (2010). Computational Modelling of Early Olfactory Processing.

Saniasiaya, J., Islam, M. A., & Abdullah, B. (2021). Prevalence of Olfactory Dysfunction in Coronavirus Disease 2019 (COVID-19): A Meta-analysis of 27,492 Patients. The Laryngoscope, 131(4), 865–878. https://doi.org/10.1002/lary.29286

Sharma A, Kumar R, Aier I, Semwal R, Tyagi P, Varadwaj P. Sense of Smell: Structural, Functional, Mechanistic Advancements and Challenges in Human Olfactory Research. Curr Neuropharmacol. 2019;17(9):891-911. doi: 10.2174/1570159X17666181206095626. PMID: 30520376; PMCID: PMC7052838.

Shohami, E., and Kohen, R. (2011). “The role of reactive oxygen species in the pathogenesis of traumatic brain injury,” in Oxidative Stress and Free Radical Damage in Neurology, eds N. Gadoth, and H. H. Göbel (Humana Press), 99–118.

Singh, I. N., Sullivan, P. G., Deng, Y., Mbye, L. H., and Hall, E. D. (2006). Time course of post-traumatic mitochondrial oxidative damage and dysfunction in a mouse model of focal traumatic brain injury: implications for neuroprotective therapy. J. Cereb. Blood Flow Metab. 26, 1407–1418. doi: 10.1038/sj.jcbfm.9600297

Smith, C. J., Xiong, G., Elkind, J. A., Putnam, B., & Cohen, A. S. (2015). Brain Injury Impairs Working Memory and Prefrontal Circuit Function. Frontiers in Neurology, 6, 240. doi: 10.3389/fneur.2015.00240

Smith, D. H., Meaney, D. F., and Shull, W. H. (2003). Diffuse axonal injury in head trauma. J. Head Trauma Rehabil. 18, 307–316. doi: 10.1097/00001199-200307000-00003

Srinivas, S., Watanabe, T., Lin, C. S., William, C. M., Tanabe, Y., Jessell, T. M., & Costantini, F. (2001). Cre reporter strains produced by targeted insertion of EYFP and ECFP into the ROSA26 locus. BMC developmental biology, 1, 4. https://doi.org/10.1186/1471-213x-1-4

Stern, T. A., Smith, F., Brennan, M. M., & Huffman, J. C. (2010). Patients with Neurologic Conditions I. Seizure Disorders (Including Nonepileptic Seizures), Cerebrovascular Disease, and Traumatic Brain Injury. In Massachusetts General Hospital Handbook of General Hospital Psychiatry (6th ed., pp. 237–253). essay, Saunders/Elsevier.

Sun, D., & Rolfe, A. (2015). Stem Cell Therapy in Brain Trauma: Implications for Repair and Regeneration of Injured Brain in Experimental TBI Models. In Brain Neurotrauma: Molecular, Neuropsychological, and Rehabilitation Aspects (Chapter 42). CRC Press/Taylor & Francis. https://www.ncbi.nlm.nih.gov/books/NBK299210/

Sun D. Endogenous neurogenic cell response in the mature mammalian brain following traumatic injury. Exp Neurol. 2016 Jan;275 Pt 3(0 3):405-410. doi: 10.1016/j.expneurol.2015.04.017. Epub 2015 Apr 30. PMID: 25936874; PMCID: PMC4627904.

Tang-Schomer, M. D., Patel, A. R., Baas, P. W., and Smith, D. H. (2010). Mechanical breaking of microtubules in axons during dynamic stretch injury underlies delayed elasticity, microtubule disassembly and axon degeneration. FASEB J. 24, 1401–1410. doi: 10.1096/fj.09-142844

The Importance of Blocking When Using Nano-Secondary Reagents for if: Proteintech. Proteintech Group. (2022, August 24). https://www.ptglab.com/news/blog/the-importance-of-blocking-when-using-nano-secondary-reagents-for-if/#:~:text=Blocking%20is%20an%20essential%20step,even%20mask%20the%20specific%20signal.

The Jackson Laboratory. (2022, October 26). What Does This Nomenclature Mean?. 006148 - R26R-EYFP strain details. https://www.jax.org/strain/006148

von Bartheld, C. S., Hagen, M. M., and Butowt, R. (2020). Prevalence of chemosensory dysfunction in COVID-19 patients: A systematic review and meta-analysis reveals significant ethnic differences. ACS Chem. Neurosci. 11:2944. doi: 10.1021/ACSCHEMNEURO.0C00460

Martinez, Diane P.; Freeman, Walter J. (1984). "Periglomerular cell action on mitral cells in olfactory bulb shown by current source density analysis". Brain Research. 308 (2): 223–233. doi:10.1016/0006-8993(84)91061-8.

Weston, N. M. (2022). The Injury-Induced Neurogenic Response and the Role of Notch1 in Regulating This Process [Doctoral dissertation, Virginia Commonwealth University].

Weston NM, Sun D. The Potential of Stem Cells in Treatment of Traumatic Brain Injury. Curr Neurol Neurosci Rep. 2018 Jan 25;18(1):1. doi: 10.1007/s11910-018-0812-z. PMID: 29372464; PMCID: PMC6314040.

Wilson, R. S., Arnold, S. E., Schneider, J. A., Tang, Y., & Bennett, D. A. (2007). The relationship between cerebral Alzheimer's disease pathology and odour identification in old age. Journal of neurology, neurosurgery, and psychiatry, 78(1), 30–35. https://doi.org/10.1136/jnnp.2006.099721

Wu, J., Cai, Y., Wu, X., Ying, Y., Tai, Y., & He, M. (2021). Transcardiac Perfusion of the Mouse for Brain Tissue Dissection and Fixation. Bio-protocol, 11(5), e3988. https://doi.org/10.21769/BioProtoc.3988

Xiong, Y., Gu, Q., Peterson, P. L., Muizelaar, J. P., and Lee, C. P. (1997). Mitochondrial dysfunction and calcium perturbation induced by traumatic brain injury. J. Neurotrauma 14, 23–34. doi: 10.1089/neu.1997.14.23

Xiong, Y., Mahmood, A., & Chopp, M. (2013). Animal models of traumatic brain injury. Nature reviews. Neuroscience, 14(2), 128–142. https://doi.org/10.1038/nrn3407

Yan X, Joshi A, Zang Y, Assunção F, Fernandes HM, Hummel T. The Shape of the Olfactory Bulb Predicts Olfactory Function. Brain Sci. 2022 Jan 18;12(2):128. doi: 10.3390/brainsci12020128. PMID: 35203892; PMCID: PMC8870545.

Yang, J., & Pinto, J. M. (2016). The Epidemiology of Olfactory Disorders. Current otorhinolaryngology reports, 4(2), 130–141. https://doi.org/10.1007/s40136-016-0120-6

Yu L, Li W. Abnormal activation of notch 1 signaling causes apoptosis resistance in cervical cancer. Int J Clin Exp Pathol. 2022 Jan 15;15(1):11-19. PMID: 35145579; PMCID: PMC8822208.

Zapiec, B., & Mombaerts, P. (2015). Multiplex assessment of the positions of odorant receptor-specific ... PNAS. https://www.pnas.org/doi/10.1073/pnas.1512135112

Zhao C, Deng W, Gage FH. Mechanisms and functional implications of adult neurogenesis. Cell. 2008;132:645–660

Zhao X, van Praag H. Steps towards standardized quantification of adult neurogenesis.Nat Commun. 2020 Aug 26;11(1):4275. doi: 10.1038/s41467-020-18046-y. PMID: 32848155; PMCID: PMC7450090.

Zou, Y. M., Lu, D., Liu, L. P., Zhang, H. H., & Zhou, Y. Y. (2016). Olfactory dysfunction in Alzheimer's disease. Neuropsychiatric disease and treatment, 12, 869–875. https://doi.org/10.2147/NDT.S104886

Zou, B., Zhou, X., Lai, S., & Liu, J. (2018). Notch signaling and non-small cell lung cancer (Review). Oncology Letters, 15, 3415-3421. https://doi.org/10.3892/ol.2018.7738

Zusho H. (1982). Posttraumatic anosmia. Archives of otolaryngology (Chicago, Ill. : 1960), 108(2), 90–92. https://doi.org/10.1001/archotol.1982.00790500026006